MAFIAS

AN INTEGRATED LAB-ON-A-CHIP FOR AMMONIUM MEASUREMENT

Theo Veenstra

The research described in this thesis was carried out at the Transducers Technology Group of the MESA+ Research Institute, Universiy of Twente, Enschede.
The project was financially supported by the Dutch Science Foundation (STW)

Promotiecommissie :

Voorzitter		
	Prof.dr. Wallinga	Universiteit Twente
Secretaris		
	Prof.dr. Wallinga	Universiteit Twente
Promotoren		
	Prof.dr.ir. A. van den Berg	Universiteit Twente
	Prof.dr. M.C.Elwenspoek	Universiteit Twente
Co-promotor		
	Dr. J.G.E.Gardeniers	Universiteit Twente
Leden		
	Prof.dr. P.French	Technische Universiteit Delft
	Prof.dr. P.Bergveld	Universiteit Twente
	Dr. E.Verpoorte	University of Neuchatel
	Dr. A.Driessen	Universiteit Twente

Veenstra, Tjitze Theodoor
MAFIAS - An Integrated Lab-On-A-Chip for Ammonium Measurement
Ph.D. thesis, University of Twente, Enschede, the Netherlands
ISBN 90-365-1602-1

MAFIAS

AN INTEGRATED LAB-ON-A-CHIP FOR AMMONIUM MEASUREMENT

PROEFSCHRIFT

ter verkrijging van
de graad van doctor aan de Universiteit Twente,
op gezag van de rector magnificus,
prof.dr. F.A. van Vught,
volgens besluit van het College voor Promoties
in het openbaar te verdedigen
op vrijdag 22 juni 2001 te 13.15 uur.

door

Tjitze Theodoor Veenstra
geboren op 5 mei 1972
te Smallingerland

Dit proefschrift is goedgekeurd door de promotoren:

Prof.dr.ir. A. van den Berg

Prof.dr. M.C.Elwenspoek

Index

Chapter 1: Introduction

The background of the Micro Ammonium Flow Injection Analysis System (MAFIAS) project that has led to this thesis is given. The important role of microfluidics is indicated, and the aim of the research described in this work, the design, realization and evaluation of an integrated microsystem for ammonium analysis, is discussed. Finally, a brief overview of the content of the different chapters of this thesis is given.

1.1 Introduction: The Dream

The title of this thesis, "MAFIAS – An integrated Lab-on-a-Chip for ammonium measurement" needs some explanation. The name of the project from which this thesis evolved is the MAFIAS project. MAFIAS is an acronym for Micro Ammonium Flow Injection Analysis System, i.e. a system for the measurement of ammonium using the flow injection analysis (FIA) method, realized with the use of micromachining techniques.

The title also refers to the dream of a fully integrated chemical analysis system on a single chip. This system should be functionally equivalent to a conventional table-top system, but with dimensions that make it easily fit in ones hand. The downscaling of such a system results in a number of advantages. Not only becomes the system readily transportable, but also the consumption of energy (to drive the system) and consumption of chemicals are significantly reduced. Also the small dimensions can considerably reduce the needed analysis time, opening the way to near real time measurements. Last but not least, the sample size needed for a reliable measurement is smaller.

1.2 Microfluidics

The field of microfluidics has recently emerged as a very important application area of microelectromechanical systems (MEMS). Simply stated, MEMS covers the area of (multi) functional sub-millimeter sized systems and structures, realized with the help of technologies derived from microelectronics. Those MEMS structures that involve fluid mechanics are said to be part of the microfluidics field. A well-known example

of a microfluidic device is the inkjet nozzle [1], whereas micromechanical devices include the airbag sensor [2] and pressure transducers [3,4]

Downscaling of systems results in a number of advantages. The response of smaller systems is faster than for large systems. Just as a hand of a wristwatch can move faster than the hand of a church clock, also a micromachined structure can move faster than its macroscopic equivalent. A number of effects, which are hardly noticed in the macroworld, become very important on the microscale. The much larger relative magnitude of forces due to viscosity and surface tension results in completely different phenomena at the microscale.

Microfluidic systems, which are created to perform the detection of a chemical substance, are known as μTAS, Micro Total Analysis Systems. μTAS's that have been presented so far involve (among others) systems for genetic, protein and cell analysis, diagnostic applications, process control and environmental monitoring [5-12]. The system presented in this thesis also falls in the category of μTAS.

1.3 Research Goal

In the MAFIAS project the development of a monolithic fluid-handling chip is undertaken. The chip should be capable of performing Berthelot's reaction, a standard method used in FIA systems, for the measurement of ammonium in water. In the Berthelot reaction two reagents are added to the ammonium sample leading to the formation of indophenol, a blue dye. The concentration of this blue dye can be measured using a detection cell and is a good measure for the original ammonium concentration. To optimize the reaction, the temperature at which the reaction takes place has to be kept constant for at least 30 seconds.

Though the detection cell does not have to be incorporated in the system, the design of the system depends on the size and specifications of a detection cell. The development of such a MAFIAS system is quite multidisciplinary. Chemistry is needed to understand and control the Berthelot reaction. Physics is needed to control the microfluidics and design the optical detection cell and to split the whole system into subsystems, which can be combined to form a complete detection system. Understanding of mechanical engineering is necessary to end up with a working design of the subsystems. And finally, knowledge and understanding of the fabrication processes used in the cleanroom are a must. The relevance and timelines of the efforts to realize a miniaturized system as described in this thesis is illustrated by the recent startup of a European project aiming at the development of a similar miniaturized ammonium detection system based upon the same reaction mechanism as used in the MAFIAS project [13-15].

The system as described in this thesis is only capable of performing the Berthelot method for the measurement of ammonium. The design route followed in this thesis however can be easily adapted to come to a design of a chip that can accommodate any other detection reaction.

1.4 Outline of this Thesis

As has been explained, the aim of the research is to create a micromachined FIA system for the detection of ammonium using a well-known method. The thesis describes in a logical order the steps that have been performed to come to the design, realization and testing of such system.

First the involved analytical-chemical aspects are investigated. Not only the reaction kinetics for ammonium using Berthelot's reaction, but also the FIA principle itself are discussed in *chapter 2*. From this chapter a number of guidelines for the design of the whole system are deduced.

The first systems component that is designed is a mixing unit. Mixing in the micro world is not as trivial as it seems. Frictional forces prohibit any turbulence in the fluids stream, resulting in laminar flow regimes. Merging two fluids into one channel will not automatically result in a homogeneously mixed fluid inside a channel or at the outlet of the channel. A diffusion mixer ensuring complete mixing of two fluids has been developed as described in *chapter 3*.

In *chapter 4* a temperature-controlled reaction chamber is described. This reaction chamber is needed to guarantee a fixed temperature for the ammonium conversion. A temperature sensor and a heating element are needed to control the temperature within in a very narrow range (<0.1 °C).

In *chapter 5* the design and realization of a micropump that has to force the liquid through the system is presented. The pump has to be user friendly, i.e. it should be self-priming and bubble-tolerant. These qualities again are not trivial. In the micro-world the forces due to surface tension (or better: surface energy) can cause a serious pressure drop at places where a surface changes from one material to another, which may prevent proper pump functioning.

As mentioned before, the chemical reaction involved in the MAFIAS system results in the formation of a blue dye. The concentration of this blue dye is proportional to the initial ammonium concentration. For the determination of the dye concentration the absorption of light in a small cuvette measured. The design of this cuvette is explained in *chapter 6*. Critical parameters for the design of the cuvette are the path length of the light through the cuvette and the light efficiency of the cuvette. Since about 75% of the light is absorbed at every reflection at a silicon-water interface, the number of reflections has to be minimized in order to end with sufficient light intensity exiting from the cuvette.

The integration of the four previously described type of components, the pumps, reactor, mixer and optical detection cell into one design is presented in *chapter 7*. Since in the MAFIAS project the explicitly mentioned goal was to realize a monolithic system, the most important challenge has been the integration of the different steps of

the process schemes for the different components into one process scheme for the whole system. After this, the physical layout of the different components has been determined, and finally, the resulting design was equipped with electric and fluidic connections to the macro-world.

In this thesis also two related topics are presented. In *chapter 8* the development of so-called 'selective anodic bonding' is described, a process that turned out to be of fundamental importance for the design of the pumps of the system. The chapter presents a number of observations on the bonding process as well as the explanation for the local prevention of bond formation between silicon and glass.

In *chapter 9* a microfluidic compliance structure is described. Such a structure is usually added to macroscopic fluidic systems in order to dampen pressure waves traveling through the system, by taking up fluid upon pressure increase. Important parameters are the total volume that can be taken in as well as the volume that is taken in per unit of pressure.

A comprehensive summary and conclusions of the most important findings of the performed research are given in *chapter 10.* The last part of that chapter reflects on the chosen method of creating a monolithically integrated, multi-component fluidic system as described in this thesis. An alternative way to create the system would be to couple different fluidic modules to each other, and one possible realization of such a "hybrid" integration is discussed.

1.5 Literature

[1] E.Bassous, H.H.Taub, L.Kuhn, Ink jet printing nozzle arrays etched in silicon, Appl. Phys.Lett., **31-2** (1977) pp135-137

[2] W.Kuehnel, S.J.Sherman, A surface micromachined silicon accelerometer with on-chip detection circuitry, Sensors and Actuators A **45-1** (1994) pp7-16

[3] Product information catalogue 15: Pressure and airflowsensors, Honeywell, Freeport, Illinois, USA (1997)

[4] E.M.Blaser, W.H.Ko, E.T.Ton, A miniature digital pressure transducer, 24th annual conference on Engineering in Med and Biol. (1971) pp211

[5] I.Amato, Microchip arrays put DNA on the spot, News focus in Science **282** (1998)

[6] R.C.Anderson, G.J.Bogdan, A.Puski, X.Su, Advances in integrated genetic analysis, in: J.D.Harrison, A.van den Berg, Micro Total Analysis Systems (1998) pp11-16

[7] C.S.Effenhauser, integrated chip-based microcolumn separation systems, in: A.Manz, Microsystem technology in Chemistry and Life Sciences **194** (1998) pp51-82

[8] M.A.Burns, B.N.Johnson, S.N.Brahmasandra, K.Handique, J.R.Webster, M.Krishnan, T.S.Sammarco, P.M.Man, D.Jones, D.Heldsinger, C.H.Mastrangelo, D.T.Burke, An integrated Nanoliter DNA Analysis Device, Science, **282** (1998)

[9] S.J.Haswell, Development and operating characteristics of micro flow injection analysis systems based on electroosmotic flow, The Analyst, Jan. 1997, **122**, 1R-10R

[10] R.Miyake, K.Tsuzuki, T.Takagi, K.Imai, A highly sensitive and small flow-type chemical analysis system with integrated absorptiometric micro-flowcell, in proc MEMS 1997 (1997), pp102-107

[11] E.M.J.Verpoorte, B.H.vanderSchoot, S.Jeanneret, A.Manz, H.M.Widmer, N.F.deRooij, 3-dimensional micro flow manifolds for miniaturized chemical analysis systems, Journal Micromech. Microeng 4 (1994) 246

[12] P.Woias, K.Hauser, E.Yacoub-George, B.Hillerich, A Silicon-based Microreaction System for Analytical Applications, In proc. IMRET3, FrankFurt, Germany, April18-21 (1999)

[13] J.P.Krog, *et al*, realization of a prototype industrial on-line sensing system for ammonium based on micro system technology: Results and future perspectives, in: A. van den Berg, W.Olthuis, P.Bergveld, MicroTotal Analysis Systems 2000 (2000) pp419-422

[14] H.Dirac, J.P.Krog, P.Gravesen, B.Bunk, B.Fabius, Design and Flow Strategies of a Pressure Driven µ-TAS Sensor with Short Response Time and Low Reagent Consumption, in Proc. Eurosensors XIV, Copenhagen, Denmark (2000) pp877-880

[15] A.Daridon, M.Sequeira, G.Pennarun-Thomas, J.Lichtenberg, E.Verpoorte, D.Diamond, N.F.de Rooij, Comparative Kinetic Studies of The Berthelot Reaction for Ammonium Determination in Microfluidic and Spectrophotometric Systems, in Proc. Eurosensors XIV, Copenhagen, Denmark (2000) pp815-818

Chapter 2 : The System Definition

The principle of the Berthelot reaction in a Flow Injection Analysis (FIA) setup for the determination of ammonium concentrations is described. Several aspects of the chemistry involved such as the influence of pH, reaction time and temperature, as well as the formation of the light absorbing product (indophenol) are discussed. The principle of FIA and a practical setup for the MAFIAS are presented, whereas the effects of axial and radial dispersion on the system's performance are discussed.

2.1 Introduction

For the continuous measurement of aqueous ammonia several chemical sensors exist, e.g. based on the ChemFET [1]. Such sensors however suffer from drawbacks such as poor selectivity or aging [2]. Therefore, for a variety of applications such as environmental and process control a need exists for a measurement system that does not suffer from these drawbacks. A classical analytical chemical method for ammonium determination is based upon the Berthelot reaction mechanism [3]. Although the completion of the reaction takes about 15 minutes, it is common practice in flow injection analysis (FIA) setups to measure at reproducible points of time shorter than that, e.g. 30 seconds, which for practical purposes can be considered as on-line. Similarly a sample rate of $1\ min^{-1}$ is considered as continuous. Clearly, ammonium determination in such an FIA requires both repeatability of the measurement and calibration.

In this chapter the Berthelot reaction mechanism and the basic layout of the FIA system are shown. From this basic layout the fluidic components needed to implement the ammonium detection system are determined. The last part of this chapter deals with the phenomena of dispersion (i.e. the effect that an injected sample redistributes itself over the FIA systems' main channel such that the maximum peak height is reduced).

2.2 Chemistry: Berthelot

The conversion of ammonia into an easily detectable compound (a blue dye) is done by means of the Berthelot reaction mechanism. In 1859 Berthelot presented his findings on the formation of a blue coloration when mixing phenol with hypochlorite and ammonia [4]. Though he wanted to find a use for this blue coloration in detecting aniline (a poisonous substance used to make dyes), the reaction now is used as a reference method for determining ammonium concentrations in water [3]. This Berthelot reaction mechanism is highly selective for ammonium [5] and is suitable for very low concentrations [6].
The Berthelot reaction scheme is a three-step reaction mechanism. The first is a well-defined second order reaction, the second and third are not fully understood but are fairly well documented. All steps have their optimum environment. These settings will have to be provided by the MAFIAS system.

2.2.1 Berthelot: Step one

The first reaction step in the Berthelot reaction scheme is the conversion of ammonia into mono-chloramine (Figure 1) in an aqueous solution.

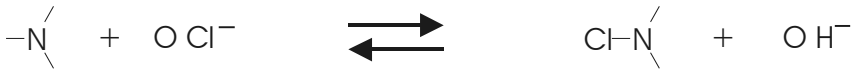

Figure 1: The first reaction step.

This step is pH dependent (see Figure 2). A high pH (>12) prevents the reaction from taking place at all, while at a lower pH (<10), the formed mono-chloramine will react further with the available hypo-chlorite into di-chloramine or even tri-chloramine. These last two reaction products do not contribute to the formation of indophenol but do take away the available ammonia. Therefore care has to be taken choosing the pH at which the reaction takes place. Figure 2 shows the dependency of the reaction rate *k* for the reaction as function of pH.

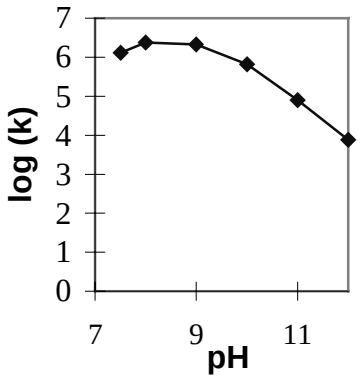

Figure 2: pH dependence of the reaction rate *k* [l mol^{-1} sec^{-1}] of the first reaction step [6]

From this graph it is clear that a pH of about 8 will result in the fastest conversion of ammonia in mono-chloramine. Unfortunately, as indicated before, at this pH the unwanted di-chloramine already will be formed at an unacceptable rate [7]. Therefore

the pH at which the reaction has to be performed should be within the mentioned range of pH 10-12. For the MAFIAS system a pH of 11 is chosen.

According to literature [8], hypochlorite should be available in large excess relative to the ammonia. To ensure excess hypochlorite even for the highest ammonia concentrations, the concentration of the hypochlorite should be at least tenfold the highest ammonia concentration. Therefore, the concentration to be used is 0.3 g l^{-1} (as the maximum ammonia concentration is 10 mg l^{-1}).

2.2.2 Berthelot: Step two and three

During the second and third step of the Berthelot reaction scheme the mono-chloramine is to be converted into indophenol-blue, the final reaction product. In the second step, one benzene ring is attached to the nitrogen atom of the mono-chloramine molecule forming quinone-chlorimine (figure 3).

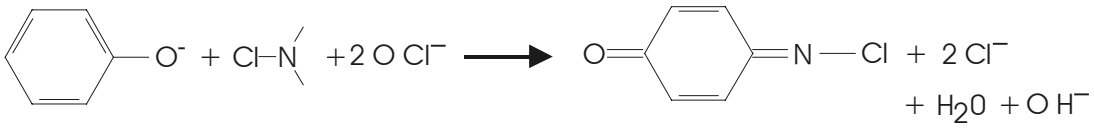

Figure 3: The second reaction step.

The last step of the reaction scheme is the bond of another benzene ring to the nitrogen atom. In this way an almost symmetrical molecule is built: indophenol. In high pH environments, the hydrogen atom at the OH group at the end of the molecule dissociates from the indophenol, leading to a free moving excess electron, which is responsible for the red-light absorption and hence the blue coloration of indophenol.

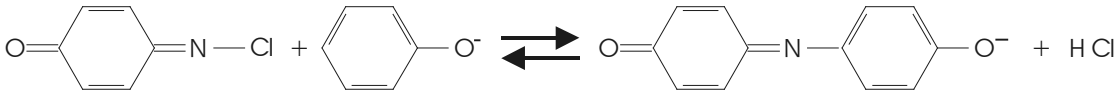

Figure 4: The third reaction step.

The combination of the second and third reaction steps is very slow and also highly temperature dependent (Figure 5). The first graph shows the formed coloration for different temperatures. The reaction time was kept constant during these experiments [9]. The second graph shows the coloration as function of time for different concentrations of ammonia.

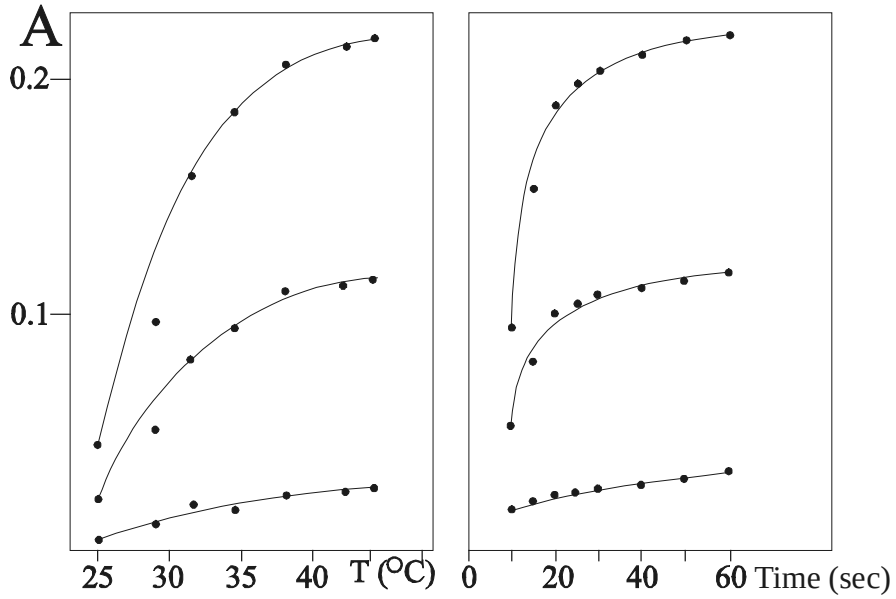

Figure 5: Color development as function of temperature (all after 26 seconds reaction time) and time (all at 38°C). The different curves refer to concentrations of the samples of 0, 250 and 500 μg l^{-1} (reproduced from [9]).

As is seen, the reaction rate for temperatures below 25°C drops to zero. For a temperature of about 60°C, the reaction rate is at 90% of its maximum [6]. Therefore the temperature at which the reaction will take place in the MAFIAS system should be as high as possible.

It is reported however [8, 9] that air bubbles easily appear in the system for reaction temperatures higher than 38°C as a result of the lower air solubility. For a batch-type detection system this does not interfere with the detection process since the air bubbles can leave the sample into open air. In a FIA system though, the air bubbles will interfere with the measurement as they come along with the sample into the cuvette. Here the light passing through the cuvette will be distorted severely. Depending on the design of the cuvette, the light will pass through the bubble resulting in a seemingly very low concentration of indophenol or the light will not be reaching the detector at all, resulting in a seemingly very high concentration of indophenol. In order to prevent such air bubbles the reaction temperature is chosen below 38°C.

The concentration of the phenol should be very high with respect to the concentration of the intermediate compound mono-chloramine, since two phenol molecules are needed to form one indophenol molecule, but also to compensate for the very slow reaction rate. To drive the equilibrium of the reaction towards the indophenol-end, the availability of phenol should not be the limiting factor. The same tenfold excess as mentioned for the hypochlorite is chosen and results in a concentration of 0.55 g l^{-1}.

2.2.3 Berthelot: Catalyst

It has been found that the compound nitro-prusside (hexa-cyanoferrate, $[Fe(CN)_6]^{4-}$) acts as a catalyst to the second reaction step [8, 10]. This nitro-prusside has a red color. Therefore it will not interfere with the detection in the cuvette.

The optimal concentration for the nitro-prusside cannot be determined in the same way as the other two reagents. In literature the nitro-prusside concentration used as catalyst for the Berthelot reaction is around 40 mg l^{-1}. Since this concentration is used in practice, this value will be used for the MAFIAS system also.

2.2.4 Berthelot: In practice

As is seen, a number of chemicals have to be added together in order to convert ammonia into indophenol. The involved chemicals are listed in Table 1. All chemicals are dissolved in water.

Chemical compound	Function	Concentration
H_2O	Carrier	-
NH_3	Sample	0.1 – 10 mg l^{-1}
OCl^-	First reagent	300 mg l^{-1}
pH 11 buffer (H_2KPO_4)	Optimum condition for 1st reaction step	-
Phenol	Second reagent	550 mg l^{-1}
NitroPrusside	Catalyst	40 mg l^{-1}

Table 1 : Chemicals involved in the MAFIAS system

In order to minimize the amount of fluids to be added into the carrier stream, some of the mentioned compounds can be premixed. The mono-chloramine can be premixed with the pH 11 buffer and the catalyst nitro-prusside can be premixed with the phenolic solution. In this way only three fluids have to be injected into the carrier stream. First the sample is injected, second the pH buffer with the hypochlorite mixture is added and at last, the catalyst with the phenol is injected into the carrier stream.

2.3 The FIA principle

A number of ways are available to use a continuously flowing system to process a sequence of samples. A FIA (Flow Injection Analysis) system is one of these. FIA systems are known for their inherent high reproducibility [11-14].

In a true FIA system the samples are injected into a continuous flowing carrier stream. The samples are separated by a certain amount of pure carrier fluid. As the sample plug travels along the channel, treatments (heating, addition of chemicals) are done in the plug.

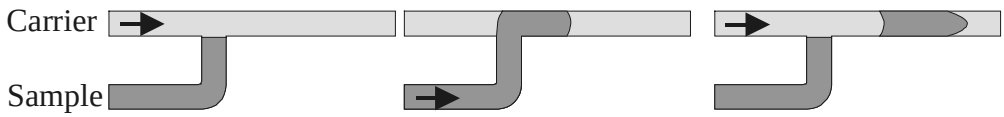

Figure 6: In a FIA system, the sample is injected into the carrier stream.

This setup has as a big advantage that the whole treatment sequence can be performed completely identical to all subsequent samples. E.g. reagent can be added at exactly the right timing and temperature steps can be introduced at the right moment. With commercial FIA systems, sample rates of up to 90 hr^{-1} are performed [15]. With a FIA system setup, complex reaction schemes as Berthelot's are implemented easily and very reproducibly [13]. This high reproducibility enables the FIA system to perform a measurement before the chemical reaction on hand has been fully completed.

2.3.1 Berthelot in FIA: MAFIAS

Needed for the design of the system is a clear overview of which processes have to be performed. Table 2 gives an overview of the processes that have to be controlled by the system in order to perform Berthelots' reaction mechanism.

Step #	Process
1	Sample injection in carrier stream
2	Control of pH at 11
3	Addition of first reagent to sample
4	Mixing of sample with first reagent
5	Control of temperature at 37°C for 30 seconds
6	Addition of second reagent
7	Addition of catalyst
8	Mixing of all compounds
9	Measurement of absorption of light at 590nm

Table 2 : Sequence of processes to be performed by the MAFIAS system.

In practice premixing the first reagent hypochlorite with a pH buffer will combine steps 2 and 3. In a similar way premixing the second reagent with the catalyst will combine step 6 and 7. The basic design of a system that joins all mentioned functions is shown in Figure 7.

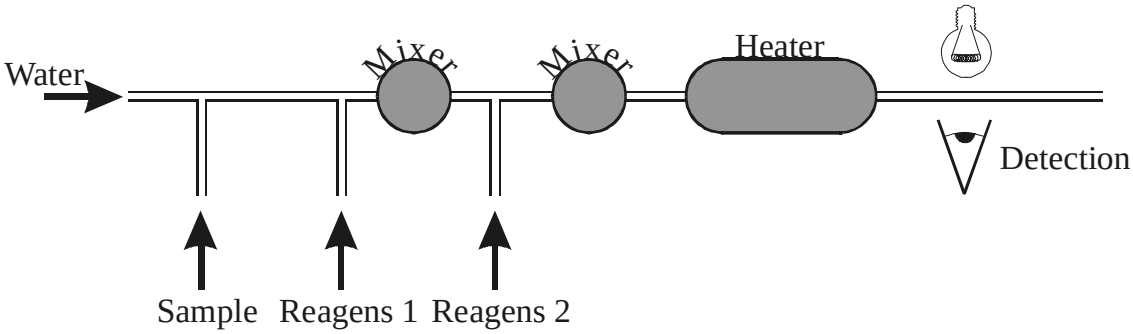

Figure 7 : Basic design of the Berthelot system

Not shown in this figure are the pumps needed to propel the fluids into the system. All components of the system can be modeled and designed as stand alone components

after which they are joined to form a complete system. In chapters 3-6 the mixer, the heater (reaction chamber), the pump and the detection cell will be treated. Chapter 7 will show how these components are combined on one chip to form a complete analysis system.

2.4 FIA - Dispersion

A factor to take into account when designing a FIA system is the so-called dispersion effect. Due to diffusion and the flow profile in the tubing of the system, the sample plug will be distorted (Figure 8, [17-19]).

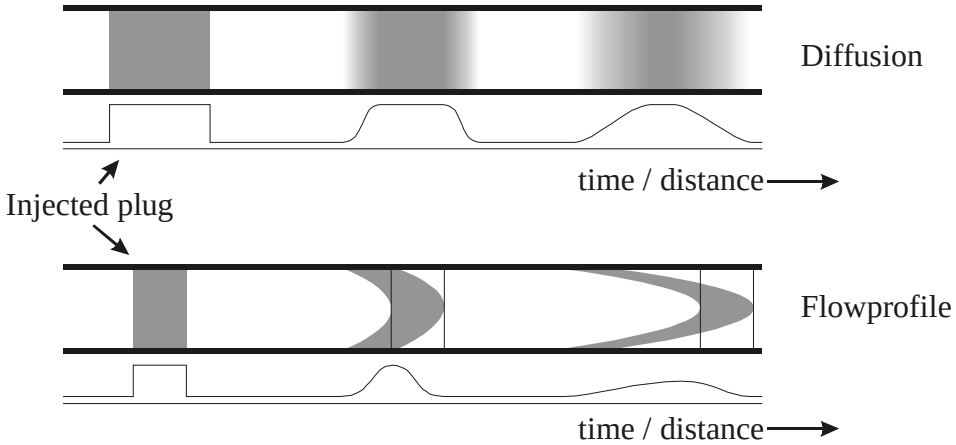

Figure 8: Dispersion due to axial diffusion and the flow profile

Due to these effects, the detection mechanism does not ‘see’ the original square sample plug. Depending on the severity of the effects, the output signal can be less than the maximum as it would be for a square plug. The ratio of the theoretical maximum detector signal and the actual maximum detector signal is defined as the dispersion (Figure 9).

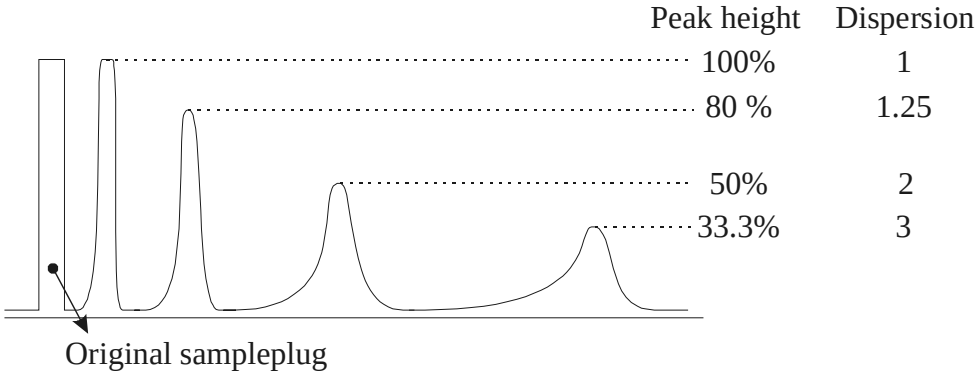

Figure 9: Plug dispersion of the injected sample versus time/distance.

A number of sources of dispersion are discussed below. First ‘dead volume’ is described. Second, the axial diffusion is modeled. Finally the radial diffusion is discussed.

2.4.1Dead volume

Whenever a change in geometry (i.e. a bend or a cross-section change) of a flow channel occurs abruptly, plug smearing will occur. At abrupt channel cross-section changes only part of the channel is used by the flowing fluid. In the remaining part of the channel the fluid flows very slowly or is even occupied by secondary flow. See Figure 10 for two examples.

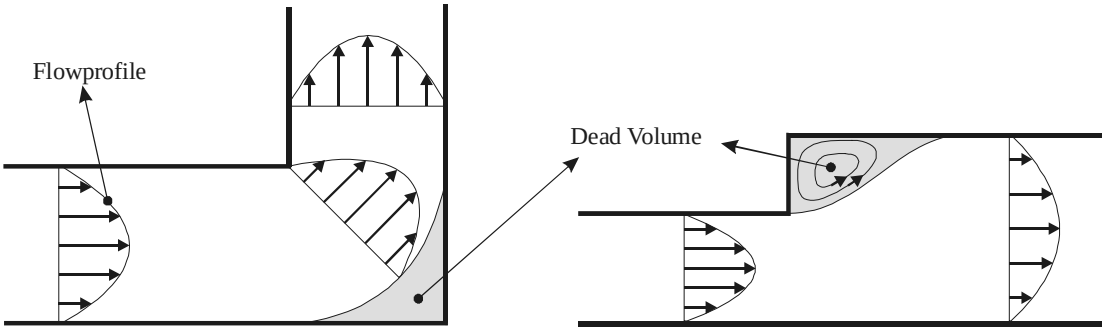

Figure 10: Dead volume at places of sudden change of cross section of channels.

The sample plug will partly diffuse into these dead volumes and is released only when the concentration in the carrier stream is lower than in this dead volume, i.e. when the sample has passed. Therefore the sample plug is dispersed by these dead volumes.

Since exact figures on dispersion due to these dead volumes can only be gathered using simulation tools (which is really beyond the scope of this thesis), only the simple rule of thumb ‘avoid any dead volume’ will be apllied.

2.4.2 Axial Diffusion

Axial diffusion is shown in Figure 8. Due to the random walk of molecules (Brownian motion), the sample plug will diffuse along the axis of the microchannel. Since diffusion times are proportional to the square of the distance (eq. 1) and the axial dimensions of the injected sample typically are a few orders of magnitude larger than the radial dimensions, the axial dispersion usually plays a minor role, and will therefore be neglected in this work.

2.4.3 Radial Diffusion

The diffusion process in combination with the parabolic flow profile in the channels of the FIA system gives rise to the effect of radial diffusion. The velocity in the center of the channel is much higher than the velocity at the edges. At the front end of the plug, the sample will diffuse from the middle of the channel to the walls. At the back end of the plug, the sample will diffuse from the walls to the center of the channel. See Figure 11.

Plug diffuses to middle Plug diffuses to sides

Figure 11: Peak broadening due to radial diffusion.

The diffusion at the front end of the plug causes the plug to disperse. The sample is more or less ‘dropped’ in a region of lower fluid velocity. As the end of the plug passes by, the fresh carrier fluid picks up this ‘dropped’ sample again.

The effect of radial diffusion only exists because of the (parabolic) flow profile in a channel. Its effect on the dispersion however is opposite to the effect of the flow profile: radial diffusion minimizes the dispersion due to the flow profile.

If the time it takes for the sample to diffuse from the middle of the channel to the sides is about the same as the time it takes for the back-end of the plug to overtake the front-end (“plug-passing time”), then the sample profile will become Gaussian very quickly. This Gaussian profile will not change too much in time [16, 17]. From this consideration, it is concluded that the length of the sample plug in combination with the linear flow velocity in the system should match the width of the channel in combination with the diffusion-constant (Figure 12). In order to avoid further dispersion of the Gaussian profile, the radial diffusion time should be smaller than the “plug-passing-time”:

$$t_{diffusion} = \frac{x^2}{D} < t_{plug-overtake} = \frac{l}{v} \qquad \text{Eq. 1}$$

with

$t_{diffusion}$	time it takes for a particle to diffuse from the middle of the channel to the side [sec]
x	diffusion distance, here the half channel width [m]
D	diffusion constant [m^2 sec^{-1}]
$t_{plug-overtake}$	time it takes for the back end of the plug to reach the front [sec]
l	the plug length [m]
v	the linear flow velocity [m sec^{-1}]

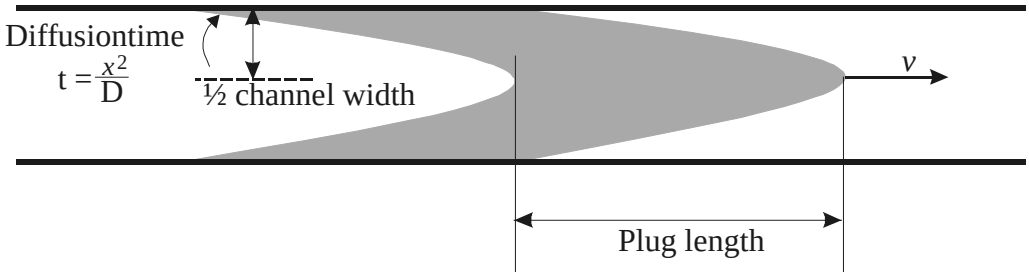

Figure 12: Graph representing design considerations of channel width and plug length.

Once the width of the channels in the system is known, the minimum needed length of the sample plug can be determined using equation 1.

2.5 Discussion and Conclusions

In this chapter, the Berthelot reaction mechanism for the detection of ammonium was discussed. The Berthelot reaction is a three-step reaction mechanism which converts ammonium into indophenol blue, a blue dye with a peak in its absorption spectrum around 600 nm. The first step converts ammonium into mono-chloramine. At a pH lower than 10, not only mono-chloramine is produced, but also di-chloramine, which won't be converted into the desired indophenol. A pH of 11 is chosen as the working pH for the system.
Phenol is added for the second and third step. Connecting two phenol molecules to the mono-chloramine creates indophenol. These last two steps are fairly slow. For speeding up the reaction, a catalyst –nitro-prusside– is added. The reaction temperature is raised also, but for temperatures higher than 37°C bubbles are formed.

Implementing this reaction in a FIA system requires a number of components. Four pumps are needed to propel a carrier fluid, the sample and two reactants through the system. Mixers are needed to make sure the reactants are mixed through the sample. A reaction chamber will be implemented to make sure the reaction temperature will be at 37°C for about 30 seconds. Finally the actual absorption measurement is done in a small cuvette.

The effect of dispersion is explained. Two mechanisms are responsible for the fact that the peak of the sample gets lower as the sample travels through the system. The first mechanism is the parabolic flow profile in the system's channels. This causes the sample plug to smear out over the length of the tube. The second effect involved in dispersion is diffusion. Diffusion of the sample in the axial direction of the channel will slowly spread the sample over the channel. This effect can in most cases be ignored. The diffusion in radial direction however partly corrects the dispersion due the flow profile. At the front-end of the plug, sample is transported to the sidewalls of the channel. At the back end of the plug sample is transported back to the center. The net effect is, that the sample is more or less kept together.

The last item discussed in this chapter concerns the sample size. It is concluded, that the length of the injected sample plug should be such, that the time it takes for the back-end of the plug to overtake the front end is longer then the time that is needed for the sample to diffuse from the middle of the channel to the sides.

2.6 Literature

[1] M.Dawgul, D.G.Pijanowska, Z.Brzozka, W.Torbicz, Urea Biosensor Based on a durable NH4+ - sensitive CHEMFET, Proceedings Eurosensors XIII, The Hague, pp305-307, 1999

[2] W.Göpel, J.Hesse, Sensors, a comprehensive survey, Vol3: Chemical and Biochemical Sensors, Weinheim VCH, 1991

[3] Water – Fotometrische bepaling van het gehalte aan ammonium, Nederlandse Norm, NEN6472, 2e druk september 1983

[4] M.P.E.Berthelot, Violet d'aniline, Repertoire Chimique Application 1, pp284, 1859

[5] T.T.Ngo, A.P.H.Phan, C.F.Yam, H.M.Lenhoff, Interference in determination of ammonia with the hypochlorite-alkaline phenol method of Berthelot, Analytical Chemistry 54, 46-49, 1982

[6] G.Schulze, C.Y.Liu, M.Brodowski, O.Elsholz, W.Frenzel, J.Moller, Different approaches to the determination of ammonium ions at low levels by FIA, Analytica Chimica Acta 214, pp121-136, 1988

[7] CJ Patton, SR Crouch, Spectrophotometric and kinetics investigation of the Berthelot reaction for the determination of ammonia, Analytical Chemistry 49(3), pp 464-469, 1977

[8] P.L.Searle, The Berthelot or indophenol reaction and its use in the analytical chemistry of nitrogen - A review, Analyst 109, pp549-568, 1984

[9] F.J.Krug, B.F.Reis, M.F.Gine, E.A.G.Zagatto, Zone trapping in flow injection analysis-spectrophotometric determination of low levels of ammonium ion in natural waters, Analytica Chimica Acta 151, pp39-48, 1983

[10] R.G.Harfmann, S.R.Crouch, Kinetic study of Berthelot reaction steps in the absence and presence of coupling reagents, Talanta 36, pp 261-269, 1989

[11] J.Růžička, E.H.Hansen, Flow injection analysis, J.Wiley & Sons, 2nd edition, 1988

[12] J.Růžička, Flow Injection Analysis, from test tube to Integrated Microconduits, Analytical Chemistry 55, pp1040A-1053A, 1983

[13] G.D.Christian, Evolution and revolution in quantitative analysis, Analytical Chemistry september 1995, pp532-538, 1995

[14] B. Karlberg, G.E.Pacey, Flow Injection Analysis, A practical Guide, Chap 8: developing a FIA method, Elsevier, 1990

[15] Lachat product specification sheet for the Lachat QuikChem FIA+, www.zelana.com, 1999

[16] E.van Akker, Convection and diffusion in a micro flow injection

analysis system, PhD thesis, University of Twente, The Netherlands, 1999

[17] J.T.Vanderslice, A.G.Rosenfeld, G.R.Beecher, Laminar-flow bolus shapes in flow injection analysis, Analytica Chimica Acta 179, pp119-129, 1986

[18] C.C.Painton, H.A.Mottola, Dispersion in continuous-flow sample processing, Analytica Chimica Acta 154, pp1-16, 1983

Chapter 3: Micro Fluidic Mixer*

In this chapter a microfabricated passive mixer, indispensable for the realization of a miniaturized FIA-based system, is described. The requirements for sufficiently fast mixing are determined using calculations and numeric modeling resulting in design parameters for the micromixer. A number of mixers are realized, and a characterization setup using four coupled syringe pumps is used for characterization. It appears that complete mixing can be obtained within 1 second. Finally, it is shown that the mixer can be used to mix two chemical components in arbitrary ratios.

3.1 Introduction

Given the typical dimensions of microfluidic systems (~100 μm) and commonly used flow rates (~10 μl min^{-1}) it can be easily understood that the flow conditions are well within the laminar flow regime, since the Reynolds number *Re* for these dimensions is around unity [1]:

$$\mathrm{Re} = \frac{\rho v d}{\eta} = \frac{v d}{\nu} \approx 1 \qquad \text{Eq. 1}$$

in which ρ the specific density of the fluid, v the linear flow velocity, d the channels diameter, η the viscosity and ν the kinematic viscosity.

Under these laminar conditions any mixing of different fluids is only governed by diffusion [2, 3], the random walk of molecules (i.e. Brownian motion). The average distance ($\bar{x}$) traveled by a particle with diffusion constant D in a given time t is given by:

$$\bar{x} = \sqrt{Dt} \qquad \text{Eq. 2}$$

From this formula it is clear that if diffusion over 50 μm takes 2 seconds, then diffusion over a distance of a millimeter will be extremely slow: more than 10 minutes (see paragraph 3.4). This brings us to an important concept: in order to minimize mixing time, the distance that has to be overcome by the diffusion process has to be minimized.

* This chapter has been published in: Journal of Micromechanical Microengineering **9**, 1999, pp199-202.

In this chapter an overview of earlier miniature mixer designs will be given. Next, the needed theory of diffusion is presented followed by the design of the mixer, as it will be implemented in MAFIAS. At last the characterization setup with measurements conforming the expected mixing behavior will be presented.

3.2 History – brief overview

A number of devices have been developed to overcome the mixing problems under laminar conditions. Most of the mixers presented in literature [4-10] aim at generating multiple layers of alternating fluid I and fluid II by lamination. The thickness of the so-constructed layers defines the diffusion distance. Some of these multilayer mixers are modular in that each mixer element doubles the number of layers [11,12]. Cascading a series of these mixer elements results in very thin layers and hence very fast mixing.

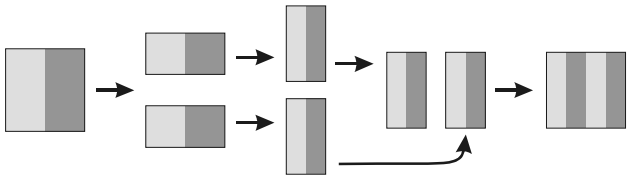

Figure 1: principle of lamination.

Next to these so-called laminating mixers also an injection mixer has been presented [13]. This mixer injects an array of micro-plumes into a carrier stream. The distance between the different plumes now defines the maximum diffusion distance and hence the mixing time.

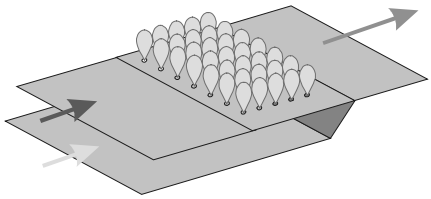

Figure 2: Mixing principle of the micro-plumes injection mixer.

Apart from all these passive micro mixers (mixing is based upon diffusion instead of actively stirring the fluids), very few active mixers are known. Only Woias *et al* [14] presented a mixer consisting of a piezo-driven membrane underneath which fluid motion is forced to be turbulent by inducing very high local flow rates, which causes mixing action. Nevertheless, the concept of controlled, active mixing may become important in the near future.

Most of these micro mixer designs involve a production scheme using process steps on multiple wafers. This makes these mixers less interesting for integration in a complete fluidic system since it will be harder to match the process steps for the mixer with the

process steps necessary for the remaining components. It is for this reason that a new simpler micro mixer has been designed.

3.3 Optimum design

In order to create a micromachined passive mixer that mixes any arbitrary concentration distribution perfectly in a very short time, the following channel structure is presented (Figure 3). The mixer is a rectangular channel with varying cross-section. The incoming channel has a square cross-section. First this is changed into a cross-section that is deep and narrow. In this part, the concentration distribution in the lateral direction is equalized. Next, the cross-section is changed to a wide and shallow channel. Here the concentration distribution in the vertical direction is equalized. The minimum dimensions of the channel determine how fast the diffusion process will have equalized the concentration distribution completely.

It should be noted, that the change in the cross-section should be smooth, to ensure that no excessive dispersion due to dead volume will occur (this thesis, chapter 2.4).

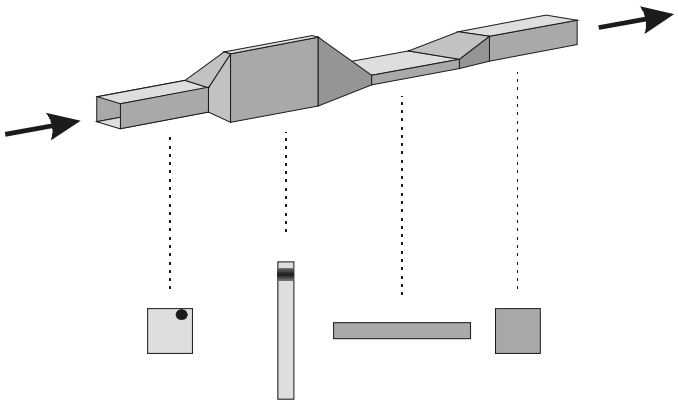

Figure 3 : layout of the proposed micro mixer.

Another factor that determines the performance of the mixer is the length of the narrow parts. Since the fluid has to be in this narrow part for a certain amount of time to let the diffusion process do its work, the length of these narrow parts determines the maximum allowable flow rate. The narrower the mixing parts, the higher the flow rate can be without deteriorating the functioning of the mixer.

The last parameter that is of interest is the pressure drop over the mixer, which is dependent on the flow rate as well as the desired mixing time. For higher flow rates, the pressure drop over a fixed channel structure will be linearly higher. However, for higher flow rates the mixer also needs to be longer in order to keep up mixing performance. The channel being longer will also contribute to a higher flow resistance. A higher flow rate therefore will result in a squared higher pressure drop.

$$\Delta P = \frac{8\mu l}{\pi r^4} \cdot \varphi \qquad \text{Eq. 3}$$

Eq.3 gives the pressure drop ΔP over a channel with radius r, length l, fluid viscosity μ at flowrate φ. Though eq.3 only yields for round channels, the influence of the channellength and flowrate are the same for any crossection.

From this reasoning it can be seen, that the optimum mixer design will be a trade-off between the desired mixing time and the desired flow rate, with the maximum allowable pressure drop as a constraint to the design.

With the use of the available clean room technology it is very hard to fabricate the mixer as shown in Figure 3. Therefore the optimum mixer design has been adapted. The resulting design is described in the next section.

3.4 MAFIAS mixer design

For the design of the mixer, the starting point is the perfect mixer as described in the previous section. The most important assumption that is made is that the concentration distribution is strictly one-dimensional. This assumption is valid as will be shown. With that assumption the mixer as described in the previous section does only need one cross-sectional transition instead of two. If a horizontal concentration distribution comes in, only the deep and narrow channel part is needed.

Figure 4: The incoming concentration distribution in the MAFIAS mixer.

The next adaptation is of a practical nature. Since it is very hard to create channels with a controlled gliding depth profile, the mixer channel will have the same depth from the beginning to the end. Creating a channel structure with two or three discrete depths will cause problems with dispersion through dead volume (this thesis, chapter 2.4). This leaves only the channel width to be varied. The resulting mixer design is shown in Figure 5. Since the fluids are injected into the mixer in the plane of the wafer (and not from above or below), the concentration distribution will be strictly horizontal.

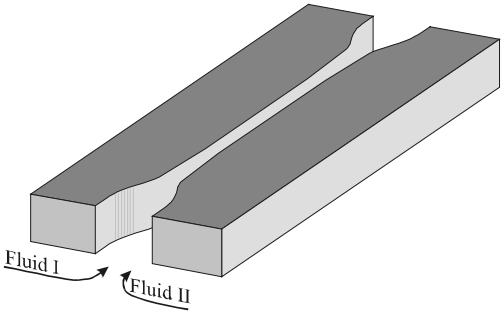

Figure 5: the mixer design that is employed.

Coming to a set of design rules, first the time needed for equalizing the concentration distribution will be determined. We shall estimate this by an estimation of the *time t* it takes for a particle with *diffusion constant D* to travel an *average distance* <*x*> [15]:

$$t = \frac{\langle x \rangle^2}{D} \qquad \text{Eq. 4}$$

The average distance such a particle has to travel is at most half the channel width (see Figure 6):

$$\langle x \rangle = \frac{w + w/2 + w/2 + 0}{4} = \frac{w}{2} \qquad \text{Eq. 5}$$

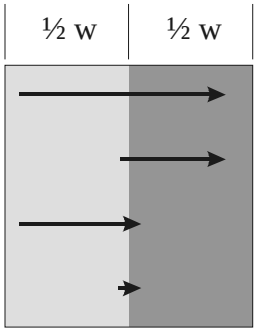

Figure 6 : graph for finding the average distance a particle has to travel.

The time that the fluid is present in the narrow part of the mixer-channel is simply found by dividing the *volume of the narrow part of the mixer channel V (= l×w×d)* by the *governing flow rate in the final system,* φ_{system} :

$$t = \frac{l \times w \times d}{\varphi_{system}} \qquad \text{Eq. 6}$$

With the equations above, the geometry of the mixer can be determined. For a geometry with a maximum aspect ratio of three (d/w~3), the fluid resistance of the mixer can be determined by calculating the hydraulic diameter of the channel (for higher aspect ratios, the channel has to be treated as a slit):

$$D_h = \frac{4A}{P} \qquad \text{Eq. 7}$$

in which *A* is the cross-sectional area of the channel, and *P* the wetted perimeter of the channel.

From this hydraulic diameter the fluid resistance is calculated:

$$\Delta P = \varphi_{system} \frac{128 \eta l}{\pi D_h^4} \qquad \text{Eq. 8}$$

in which η is the kinematic viscosity of the fluid in the mixer.

The parameters and constraints determining the mixer design are presented in Table 1.

Parameter	Value	Units
Viscosity of water (37°)	0.7×10^{3}	N sec m^{-2}
Diffusion constant of phenol (in water)	0.89×10^{-9}	m^2sec^{-1}
Flow rate in the system	10	µl min^{-1}
Depth of channels	200	µm
Desired mixing time	3	Sec

Table 1: relevant parameters and constraints for the MAFIAS mixer design.

The parameters in Table 1 lead to the following relationship for the diffusion time as function of the channel width.

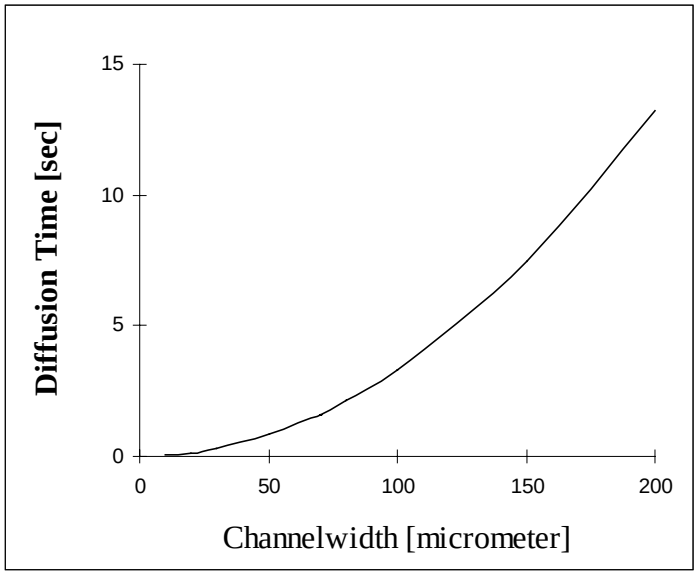

Figure 7: The calculated diffusion time of Phenol as function of the channel width.

From Figure 7 it is read what the channel width should be. With the help of Eq. 7 the length *l* of the mixer channel is found. Now the pressure drop over the mixer (Figure 8) is easily obtained.

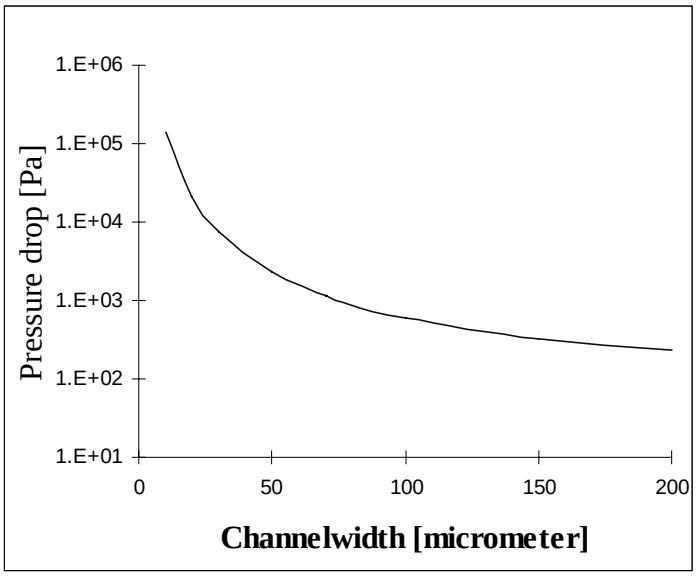

Figure 8 : The calculated pressuredrop over the mixer channel as function of the channel width.

From the shown graphs it is seen, that a channel width of 100 µm results in a mixing time of 3.3 seconds. The corresponding length of the mixing channel is 27.5 mm. The pressure drop over the mixer will be 6 mBars for this channel width. These figures are acceptable for the MAFIAS system.

3.5 Simulations

To confirm the model of the mixer, simulations have been performed. Using the simulation software FLOW-3D (module CFX-4.2) a straight channel of 200 µm deep, 300 µm wide and 13000 µm long is defined. Simulations have been performed for particles with the same diffusion constant as Phenol. The flow rate in the simulations is 1.25 µl/min. According to the analytical model it will take 25 seconds for a particle to diffuse over a distance of 150 µm. At the flow rate of 1.25 µl/min, mixing should be complete at 8.6 mm after the injection point.

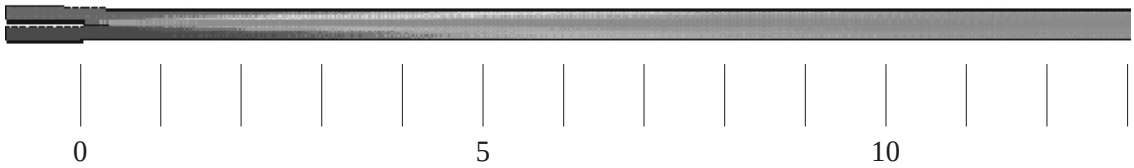

Figure 9: Simulation results for the mixer. Indicated units are mm's along the channel.

From the mixer simulations it is seen that mixing indeed is complete after 10 mm behind the injection point. This is in reasonable agreement with the analytical model.

3.6 Characterization

Now the mixer has been designed, verification of the mixing principle is still needed. For testing purposes, a number of mixers have been created and tested. The mixers were designed for the mixing of aquatic Phenol with water at a flow rate of 2 µl/min. In order to be able to measure the extent of mixing, the outlet of the mixer is divided into two outlets, each located to correspond to one of the inlets (see photograph in Figure 10). If the flow rate is very high, almost no mixing will occur. As the flow rate gets smaller, the mixing becomes more complete. For flow rates lower than 2 µl/min, mixing should be perfect and both outlets should contain the same concentration of phenol.

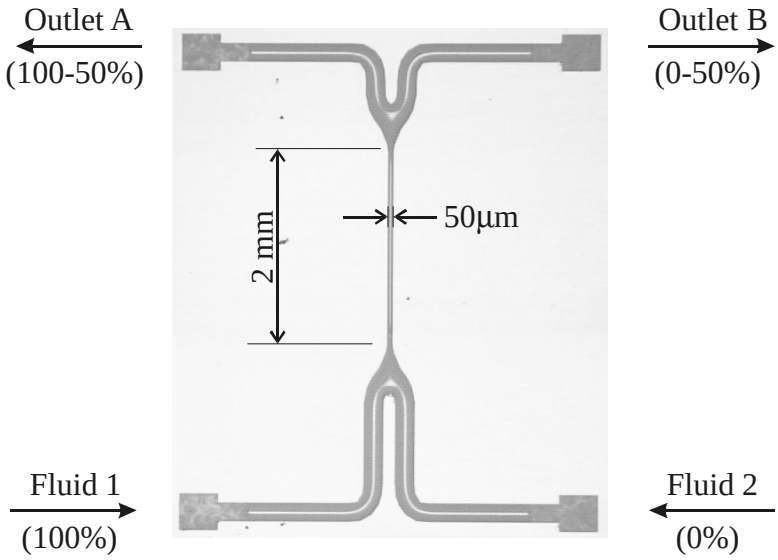

Figure 10: Photograph of one of the fabricated mixers.

3.6.1 Characterization setup

The setup that is used to characterize the mixer is schematically shown in Figure 11.

Four syringes are mounted on one translation table. They are coupled in such a way, that while two are discharging, the other two will simultaneously draw in the same amount of fluid. These syringes are connected to respectively the in- and the outlets of the mixer. This construction is chosen in order to ensure that the samples that are taken from the different outlets indeed correspond to their inlets. Possible problems with open outlets include pressure differences due to surface tension, fluid resistance differences and outlet level differences. All of those problems would cause cross talk between the outlet samples. Three way valves are incorporated in the system to be able to refill the system.

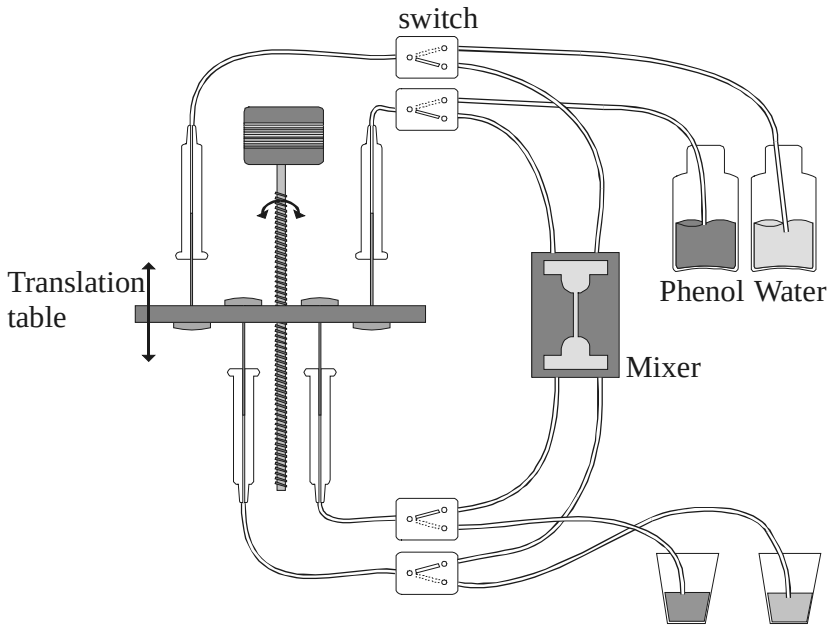

Figure 11: schematic of the mixer characterization setup.

The concentration of the phenol in the samples is determined by a conductivity measurement.

3.6.2 Measurements

Measurements were performed using de-ionized-water in one syringe and a phenol solution (in water) in the other syringe. Since the conductivity of the solution in one of the connecting channels is proportional to the average phenol concentration, the conductivity ratio of the outlet channels represents the amount of mixing. Results from the measurements are shown in Figure 12, in which the conductivity ratio of the samples from the outlets is plotted against the flow rate through the mixer.

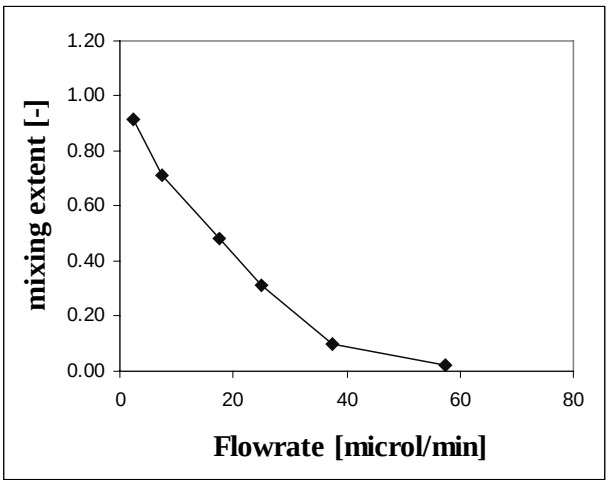

Figure 12: Extent of mixing as function of flow rate. The used mixer was 2 mm long. The depth of the channel was 200 μm, the width 50 μm.

It is clearly seen that for high flow rates the mixer does not function at all. However, the lower the flow rate, the more complete the mixing is. Though no measurements could be performed below 2 µl/min, it can be read from the graph, that the mixing in this region is better than 0.9.

3.7 Using the mixer as a "concentration synthesizer"

The developed flow-driven mixer (as depicted in Figure 10) can also be used as a flow-driven "synthesizer" in the case of incomplete mixing, which occurs when the flow rate through the mixer is higher than the flow rate needed for complete mixing. In that case within certain limits any combination of the two compounds at the inlet can be obtained at the outlet, depending on the chosen flow rates, as is illustrated (Figure 12).

Feeding the mixer with a neutral fluid (e.g. de-ionized water) on one side and a fluid with a high concentration active component, the concentration at one of the outlets can be controlled between 0 and 50% of the concentration at the inlet by varying the flow rate through the mixer (using the other outlet, the concentration range is from 100% to 50%). A high flow rate will result in a low diffusion efficiency, and hence a low concentration at the outlet. A low flow rate however will give enough time to let the active component diffuse to the 'clean' side resulting in a high relative high concentration at this outlet.

Tests were performed using the same setup as shown in Figure 11. The flow rate through the system was changed a number of times from 3 µl/min to 6 µl/min (corresponding to a measured conductivity ratio (Figure 12) of approximately 0.7 and 0.82). The conductivities at both outlets were measured. Finally the ratio of the found conductivities was calculated. The results from this experiment are shown in Figure 13.

As is seen from this figure, the conductivity ratios stay within a small range. For the measurements at 0.3 µl/min the ratio ranges from 0.83-0.85, whereas the ratio for the flow rate of 0.6 µl/min ranges from 0.72-0.73.

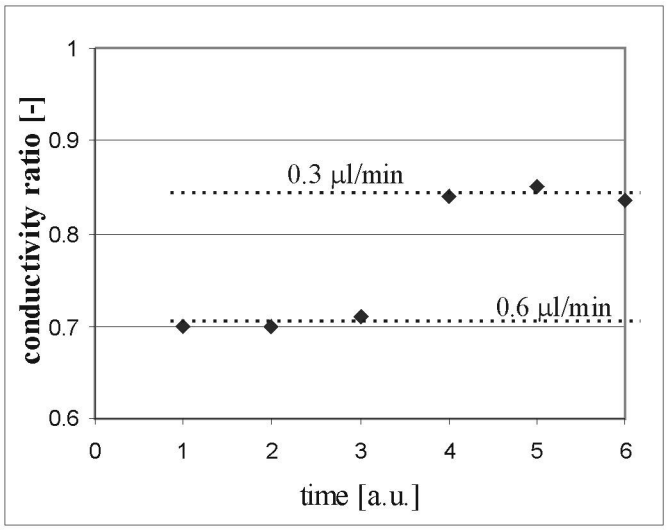

Figure 13: Consistency measurements on the mixer/synthesizer

From these measurements it can be concluded, that the mixer structure can be used as a concentration synthesizer: a device with which the concentration of a chemical compound in a fluid can be tuned. Theoretically a measurement of the concentration at the unused outlet could be used to calculate the concentration at the real outlet. With a feedback loop to the flow generating system, the concentration at the outlet could be controlled perfectly.

3.8 Discussion and conclusions

This chapter has shown the design of a microfluidic mixer. Since the flow regime in microfluidics is such that all flow is laminar, mixing has to be based on diffusion. Only for small diffusion distances (~50 µm) the diffusion process is fairly fast (~1 sec). For longer distances, diffusion time goes up with the square of the diffusion distance. The only way therefore to reduce mixing time is to reduce the diffusion distance.

The mixer that is presented in this chapter also applies this rule: the dimensions of the channel in which the fluids to mix come together are reduced such that mixing will occur within the desired mixing time. To ensure complete mixing, the length of the narrow part has to be chosen such that the fluids will stay in the narrow part as long as needed. The pressure drop over this narrow channel part will increase with respect to the normal channel due to two facts. First, the narrow part of the channel has a higher fluid resistance because of its smaller dimensions. Second, the fluid will flow faster through the narrow part, resulting in larger shear forces within the fluid.

For this mixer, a model is presented from which for a compound with known diffusion constant the geometry of the mixer can be calculated. From simulation as well as experiment, it is seen, that the mixer behaves as the model predicts. Dimensions of the mixer to be employed are 200 µm deep, 100 µm wide and 27.5 mm long. This ensures mixing in about 3.3. seconds at a flowrate of 10 µl/min.

Using this mixer, it should be noted that the mixer is designed for a specific range of diffusion constants, and thus a limited number of compounds with diffusion constants within this range. Compounds with larger diffusion constants are mixed completely, but compounds with smaller diffusion constant are only partly mixed at the outlet of the mixer.

At last it is shown, that the mixer structure can be used as a concentration synthesizer. Varying the flow rate through the mixer, the extent of mixing can be influenced in such a way that the concentration at one of the outlets can be controlled within a small range. Implementing a feedback loop from the unused outlet to the flow generating system, the synthesizer is capable of delivering any concentration from 0-50% (or using the other outlet 50-100%) of the concentration of the incoming fluids.

3.9 Literature

[1] R.W.Fox, A.T.McDonald, Introduction to fluid mechanics, chapter 7, 3rd edition, Wiley & Sons, 1985

[2] J.B.Knight, A.Vishwanath, J.P.Brody, R.H.Austin, Hydrodynamic focusing on a silicon chip: Mixing nanoliters in microseconds, Physical Review Letters 80, pp3863-3866, 1998

[3] B.H.Weigl, P.Yager, Microfluidic diffusion-based separation and detection, Science15-01-1999, pp 346, 1999

[4] U.D.Larsen, J.Branebjerg, G.Blankenstein, Fast mixing by parallel multilayer lamination, Proceedings MicroTAS '96, pp228, 1996

[5] J.P.Krog, J.Branebjerg, C.R.Nielsen, P.Gravesen, Experiments and simulations on micromixer fabricated using a planar silicon/glass technology, Proceedings MEMS ASME 1996, pp177, 1996

[6] M.Koch, D.Chatelain, A.G.R.Evans, A.Brunnschweiler, Two simple micromixers based on silicon, JMM 8, pp123-126, 1998

[7] M.Koch, H.Witt, A.G.R.Evans, A.Brunnschweiler, Improved characterisation technique for micromixers, JMM 9, pp156-158, 1999

[8] Erbacher C, Bessoth FG, Busch M, Verpoorte E, Manz A, Towards integrated continuous-flow chemical reactors, Mikrochimica Acta 131 (1-2), pp19-24, 1999

[9] J.Branebjerg, B.Fabius and P.Gravesen, Application of miniature analyzers: from microfluidic components to μTAS, Proceedings MicroTAS '94, pp141, 1994

[10] J.Branebjerg, P.Gravesen, J.P.Krog, C.R.Nielsen, Fast mixing by lamination, Proceedings MEMS-96, SanDiego,1996

[11] H.Mensinger, T.Richter, V.Hessel, J.Dopper,W.Ehrfeld, Microreactor with integrated static mixer and analysis system, Proceedings MicroTAS '94, pp237, 1994

[12] N.Schwesinger, T.Frank, H.Wurmus, A modular microfluid system with an integrated micromixer, JMM 6, pp99-102, 1996

[13] R. Miyake, K.Tsuzuki, T.Takagi, K.Imai, A highly sensitive and small flow-type chemical analysis system with integrated absorptiometric micro-flowcell, Proceedings MEMS 97

[14] P.Woias, K.Hauser, E.Yacoub-George, B.Hillerich, A Silicon-based Microreaction System for Analytical Applications, Proceedings IMRET3, FrankFurt, Germany, April18-21, 1999

[15] P.Atkins, Physical Chemistry 4^{th} ed., Chapter 25, Oxford University Press, 1990

Chapter 4 : The Reaction Chamber

In chapter 4 the development of another essential component of the MAFIAS, the miniaturized reaction chamber, is described. First the major requirement of the microreactor is deduced, i.e. to maintain a constant reaction temperature of 37 ± 0.5 °C for 30 seconds for the mixed reagents. The heat transfer form the heated microreactor chip to the fluid is calculated and found to be far less (< 1 second) than the residence time of the fluid in the reactor. The microreactor is realized using KOH etching in silicon and anodic bonding of Pyrex, covered with a thin film platinum heater protected with PECVD silicon oxide, to the etched silicon. It is found that with the requirements for the flow rate of 10 μl/min and a desired residence time of 30 seconds, a 12.5 cm long, 200x200 μm^2 channel is needed.

4.1 Introduction

This chapter describes the design and considerations of the reaction chamber for the MAFIAS. In this reaction chamber, the conversion of ammonia into indophenol is realized. Since a measurement time of less than 1 minute is required, the reaction is not fully completed at the point of measurement in the system. Therefore, the only way to ensure a stable and repeatable measurement is to treat each consecutive sample in exactly the same way. For the reaction chamber this means that the residence time has to be exactly equal for each sample. As for the temperature: since the second reaction step is highly temperature dependent, the temperature has to be controlled to stay within a very narrow temperature range (<0.5°C).

From literature only little is found on microfluidic heating chambers for liquids. Burns [1] and Norhtrup [2] present a temperature controlled fluidic system for the pretreatment of DNA samples, whereas Miyake [3] shows us the design of a small reaction chamber which is integrated into a small detecting system.
In this chapter the design of a reaction chamber will be shown. From measurements on and experiences with the fabricated design, conclusions are drawn which lead to a final design.

---

* The contents of this chapter will be presented at the IMRET 5 conference, 27-30 may 2001, Strasbourg.
N.R. Tas, R.E. Oosterbroek, T.T. Veenstra, M. Elwenspoek and A. van den Berg, Microfluidics and Microtechnology for Microreactor Systems

4.2 Basic design

The basic design of the reaction chamber is shown in Figure 1. The reaction chamber will consist of a silicon base plate with an etched channel in it. The channel is closed with a Pyrex top plate. Thin film Platinum resistors are deposited on the bottom side of the Pyrex wafer. These resistors are used to (electrically) generate the power for heating of the fluid in the channel as well as for the measurement of the temperature of the fluid.

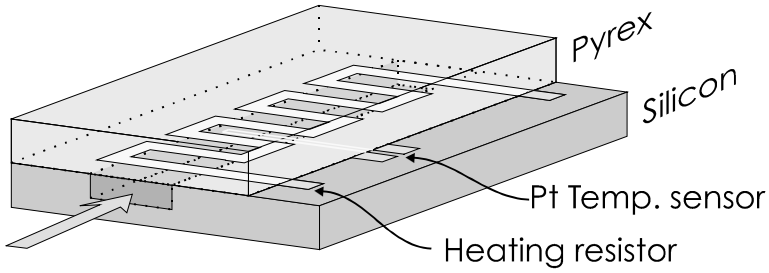

Figure 1: Principle of the design of the reaction chamber

The silicon chip has to be covered with an insulating layer to prevent shortcircuiting of the resistors through the silicon.

The fluid has to be at 37°C for 30 seconds. This can be realized in two ways. The flow can either be stopped for 30 seconds such that the sample plug stays in the temperature controlled region for 30 seconds, or the reaction chamber channel can be chosen as long as that the fluid needs 30 seconds to flow through the channel.

4.3 Theory

To come to a complete design, a number of aspects of the reaction chamber have to be modeled and/or calculated. The fluid that enters the reaction chamber has to be heated to 37°C. The power needed for that has to be brought into the system by the electrical heater. The generated heat has to be transported into the fluid. It will take some time, before the fluid is at the desired temperature. At last, the fluid has to be in the reaction chamber for 30 seconds.

First the power needed for the heating of the fluid from room temperature (T_{low}, 20°C) to T_{high} (37°C) at the governing flow rate in the MAFIAS system is calculated. Once the needed power is known, the dimensions of the electrical heater can be calculated. The last part of this paragraph will deal with the time that it will take for the fluid to reach the desired temperature.

The power P_{fluid} needed to increase the fluid temperature by ΔT degrees Kelvin is calculated with:

$$P_{fluid} = \sigma \cdot \rho \cdot \Delta T \cdot \Phi \qquad \text{Eq. 1}$$

with:

σ the specific heat of the fluid [$J \cdot kg^{-1} \cdot K^{-1}$],
ρ the mass density of the fluid [$kg \cdot m^{-3}$],
ΔT the temperature difference: $T_{high} - T_{low}$ [K],
Φ the volume flow throughout the MAFIAS system [$m^3 \cdot sec^{-1}$].

The power P_{fluid} must be delivered by the heater. The generated power in the heater P_{heater} [W] is:

$$P_{heater} = I^2 \cdot R_{heater} \qquad \text{Eq. 2}$$

Not all the generated heat will be transferred to the cold fluid. A lot of the heat will disappear heating the surroundings of the chip. Therefore the power that can be delivered by the heater resistor has to be larger than just the power needed to heat the fluid. The power that is dissipated into the surroundings depends on several factors. The size of the chip (determining the heat capacity of the chip) as well as the packaging of the chip (determining the heat loss to the surroundings) are very important factors controlling the heat loss.

The temperature of the chip will be controlled using a feedback loop. This means, that a temperature sensor has to be integrated on the chip. The most common method for integrating a temperature sensor is using a Platinum resistor. Temperature variations will be translated in variations of the absolute value of the used resistance via the *temperature coefficient of resistivity*. Considering the readout electronics, a resistance in the order of a few kOhms should be used.

The resistance of a resistor R [Ω] can be calculated with:

$$R_{heater} = \frac{\rho_{el} \cdot l_h}{A_h} \qquad \text{Eq. 3}$$

with:

ρ_{el}: the specific material resistivity [$\Omega \cdot m$], for platinum $\rho_{el} = 106 \cdot 10^{-9}$ $\Omega \cdot m$
l_h: the length of the heater [m],
A_h: the cross-sectional area of the heater [m^2].

The value of the resistance will be read with the four-point measurement method. The resistor will be connected to the readout electronics with two sets of leads. One set is used to force a current through the resistor, the other set is used to read out the voltage drop over the resistor. Once both these quantities are known, *Ohms law* gives the value of the resistance and hence the temperature.

For calculating the time needed for the fluid to be heated to the desired temperature, the heat transfer is considered. In small microfluidic systems at relatively low

temperatures, heat transfer by radiation and convection can be neglected, and thus only heat diffusion is considered. Starting point is a temperature step in a fluidic medium, and the time constant for equilibration of that temperature step can be calculated.

Theory [4] starts with the (one dimensional) differential equation for the temperature distribution in a medium as a function of time and place :

$$\frac{\partial}{\partial t}U(x,t) = D \cdot \frac{\partial^2}{\partial x^2}U(x,t) \qquad \text{Eq. 4}$$

with:
U(x,t): the temperature at time *t* at position *x* from the heating source [K],
D: the thermal diffusion coefficient [$m^2 \cdot sec$]

This thermal diffusion coefficient *D* can be expressed:

$$D = \frac{\kappa}{c \cdot \rho} \qquad \text{Eq. 5}$$

with:
κ: the thermal conductivity [$W \cdot m^{-1} \cdot K^{-1}$],
c: the specific heat per mass-unit [$J \cdot kg^{-1} \cdot K^{-1}$],
ρ: the mass density [$kg \cdot m^{-3}$].

A time constant τ [sec.] can be defined for heat diffusion over a distance *d* in a medium with thermal diffusion coefficient *D* (eq. 3) [5]:

$$\tau = \frac{d^2}{D} = \frac{c \cdot \rho \cdot d^2}{\kappa} \qquad \text{Eq. 6}$$

This time-constant indicates the time needed for the temperature profile to travel over a distance *d*. After $t = \tau$ the initial temperature difference at a distance *d* will be reduced by 93% [6]. In our case we have a channel embedded in a chip, which is held at a constant temperature of 37°C. Therefore, the temperature of the walls of the channel are at 37°C. The maximum distance the temperature has to penetrate the channel is half the smallest of either the height or the width of the channel.

Assuming the channel depth is the smallest of the channel dimension, Table 1 gives the time constant τ for heating water for several channel depths.

Depth of the channel (d_h) [μm]	Time constant τ [msec]
100	17.9
200	71.4
400	285.7

Table 1 : Time constant τ for heating water for several channel depths

As is seen from the table, the model predicts that heating the fluid in the channel is easily accomplished within a time of one second.

4.4 Process Design

Samples were designed and fabricated in order to test the feasibility of the chosen reaction chamber principle.

In Figure 2 a cross-section of the reaction chamber is drawn. The long channel of the reaction chamber is KOH etched in a silicon wafer. The channel is closed by anodic bonding of Pyrex wafer on top of the silicon wafer. The Platinum resistors that are used for the temperature measurement and heating of the chip are sputtered on the bottom side of the Pyrex chip. In order to prevent shortcircuiting of the platinum resistors via the silicon, the silicon wafer has to be covered with a silicon oxide layer (wet oxidation). A silicon oxide layer (PECVD) also protects the resistors on the Pyrex wafer itself. This to ensure that a possibly conducting fluid will not shortcircuit the resistors.

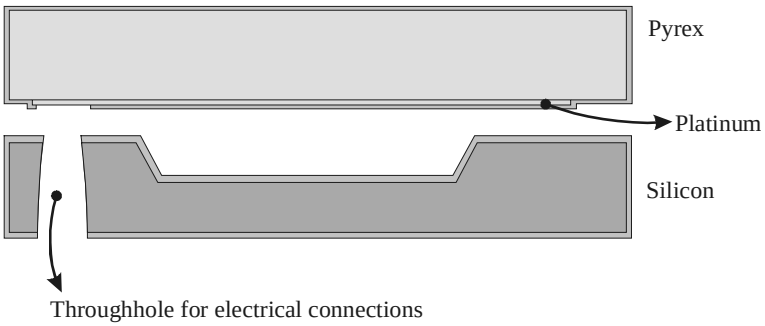

Figure 2: Cross-section of the chip design.

Access to the free-etched platinum contact pads is obtained by a powderblasted throughhole in the silicon wafer.

The length of the channel of the reaction chamber should correspond to a sample residence time of 30 seconds for the chosen flow rate. With channel dimensions $200\times200\mu m^2$ and a flow rate throughout the system of 10 μl/min a length of 12.5 cm can be calculated.

Factors to be taken into account when designing the resistors for either the heater or the temperature sensor come from the control electronics and the anodic bonding process. In order to be compatible with the anodic bonding process the Platinum layer on the Pyrex can be only as thick as 50 nm. Next to this restriction is the fact that it would be convenient for the control electronics if the heater would not need more than 5 Volts of supply voltage.

The heater design results in a 400 μm wide and 4.5 cm long resistor. The resistance will be around 240 Ohms (corresponding to 100mW of electrically generated heat at 5V driving voltage). The temperature sensor design is 20 μm wide and 4 cm length. The resistance will be around 4000 Ohms.

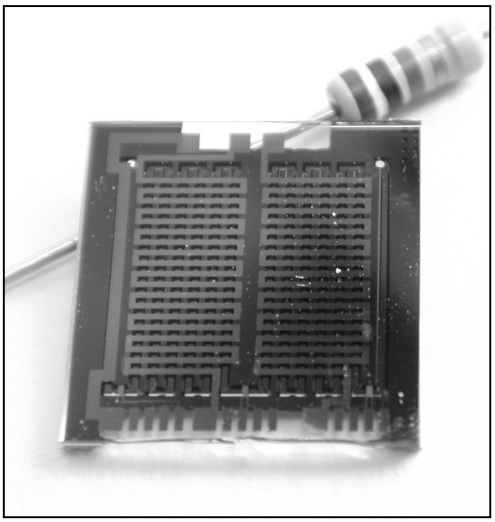

Figure 3: Fabricated reaction chamber.

In Figure 3 one of the fabricated stand-alone reaction chamber is shown. A number of experiments, presented in the next section, were done in this reaction chamber.

4.5 Experimental

First, the temperature sensors on the reaction chamber chip have to be calibrated. After this, a set of experiments heating a fluid will be performed. This test will be done with either flowing fluid and stopped fluid flow.

The calibration of the reaction chamber is done by putting the whole reaction chamber in a small oven. The oven itself has a large heat capacity (relative to the chip). The temperature in the oven is controlled by using a standard temperature sensor and a Peltier element in a feedback loop. This setup guarantees a stable temperature of the reaction chamber chip.

Using this setup, the reaction chamber chip was put through a temperature sweep. The resistor values of the temperature sensor were measured. From this sweep (Figure 4, multiple temperature sensors are shown) it is seen, that the temperature sensors behave very linear. It is also seen, that the calibration of the temperature sensors is necessary

since the resistances of different temperature sensors vary easily 500 Ohms in absolute value.

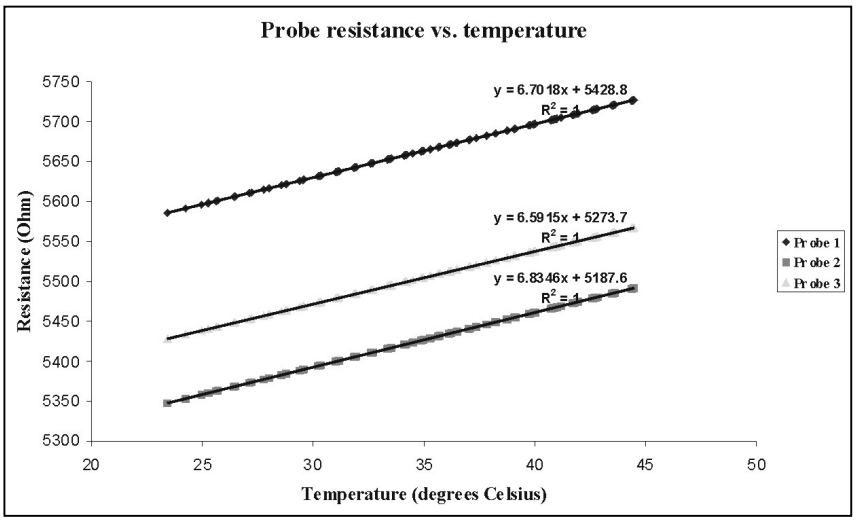

Figure 4: resistance of the temperature sensors as function of temperature.

The next performed experiment was the heating of the reaction chamber with water using the reaction chambers' own heater. From this experiment it was concluded that the SiO_x layer on the Pyrex wafer does not cover the platinum resistors completely. Not only does the water shortcircuit the resistors, but it also attacks the chromium adhesion layer on which the Platinum is deposited. Therefore, further testing is performed using the non-conductive fluid methanol.

The next experiment involves the working of a complete reaction chamber. The results of the tests are shown in Figure 5. The control-loop is set to a certain temperature, after which the resistances of the temperature sensors are read.

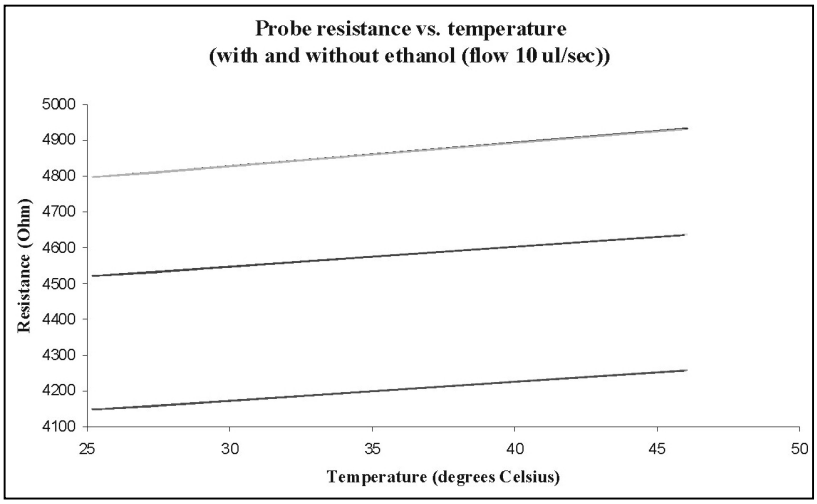

Figure 5: Test results of the reaction chamber filled with ethanol.

The lines seen in Figure 5 are the measurement results of the three temperature sensors located on one chip. Every single line in fact is a double line. First of those two lines shows the temperature-resistance curve with stopped ethanol flow. The second line shows the same curve for flowing ethanol (10 µl/min). Since the lines can't be distinguished it can be concluded that the reaction chamber with feedback loop keeps the temperature of the whole chip perfectly stable.

4.6 Conclusions and Discussion

In this chapter a design for the reaction chamber of the MAFIAS system was shown. The reaction chamber consists of a very long channel with an electric heater and temperature sensors for temperature control.

The length of the channel with the flow rate determines how long the sample fluid remains in the reaction chamber. For the MAFIAS system this has to be 30 seconds. At a flow rate of 10 µl/min, a 200x200 μm^2 channel has to be as long as 12.5 cm to meet the 30 second constraint.

Samples have been fabricated of such a channel. Testing of these samples show, that the temperature of the reaction chamber can easily be kept constant. It was found that a raise of the heating power results in a temperature raise all over the chip within milliseconds. This indicates that the heating of the chip can be done by a single heater.

To prevent shortcircuiting of the electrodes by the fluid, the electrodes were protected by an insulating layer of silicon oxide. It was found, however, that the oxide layer does not completely cover the electrode area. Using water as fluid, the temperature sensors and heaters were still short-circuited. Further testing of the reaction chamber was carried out using ethanol as fluid.

The problem of shortcircuiting the electrodes can be solved by placing the heaters and the temperature sensors next to (outside) the channel (Figure 6) instead of directly over the channel. Measuring the temperature of the chip will be a good measure for the temperature of the fluid.

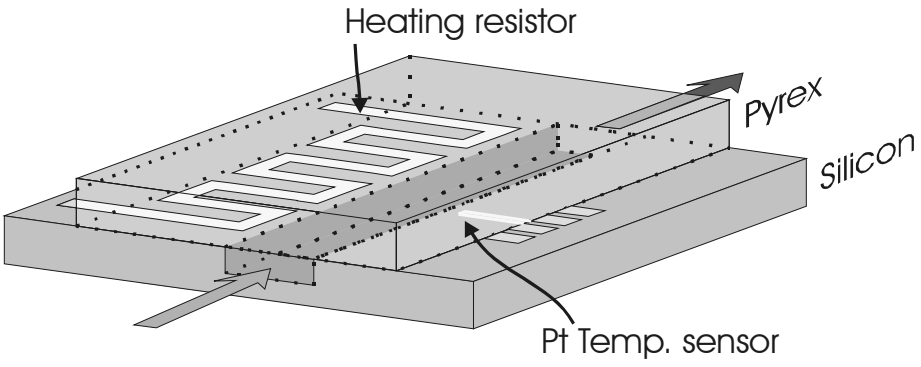

Figure 6 : New layout principle. The electrodes are placed next to the channel instead of over the channel.

4.7 Literature

[1] M.A.Burns, B.N.Johnson, S.N.Brahmasandra, K.Handique, J.R.Webster, M.Krishnan, T.S.Sammarco, P.M.Man, D.Jones, D.Heldsinger, C.H.Mastrangelo, D.T.Burke, An integrated Nanoliter DNA Analysis Device, Science vol282, pp484-487, 1998

[2] Northrup, M. Allen, A Miniature Analytical Instrument for Nucleic Acids Based on Micromachined Silicon Reaction Xhambers., Anal. Chem., Volume 70, Issue 5, 1998, Pages 918-922

[3] R.Miyake, K.Tsuzuki, T.Takagi, K.Imai, A highly sensitive and small flow-type chemical analysis system with integrated absorptiometric micro-flowcell, proceedings MEMS, pp102-107, 1997

[4] H.S. Carslaw and J.C. Jaeger, Conduction of heat in solids, Clarendon Press, Oxford, 1959

[5] C.B.P. Finn, Thermal physics, 2nd edition, Chapmann & Hall, Londen, 1993

[6] J.C.T. Eijkel, A. Prak, S. Cowen, D.H. Craston, A. Manz, Micromachined heated chemical reactor for pre-column derivatisation, Journal of Chromatography A 815, pp. 265, 1998

Chapter 5 : The Pump

For a robust operation of a microanalysis system self-priming and bubble tolerant micropumps are needed. In this chapter first the history of micropumps is briefly reiterated. The most critical properties of micropumps for use in MAFIAS are determined as the absence of back flow, capability of pumping gases and liquids, and simple fabrication. Since peristaltic micropumps with three piezo actuators fulfill all of these requirements a simple fabrication process was developed for their realization. The dependence of the flow rate on the actuation frequency and voltage is determined, and the influence of the backpressure is investigated. It is concluded that the realized pumps are well suitable for use in the MAFIAS.

5.1 Introduction

In the MAFIAS system, pumps are needed to propel all involved fluids through the system. Due to the frictional forces in the moving fluids, a pressure drop will be present over the systems channels. This pressure drop has to be overcome by the pumps. An important design parameter for the pumps therefore is the pressure drop at the desired flowrate that has to be overcome. Next to the desired pressure drop and flowrate, the capability to pump gas or even a gas/liquid mixture is a very desirable feature. A pump which is capable of pumping a gas/liquid mixture is called bubble-tolerant. A bubble tolerant pump puts less stringent demands on the fluids that have to be transported.
The design of such a pump is described in this chapter.

5.2 History

Since the late eighties, a lot of effort has been put in making an effective and easy to use micromachined pump. The opportunities that will be created by a reliable micropump are mainly based on the small sample volumes that can be handled by such a pump. If sample volumes go down, reagent volumes go down, resulting in lower costs as well as increased stand-alone operation times of such microfluidic systems. The first reported working micropump was made by van Lintel in 1987 [2]. During the

90's, a lot of research is reported on the field of micropumps. Modeling and simulation become commonly used tools. Devices that are made include (check-) valves as well as complete pumps. Reported valves can for example be found in [3-7].

Working micropumps can be divided in a number of categories. Most common are micropumps with two check valves, which are found in e.g. [8-11]. Pumps with 'open' valves are reported by [12-16]. These open valves are channel structures that have a larger fluidic resistance in one direction then in the other [e.g. 17]. The main advantage of an 'open' valve pump is the fact that such a pump will be capable of pumping fluids with particles in it. The accompanying disadvantage is that the pump will leak if it is not actuated.

Next to the 'normal' membrane pumps also a number of bi-directional pumps are presented. Zengerle et al. [18] presents a pump with active valves whereas Folta et al. and Mizoguchi et al. [1, 19, 20] propose peristaltic pumps. A peristaltic pump consists of three pump membranes along a pump channel. Actuation of the three membranes in a specific order results in a fluid displacement from the inlet to the outlet. Reversing the membrane actuation sequence results in a reversed pumping action.

In the 90's, two new trends show up. First, the electro-osmotic pump is introduced [21]. The second trend is the development of micropumps using cheaper materials (like plastics) and fabrication techniques [22-24].

Only recently, pumps are described in terms as self-priming ability and bubble-tolerancy [25]. These features describe the ability of a pump to overcome surface tension effects.

5.3 Choice of pump principle

Before the process of designing the pump for the MAFIAS system can start, a choice has to be made on which principle the pump will be based.

Here the specifications that the pump has to meet will be deduced. These specifications will be based on practical issues as well as on an estimate of the performance needed for the final MAFIAS system.

From chapter 2 it was concluded that multiple pumps have to be incorporated in the final system. This introduces the constraint on the pumps that no back flow may occur. Otherwise sample fluid might end up in the channels with reagents (or the other way around) thus disturbing the measurement on hand as well as future measurements.

From a practical point of view, it is very desirable that the pump is self-priming and bubble-tolerant. The self-priming capability of the pump means that the pump can suck in liquid through a channel (or tube) originally filled with gas (air), eventually priming itself with that liquid. The bubble tolerant feature indicates the capability of

pumping a liquid with gas (air) bubbles. The combination of these two features results in a system that is user-friendly: no priming procedure is needed.

An estimate of the flow and pressure the pump must be able to deliver is now given. The estimated needed channel length is 25 cm. A common channel cross section is $200\times200\ \mu m^2$. The system has to be capable of processing one sample in a minute time. Therefore, the channel has to be flushed once a minute. The volume of the systems main channel at the given parameters is $10^{-8}\ m^3$ which means that the flow rate throughout the system has to be $10\ \mu l\ min^{-1}$.

The fluidic resistance of a channel of the dimensions mentioned above is calculated to be 4.4×10^{12} Pa s m^{-3} [26]. At a flow rate of $10\ \mu l\ min^{-1}$ this equals a pressure drop of 740 Pa which has to be overcome by the pump.

Since the pump fabrication process has to be compatible with a number of other fluidic components, the process design has to be kept as simple as possible. Therefore the choice is made to create a peristaltic pump. A (micromachined) peristaltic pump has a number of identical membranes in a row connected by some channel. Since the membranes all are equal, the process steps can be limited to a minimum.

5.4 Theory of pumping operation

From the previous section it was decided that the pump for the MAFIAS system will be a peristaltic pump. This paragraph will present the theory needed for the design of the pump. First the peristaltic principle will be explained, after which it will be shown how the maximum achievable pressure at the outlet of the pump can be calculated. The issue of surface tension with respect to the pumping performance is discussed later.

A micromachined peristaltic pump will consist of three membranes in a row interconnected with channels. The membranes have to be actuated in a certain sequence to result in pumping action. The sequence that is applied on the pump is shown in Figure 1. Starting from a neutral position with all the membranes closed, the first membrane opens causing some fluid to be sipped in (step 1). The opening of the second membrane will draw some more fluid into the pump (step 2). Step 3 closes the first membrane, pushing some fluid back into the pump inlet. So far nothing has happened at the pump outlet. During the next three sequence steps the pump takes in some fluid from the outlet after which it pushes out twice that amount. During these six sequence steps only one stroke volume is dispensed into the pumps outlet.

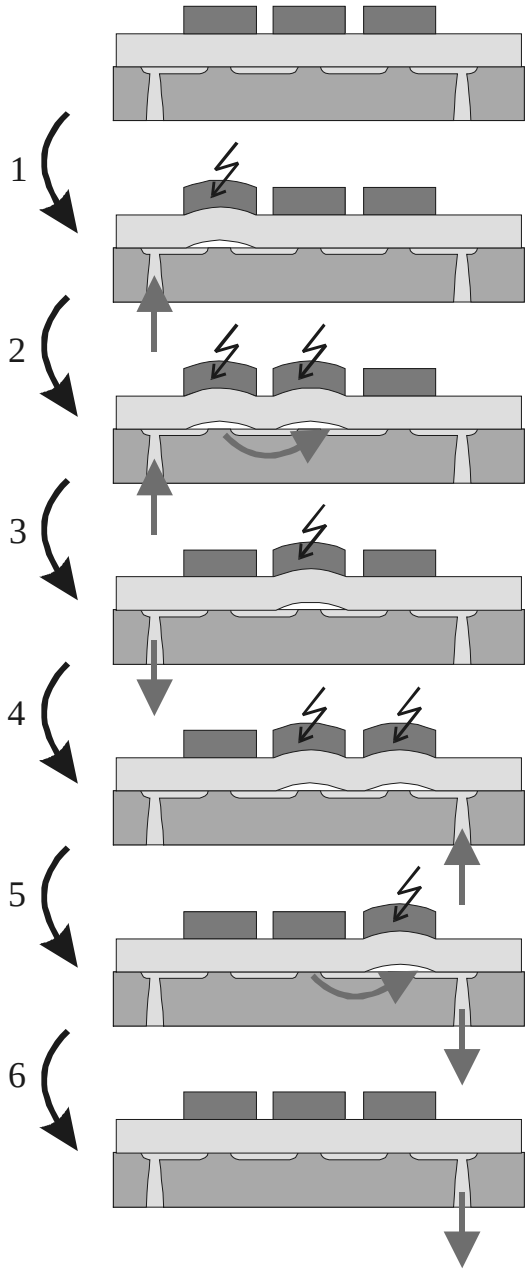

Figure 1 : Schematic of the pump actuation sequence.

The mass flow from the pump within one pump-cycle is expected to look as shown in Figure 2. After actuation of one of the membranes, the fluid underneath the membrane will not be pushed out immediately. The pressure underneath the membrane has to build up and the fluid has to be accelerated. This is indicated in the figure by presenting the steps in the generated flow as a first order system's step response.

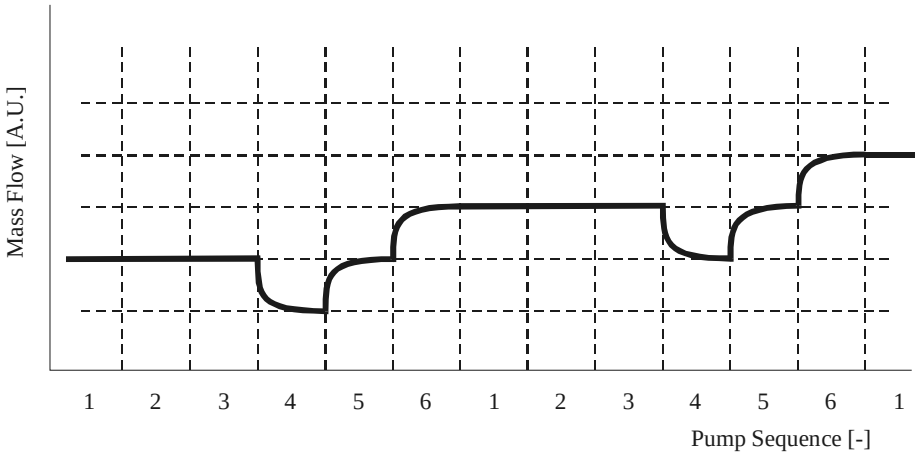

Figure 2 : The expected flow profile in time from the actuation sequence as in Figure 1.

The first order response results from the fluidic resistance underneath the membranes of the pump. Actuating the piezos on the membrane will result in a pressure change underneath the membrane. It will take some time before all fluid is squished away from underneath the membrane.

From this assumed first-order-response-like behavior it is deduced that the pump will have a linear flowrate-actuation frequency behaviour up to a certain frequency. Above this frequency the flowrate will not increase any more. This is explained with the help of the graph in Figure 3.

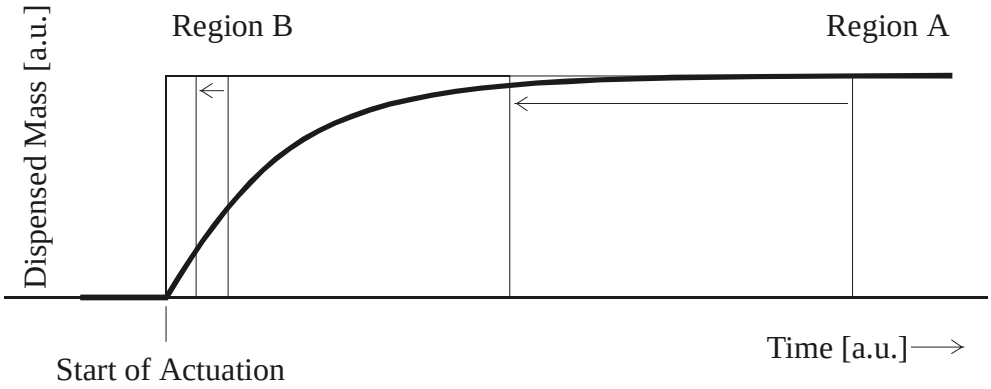

Figure 3 : The first order response of the dispensed mass from underneath the membrane after actuation of the piezo disc.

In Region A, the fluid underneath the membranes is given enough time to be completely dispensed from the pump. In this region, doubling the actuation frequency will result in a double output of the pump. For higher actuation frequencies (time constant in region B) a higher actuation frequency will result in a lower output per pump stroke. These two will cancel out: the pump will dispense half the volume at the double delivering frequency, resulting in a practically unchanged flow rate.

From the pump sequence shown in Figure 1 the maximum underpressure the pump can create pumping a compressible fluid is calculated. The pumping fluid is assumed to obey the ideal gas-law : PV=nRT, which states that the product of volume and pressure remains constant if no particles are added to the considered system and if the temperature does not change during the pumpcycle.

The modeled system is shown in Figure 4. One end of the pump is connected to its environment, which is at atmospherical pressure P_{inf}. The other end is connected to a fixed volume V_{out} at pressure P_{out}.

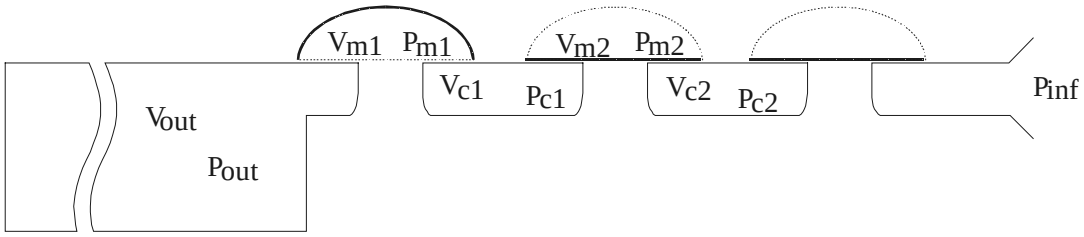

Figure 4 : The pump model as used to calculate the maximum gaspressure.

The volumes and pressures in the channels and underneath the membranes are indicated with *V* and *P* with subscripts *c* and *m*.

	Membrane status	Pressures
1		$P_{c1} = P_{c2} = P_{\inf}$
2		$P_{c1} = P_{c2} = P_{\inf}$
3		$P_{out3} = \frac{P_{out2} \times V_{out} + P_{\inf} \times (V_{c1} + V_{c2} + V_{m2})}{V_{out} + V_{m1} + V_{m2} + V_{c1} + V_{c2}}$
4		$P_{out4} = \frac{P_{out3} \times (V_{out} + V_{m1} + V_{c1} + V_{m2} + V_{c2})}{V_{out} + V_{c1} + V_{m2} + V_{c2}}$
5		$P_{out5} = \frac{P_{out4} \times (V_{out} + V_{m1} + V_{c1})}{V_{out} + V_{c1}}$
6		$P_{c2} = P_{\inf}$
1		$P_{c1} = P_{c2} = P_{\inf}$

Table 1 : Pressure at the outlet of the pump at the different stages of the pumpcycle. The pump is pumping into a fixed volume, creating overpressure.

The maximum achievable pressure $P_{out\text{-}max}$ is reached as the condition $P_{out5} = P_{out2}$ yields. For $V_{out} >> V_{m1}$ this pressure is found to be

$$P_{out,\max} = P_{\inf} \frac{V_{c1} + V_{m2} + V_{c2}}{V_{c1} + V_{c2}} = P_{\inf} \left(1 + \frac{V_{m2}}{V_{c1} + V_{c2}} \right) \qquad \text{Eq. 1}$$

So the maximum achievable overpressure is determined by the ratio of the volume of the actuated middle membrane (V_{m2}) to the volume of the connecting channels

(V_{c1}+V_{c2}). This ratio is an important design parameter in designing the selfpriming and bubble tolerant property of the pump.

If an air-water interface is present in the pump (i.e. an airbubble in the fluid) the accompanying surface tension will act as a force on the membrane trying to close the membrane (Figure 5). Before pumping action can be established, this surface tension force has to be overcome by the pressure in the pumpchamber.

$$\Delta P_{pumpchamber} > \Delta P_{surface-tension} \qquad \text{Eq. 2}$$

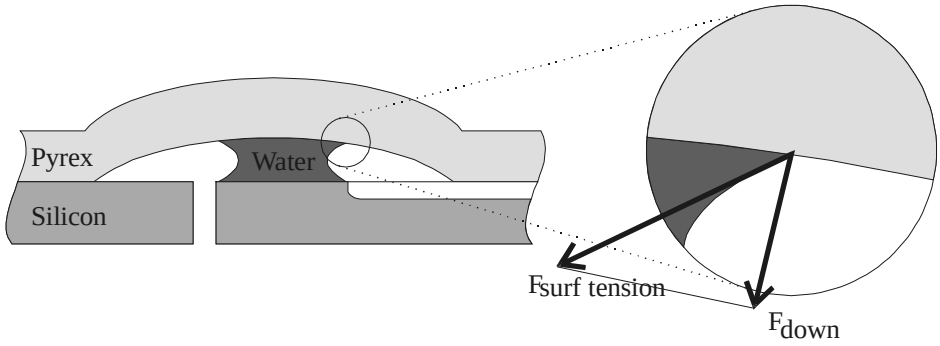

Figure 5 : Surface tension effects result in a force trying to close the valve.

Only one water/membrane interface will be present at the moment water enters the pumpchamber for the very first time. In order to be self-priming, the pump has to overcome the surface tension force due to this one interface.

The worst case surface tension scenario is found if air is present in the incoming channel as well as in the outgoing channel. Now the pump has to overcome the surface tension forces of the *two* interfaces. The pump will be bubble tolerant if it can actually handle this situation.

The pressures that the pump has to generate in order to be self-priming or bubble tolerant for water are found to be respectively 15 mBar and 70 mBar [25].

5.5 The Pump Design

Though the basic design of the pump has been shown (implicitly) in Figure 1, a number of figures and principles still have to be decided upon. The most important feature that has to be designed is the stroke volume of the pump membranes. Not only must this volume be large enough to meet the desired flowrate within only a number of pumpcycles per second, but on this figure it also depends whether the pump will be bubble tolerant.

Before the stroke volume can be calculated, the actuation mechanism of the membrane has to be decided upon.

A series of actuation methods have been proposed and used in the past (Figure 6). Of course numerous varieties exist on the shown membrane deflection actuation principles, but most of those originate from one of the shown principles.

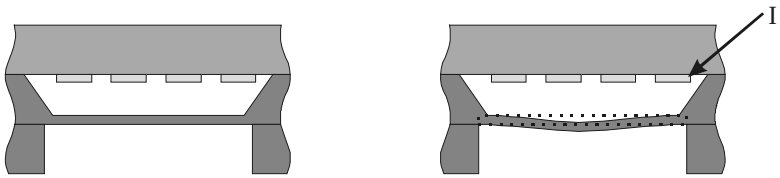

1. A pressure is built up inside an actuation chamber.

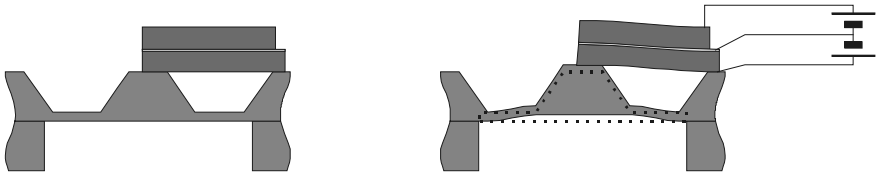

2. An actuated Piezo-bimorph lifts the membrane.

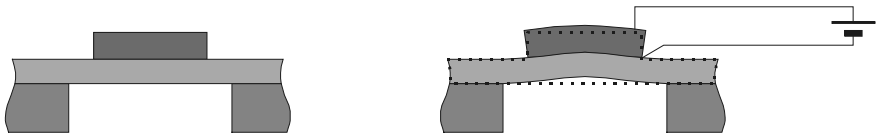

3. A Piezodisc forms a bimorph with the membrane itself.

Figure 6 : A short overview of different membrane actuation principles.

The first actuation method is based on raising the pressure in a chamber above the membrane. The gas present in the chamber above the membrane is heated by dissipating electrical energy in a resistor in that chamber. With this principle actuation frequencies up to 10 Hz have been reported [27].
The second option for deflecting a (pump)membrane is lifting the membrane using a bi-morph. A bi-morph is a stack of two piezo elements which are actuated with opposite voltages. This causes the bi-morph to bend and in our case to lift the membrane from its neutral position. The main disadvantage of membrane actuation with a bi-morph is that the membrane has to be a bossed membrane, which stiffens the membrane, thus reducing the maximum deflection [e.g. 18].
The last actuation principle shown here is the mounting of a piezo slab (or disc) to the membrane [e.g. 1]. Actuation of the piezo causes the piezo to gain somewhat in length. The membrane has to bend to compensate for the resulting stress.

It is this last actuation method that is chosen for the pump membrane. The most important reason is that this actuation mechanism is fairly easy to realize.

The actuation method will be studied in somewhat more detail here. First the deflection and hence the displaced volume that can be created will be modeled. From the results of this model it will follow if this type of membrane actuation is feasible.

Starting point will be Piezodiscs from Philips (PXE5-10/0.2-N, [28]) with a thickness of 200 μm and a radius of 1 cm. These discs have been satisfactorily used with other pumps [24]. For a maximum deflection, the stiffness of the membrane and the piezodisc have to be the same. In practice this means that the (Pyrex) membrane has to be equally thick as the piezo disc (200 μm).

An approximation of the lift height of the membrane due to an actuated piezodisc will be made here. The actuated piezo disc will elongate. It is assumed that the membrane itself will not be elongated. Therefore the geometry of the piezo/membrane is forced into a part of a sphere with radius *r* (Figure 7).

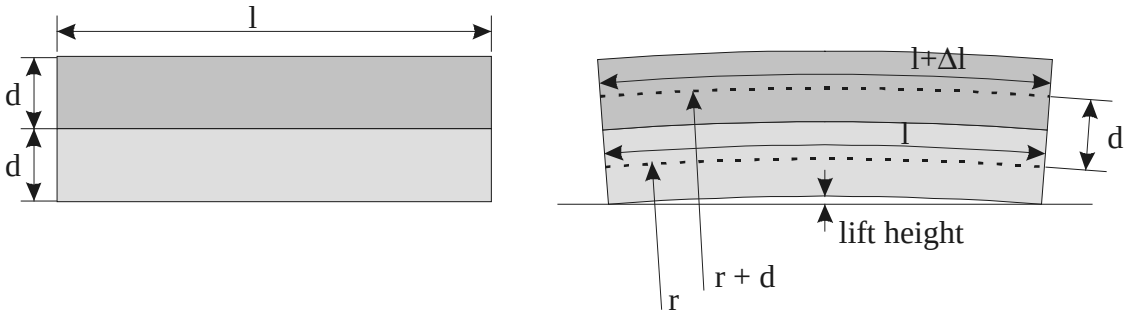

Figure 7 : Definition of symbols needed for the calculation of the lift height.

The following formulas hold for this configuration:

$$l = \alpha r \qquad \text{Eq. 3}$$

$$l + \Delta l = \alpha (r + t) \qquad \text{Eq. 4}$$

in which l is the membrane diameter, r the radius of curvature of the membrane, t the thickness of the piezodisc and the membrane, Δl the longation of the piezodisc and α the bending angle of the piezodisc.

Subtracting equation 3 from equation 4 yields:

$$\Delta l = \alpha t \qquad \text{Eq. 5}$$

First the expansion of the piezo disc will be calculated. The expansion of the piezodisc Δt in the piezos poled direction is (Figure 8):

$$\Delta t = \varepsilon(E) t\,, \qquad \text{Eq. 6}$$

in which t is the thickness of the piezo disc and ε the linear expansion coefficient as function of the electric field strength E applied to the piezo disc. From [29] it is concluded that the expansion coefficient is linear with the applied electric field. An applied field of 1 kV mm^{-1} results in an expansion coefficient of 5×10^{-4}.

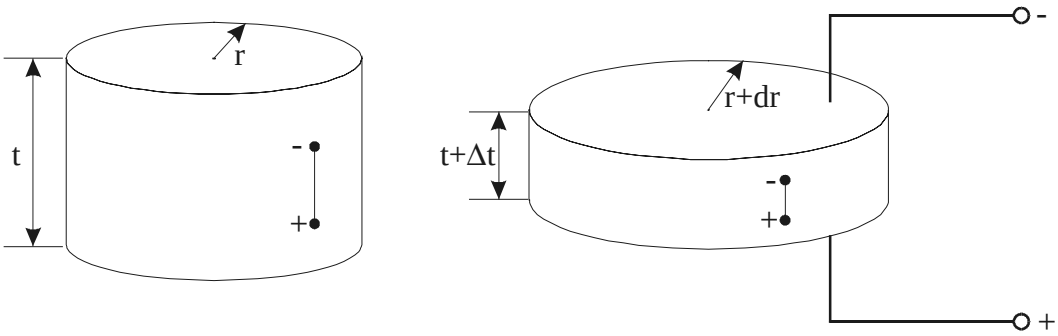

Figure 8 : The deformation of a piezo disc. Left the piezo in its neutral form, right the piezo with an applied voltage, deforming the piezo disc.

The used piezos (Philips PXE5-10/0.2-Ni) have a thickness of 200 μm. The voltage applied to these piezos is 125 V. Therefore the electric field strength is 625 kV mm^{-1}, which results in an expansion coefficient of 3.125×10^{-4} in the poled direction. The expansion in the radial direction of the piezodisc, *dr*, is found by multiplying the expansion in the poled direction with the Poissons ratio of the piezo electric material. The Poissons ratio for the piezo electric material PXE5 is 0.3 [30], therefore the radial expansion is 0.3×3.125 μm = 0.94 μm.

The lift height is found with the help of Figure 9:

$$lift = r - r\cos(\tfrac{1}{2}\alpha) \qquad \text{Eq. 7}$$

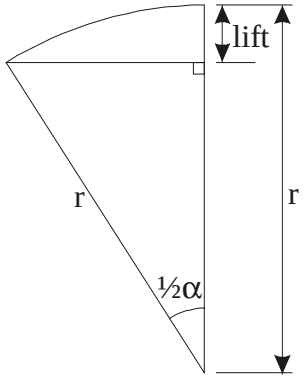

Figure 9 : Graph for finding the lift height.

From equation 5 the opening angle α is found to be $\alpha = 0.0046875$ rad. The accompanying radius of curvature of the membrane is (equation 3) $r = 2.13$ m. With these values in equation 7, the lift height of the membrane is calculated to be 4.7 μm.

The volume of a sphere segment as in our case is given by [31]:

$$V = \tfrac{1}{3}\pi\ lift^2(3r + lift)\,, \qquad \text{Eq. 8}$$

which is approximately 230 nl for our case.

The membrane is chosen to be somewhat larger (10%) as the piezodisc. This in order to reduce the stresses in the membrane along the edges and maximize the displaced volume ([32], Figure 10).

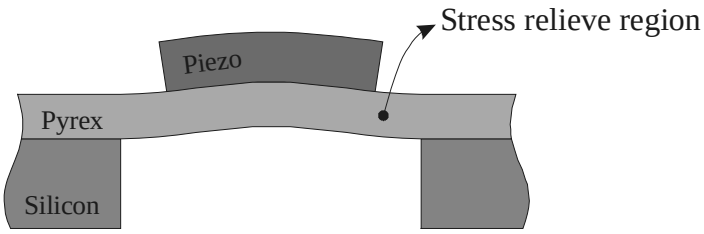

Figure 10 (not on scale) : The membrane is chosen somewhat larger as the piezodisc. Thus a stress relieve region is introduced.

The volume underneath the membrane as drawn in Figure 10 will be larger as the estimated volume from equation 8. Assuming that the membrane bends back with a radial curve, the situation as shown in Figure 11 holds. The extra lift height due to the stress relieving region is given by :

$$lift2 = lift1 \times \frac{r_2}{r_1} \qquad \text{Eq. 9}$$

This extra lift height introduces an extra displaced volume which can be estimated by a circular disc with a height of the extra lift and the radius of the membrane.

$$Volume2 = lift2 \times membraneradius \qquad \text{Eq. 10}$$

The total volume underneath the membrane is the sum of the two mentioned components, which add to 275 nl.

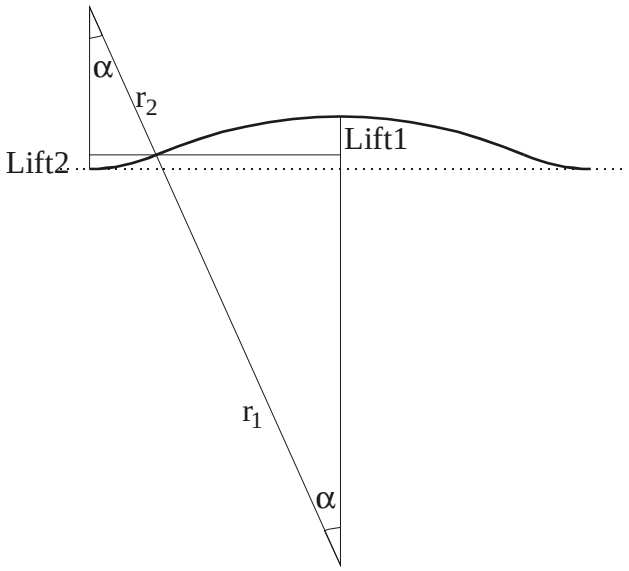

Figure 11 : graph for estimating the extra lift height due to the stress relieve region.

The needed flowrate to drive the MAFIAS system is 10 µl/min = 166 nl/sec. Therefore, at a pumping frequency of 1 Hz the pump can easily realize the needed flow.

With respect to the total volume of the connecting channels (estimate: two channels of 200µm×200µm×1cm=800 nl), a maximum pressure of 288 mBar should be feasible. This pressure is higher then the pressure needed for the system (7 mBar, paragraph 5.3) as well as higher as the estimates made by Richter for a selfpriming and bubble tolerant micropump.

It is concluded, that a peristaltic pump can be realized which meets the specifications needed for the MAFIAS system. Implicitly it was assumed that the volume underneath the membrane in the 'down' position is zero. Though this is certainly not trivial, fabrication techniques are available to realize this (Chapter 8). The fabrication process for the micropump will be discussed in the next section.

5.6 The fabrication process

This paragraph shows the fabrication process of the peristaltic pump.

The pump design consists of a two wafer stack with piezos attached to the top-wafer (Figure 12).

The bottom wafer will be a silicon wafer with powderblasted channels connecting the different membranes. Since the powderblasting technique results in an (approximately) parabolic cross-section, the cross-section will not be 200×200=40000 μm^2, but appr 25000 μm^2. The total internal volume of the channels therefore will be 530 nl,

resulting in a maximum pressure drop of 430 mBar. Through holes will be powderblasted through the wafer to make the fluidic connections.

The top wafer will be a Pyrex wafer which is anodically bonded to the bottom wafer. Before bonding the top wafer will be patterned with a thin Chromium layer. This Chromium layer prevents the formation of a bond between the silicon and the Pyrex (Chapter 8). After bonding the Pyrex wafer is thinned down to match the thickness of the piezo discs (~200 μm). The last step is to pattern the waferstack with metal electrodes at the top side which will be used as the electrical connections for the piezodiscs.

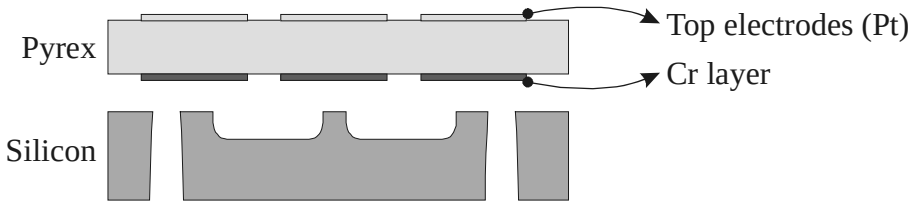

Figure 12 : The pump design

The pumps as they look at the stage shown in Figure 12 is shown in Figure 13.

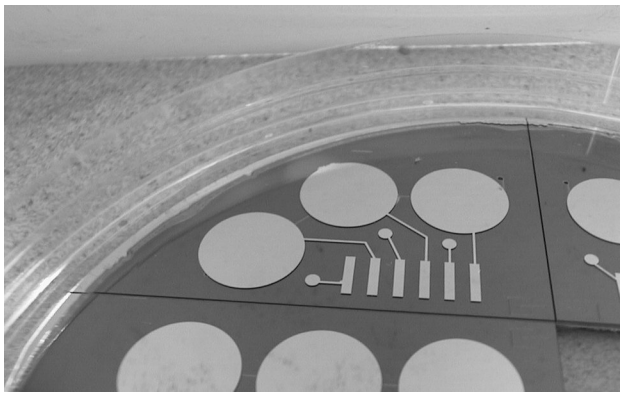

Figure 13 : Photograph of a micropump without piezo elements.

After the deposition of the electrodes the piezodiscs have to be connected to the top wafer. This is described in the next paragraph.

5.6.1 Attaching the piezo discs

The fabricated device has to be mounted with piezodiscs to be a working device. In order to maximize the lift height of the membrane, the intermediate layer has to be as thin as possible [32]. Also care has to be taken that no stresses are present in the piezo material. If a tensile stress is present in the piezodisc after the attachment procedure, the membrane will bulge down. If this pre-tension is too large, the membrane will not separate from the bottom wafer.

Options that are available for connecting the piezo discs to the membranes are gluing and soldering.

Soldering is done by heating the whole pump to the melting point of the soldering alloy (~180 °C). The piezodiscs are pushed on to the electrodes, thus pressing the surplus of the soldering alloy out from between the piezo and the membrane, which results in a thin (~10 μm) intermediate layer.

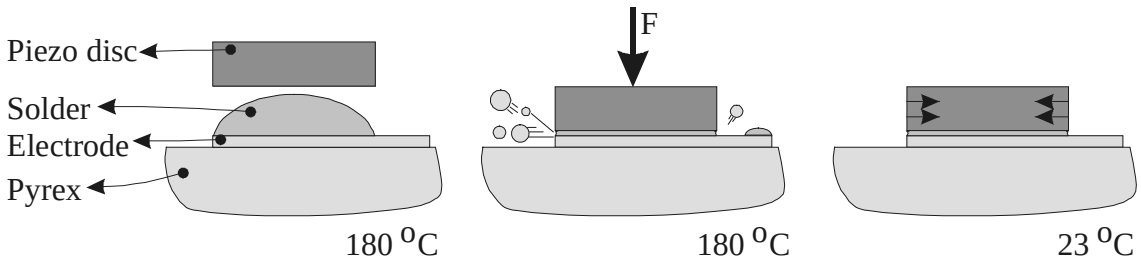

Figure 14 : The soldering procedure

Though the adhesion of the piezo discs is very good, the difference in linear expansion coefficients between the piezo electric material (Philips PXE-5) and the membrane (Pyrex) is fairly large (~5×10^{-6}). Lowering temperature from 180°C down to 23°C would result in a contraction of the piezo disc of 7.5 μm with respect to the silicon. Since the maximum elongation of the piezo (see paragraph 5.3.2) will be in the order of only 1 μm, the piezo disc will not be capable of lifting the membrane after it has been soldered to the membrane.

It is concluded that the piezodiscs have to be glued to the top wafer (using conductive glue).

Figure 15 shows a peristaltic pump after gluing and connecting the piezos to the waferstack.

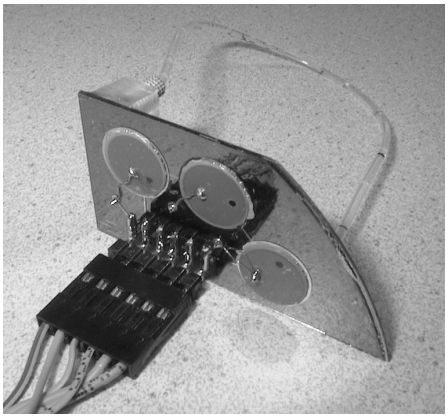

Figure 15 : Photograph of a completed micropump.

5.7 Characterization

For the full characterization of the micropump, quantities that have to be measured are the flowrate and the pressure build up over the micropump. The setup that has been built for measuring these quantities is described in the next paragraph. Results from the performed measurements are presented in paragraph 5.7.2.

5.7.1 Characterization setup

The setup that has been built for the characterization of the micropump is schematically shown in Figure 16. The pump is mounted in the setup such that it discharges into a small container on a microbalance (Mettler Toledo AT261, 0.01 mg resolution). A computer continuously reads out the microbalance. From the recorded mass over time data, the massflow produced by the micropump is calculated. Dividing the massflow by the specific weight of the fluid results in the generated volume flow.

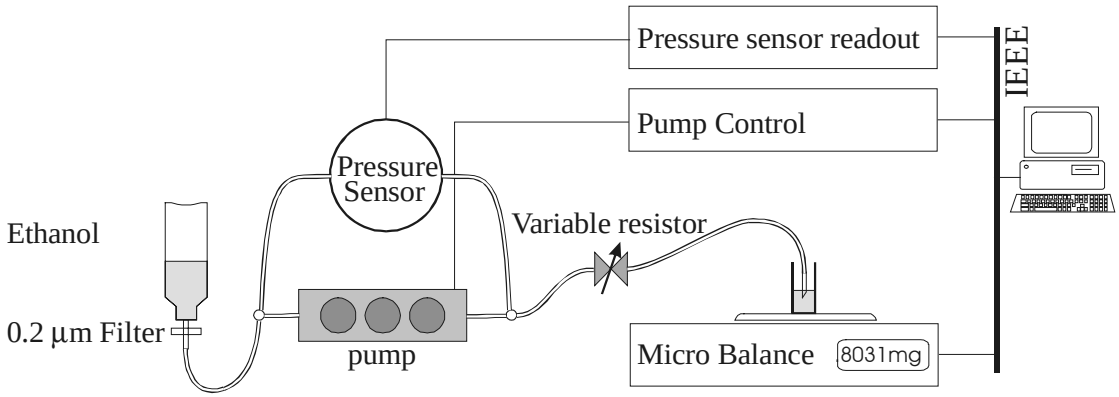

Figure 16 : Schematic of the measurement setup for the micropump

A differential pressure sensor (Honeywell 26PCC) is mounted over the micropump to be able to measure the pump head pressure. This value can be changed manually by means of a variable resistor. The pumping liquid is filtered (0.2 µm) before it enters the system to prevent the pump from clogging.

The liquid is dispensed in a small container on the microbalance via a needle. The needle pierces through the liquid surface, thus preventing any surface tension effects to disturb the measurement (Figure 17).

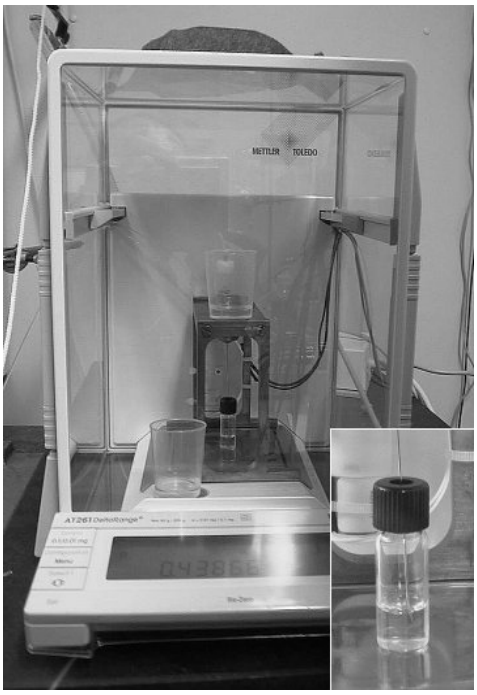

Figure 17 : The precision balance with the container. The inset shows the needle through which the pump discharges in the container.

Since the flowrates to be measured are very small, the fact of liquid evaporating from the container on the scale has to be taken into account. The measurements presented in this thesis have been corrected for the evaporation rate unless indicated otherwise.

5.7.2 Measurements

In order to characterize the micropump a number of experiments have been performed. The results of these measurements are presented here.

The first experiment is the frequency dependence of the flowrate from the micropump. The result is shown in Figure 18. The actuation frequency at the x-axis is the number of times per second the pump-cycle (Figure 1) is repeated.

From Figure 18 it is seen that the pump indeed acts as indicated in paragraph 5.3. Above a frequency of about 1.5 pump cycles per second, the pump does not gain any more in output.

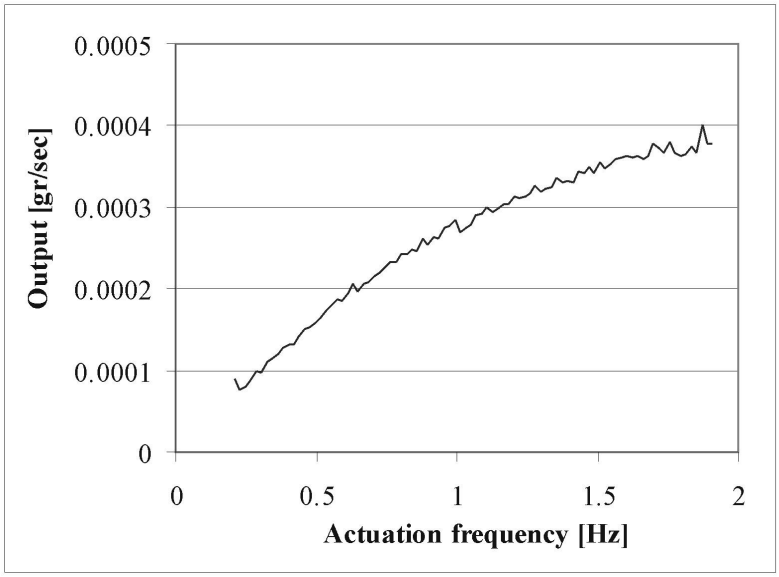

Figure 18 : The measured pump output (water) as function of the actuation frequency.

The following experiment shows the recording of the mass on the precision balance at a very low pumping frequency. This way, the subsequent steps within a pumpcycle can be measured and verified against the expected output as depicted in Figure 2. The result is shown in Figure 19.

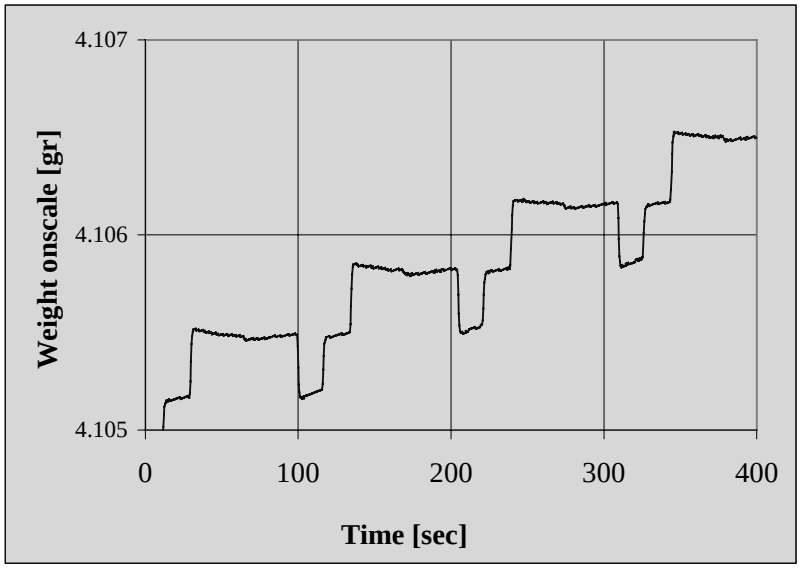

Figure 19 : The measured pump output within a pumpcycle with water as medium.

From Figure 19 it is learned that the output during the pumpcycle is indeed as expected: after three inactive periods, one amount of fluid is taken in at the outlet, after which twice that same amount of fluid is dispensed onto the scale. It is also seen, that about one third milligram of water is dispensed in one pumpcycle. This corresponds to 300 nl per pumpcycle, which is in the same range as the predicted 275 nl.

In order to test the leak-tightness of the pump a simple experiment is performed. The setup is modified such that an overpressure can be applied to the inlet of the pump. First, no pressure is applied (1). In this stage the evaporation rate of the fluid from the scale is determined. During the second stage a pressure of 33 mBar is applied to the inlet (2). The membranes are not actuated. During the next stage all the membranes are actuated **down** (3). This causes the membranes to minimize any possible gap between the Pyrex membrane and the silicon bottom wafer. The last stage consist of the membranes actuated open (4). The results of this experiment are shown in Figure 20.

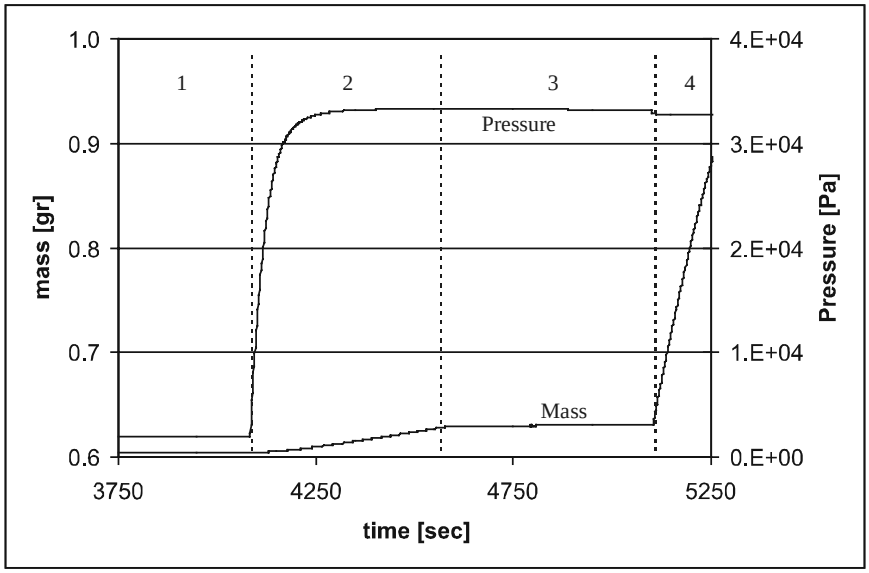

Figure 20 : The results of the leaktest of the membranes. The mass on the scale (bottom line) and the applied pressure (top line) are plotted against the elapsed time.

From Figure 20 it its clearly seen, that there's a large difference between the open and closed resistances. In Table 2 the flow resistances during the three last stages are calculated. The first column shows the flowrate as measured without any actuation on the fluid. This column includes effects as vaporizing of the liquid from the micro balance. The second column is corrected for these effects. From the measured flowrate and the measured pressure, the flow resistance of the pump can be calculated. The last column shows the relative flow resistance of the three stages with respect to the flow resistance in the case of all membranes actuated down.

	Measured flowrate [m^3 sec^{-1}]	Corrected flowrate [m^3 sec^{-1}]	Flow Resistance [Pa sec m^{-3}]	Normalized flow resistance [-]
1	-1.92E-14			
2	5.27E-14	7.19E-14	4.63×10^{17}	.037
3	-1.65E-14	0.27E-14	1.26×10^{19}	1
4	2.07E-12	209E-14	1.59×10^{16}	.0013

Table 2 : The calculated flow resistances during the three stages of the leaktest (Figure 20).

The results from the leaktest show that the fluid resistance during the ‘up’ and ‘down’ actuation of the membranes differ by a factor of approximately 800 (1/0.0013). This means that while closing the second membrane (see pumpcycle Figure 1, step 5) one part of the fluid will be dispensed back into the inlet against 799 parts dispensed into the outlet of the pump.
The absolute flow resistance of the pump with three closed membranes compared to the flow resistance expected for the final system (paragraph 5.3, 4.4×10^{12} Pa s m^{-3}), the pump can be considered leak tight.

The last performed experiment consists of driving the pump at a fixed frequency at different actuation voltages. The measurement series is started at the high voltage side, gradually lowering the actuation voltage. The flowrate of the pump is measured. The results are shown in Figure 21.

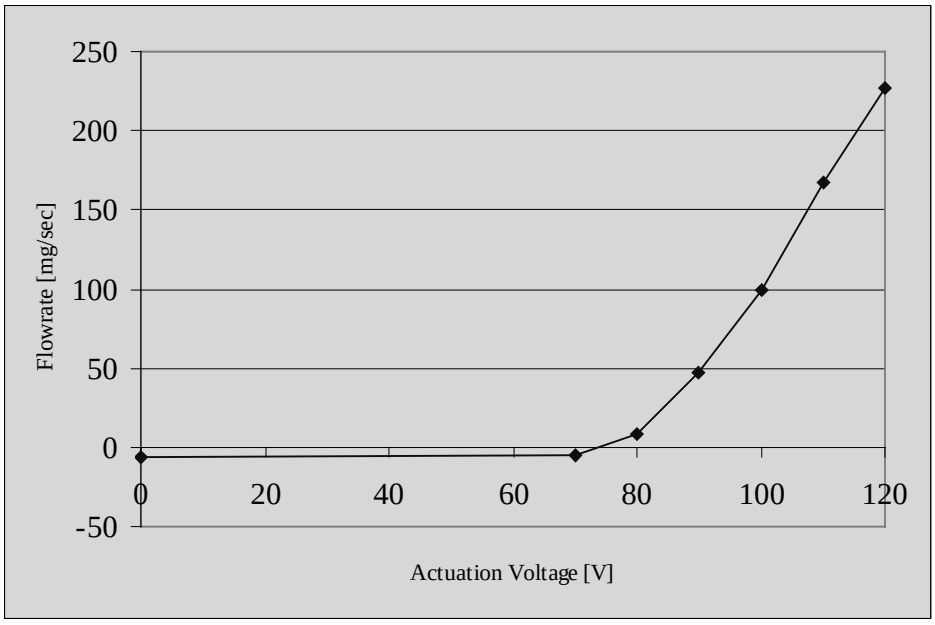

Figure 21 : Flowrate vs actuation voltage of the micropump. (Pumping water at 550 Hz)

It is clearly seen that pumping action starts only at an actuation voltage of 80 V. No fundamental reason is found for this behaviour. Whether at low actuation voltages the stroke volume is not large enough to result in pumping action or whether the piezodisc cannot deliver enough force to the membrane to sip in or dispense fluid is not understood.

During the experiments it was found that the pump membranes can withstand a maximum backpressure of about 750 mBar. Above this pressure, the last membrane (which has this pressure constantly applied to it) breaks out of the Pyrex wafer.

5.8 Discussion and Conclusions

In this chapter the design, realization and characterization of a peristaltic micropump was discussed.

The micropump will be incorporated in the MAFIAS system described in this thesis. Therefore the pump has to be able to propel fluid through this system. An estimate of the needed performance of the pump is that the pump has to be capable of delivering a flowrate of 10 $\mu l\ min^{-1}$ at a backpressure of only 7 mBar. Next to these specs, the pump also has to be selfpriming and bubble tolerant. This means that the pump has to capable of compressing air to a pressure of 70 mBar.

The design of the pump is based on the peristaltic principle. Three membranes in a row are interconnected with channels. Subsequent actuation of the membranes will result in the transportation of fluid from the first to the last membrane. The key design parameter is the ratio of the so-called dead volume by the stroke volume. This ratio has to be larger than 0.07 in order to reach the critical pressure of 70 mBar. The pump is designed with a ratio of these volumes of 0.43. A theoretical maximum pressure of 430 mBar can therefore be reached (pumping gas).

The membranes of the pump are created with a near zero gap between the Pyrex membranes and the silicon bottom wafer. The technique of selective anodic bonding that is used for creating these membranes is described in chapter 10. The membranes are actuated by a piezo disc that is glued to the membrane. Actuating the piezo disc, the piezodisc elongates a little and therefore is longer than the membrane. The thus induced stress in the material causes the membrane to bulge out.

From the measurements on the completed pumps, a number of features have been seen. The pump is capable of producing a flowrate of approximately 23 $\mu l\ min^{-1}$. The maximum backpressure the pump can withstand is 750 mBar. Higher pressures cause the membrane to break out of the Pyrex top wafer.

By applying a pressure to the inlet and measuring the induced flowrate for down-actuated and up-actuated membranes, the fluidic resistances were calculated. The resistance for the membranes actuated down are a factor 800 higher as for the membranes actuated up. The absolute value of the resistance actuated down is a factor 3500 higher as the estimated flow resistance of the final systems channel. It can therefore be concluded that the pump is leaktight with respect to the system itself.

The dependance of the flowrate from the pump on the actuation voltage shows that pumping action starts only at 80V. It is not clear why pumping action is not seen for lower voltages. Though the stroke volume at lower voltages is smaller, a well primed pump still should displace fluid from the inlet to the outlet. A possible cause is that the piezo discs at low voltages cannot exert enough force on the pump membranes to actually push fluid out from underneath the membranes.

5.9 Literature

[1] J.G.Smits, Piezoelectric micropump for peristaltic fluid displacements, NL patent 8302860, 1985

[2] H.T.G.vanLintel, F.C.M.vandePol, S.Bouwstra, A piezoelectric micropump based on micromachining of silicon, Sensors and Actuators 15, pp153-167, 1988

[3] P.W.Barth, C.C.Beatty, L.A.Field, J.W.Baker, G.B.Gordon, A robust normally closed silicon microvalve, S&A '94, pp248-250, 1994

[4] S.Matsumoto, A.Klein, R.Maeda, Development of Bi-Directional valve-less micropump for liquid, Proceedings MEMS 99, 1999

[5] B.Wagner, H.J.Quenzer, S.Hoerschelmann, T.Lisec, M.Juerss, Bistable microvalve with pneumatically coupled membranes, Proceedings MEMS '96, pp384-388, 1996

[6] O.S.Jensen, P.Gravesen, Flow characteristics of a micromachined diaphragm valve designed for liquid flows above 1 ml/min, Micromech. Microeng. 3, pp236-238, 1993

[7] C.R.Neagu, J.G.E.Gardeniers, M.Elwenspoek, J.H.J.Fluitman, An electrochemically actuated microvalve, Actuator '96, pp41-44, 1996

[8] D.Maillefer, H.vanLintel, G.Rey-Mernet, R.Hirschi, A High-performance silicon micropump for an implantable drug delivery system, Proc. MEMS 99, 1999

[9] M.Richter, R.Linneman, P.Woias, Design methodology for gas and liquid micropumps, Proc.Eurosensors XI, pp785-788, 1997

[10] J.Shinohara, M.Suda, K.Furuta, T.Sakuhara, A high pressure-resistance micropump using active and normally-closed valves, MEMS 2000, 2000

[11] R.L.Bardell, F.K.Forster, M.A.Afromowitz, N.R.Sharma, A.Blanchard, Designing high-performance micro-pumps based on no-moving-parts valves, MEMS '97, pp47-53, 1997

[12] A.Olsson, G.Stemme, E.Stemme, A numerical design study of the valveless diffuser pump using a lumped mass model, JMM 9, pp34-44, 1999

[13] S.Matsumoto, A.Klein, R.Maeda, Development of Bi-Directional valve-less micropump for liquid, Proc. MEMS 99, 1999

[14] T.Gerlach, M.Schuenemann, H.Wurmus, A new micropump principle of the reciprocating type using pyramidic micro flowchannels as passive valves, Journal Micromech. Microeng 5, 1995

[15] M.Koch, A.G.R.Evans, A.Brunnschweiler, The dynamic micropump driven with a screen printed PZT actuator, JMM 8, pp119-122, 1998

[16] W.vanderWijngaart, H.Andersson, P.Enoksson, K.Noren, G.Stemme, The first self-priming and bi-directional valve-less diffuser micropump for both liquid and gas, MEMS 2000, 2000

[17] N.Tesla, Valvular conduit, US Patent office, 1.329.559, 1920

[18] M.Stehr, S.Messner, H.Sandmaier, R.Zengerle, A new micropump with bidirectional fluid transport and selfblocking effect, MEMS '96, pp485-490, 1996

[19] J.A.Folta, N.F.Raley, E.W.Hee, Design, fabrication and testing of a miniature peristaltic micropump, Solid State Sensors and Actuators Workshop, Hilton Head Island, South Carolina, 1992

[20] H.Mizoguchi, M.Ando, T.Mizuno, T.Takagi, N.Nakajima, Design and fabrication of a light driven micropump, MEMS'92, pp31-36, 1992

[21] O.T.Guenat, D.Ghiglione, V.Pasquier, B.H.vanderSchoot, W.E.Morf, N.F.deRooij, An electro-osmotically driven nanopump for volumetric nanotitration applications, Proc Eurosensors XIII, the Hague, pp681-682, 1999

[22] Brochure from MEMStek, ProtoType Micro-miniature Gear-Pump, 1997

[23] X.Wang, Q.Lin, Y.Tai, A parylene micro check valve, Proc. MEMS 99, 1999

[24] S.Böhm, The comprehensive integration of microdialysis membranes and silicon sensors, PhD thesis, University of Twente, 2000

[25] M.Richter, R.Linneman, P.Woias, Robust design of gas and liquid micropumps, Sensors & Actuators A 68, PP480-486, 1998

[26] E.Oosterbroek, Modeling, Design and Realization of Microfluidic Components, PhD thesis, University of Twente, ISBN 90-36513464 (1999)

[27] T.S.J.Lammerink, M.C.Elwenspoek, J.H.J.Fluitman, Integrated micro liquid dosing system, In proc. Micro Electro Mechanical Systems, MEMS'95 (1995), pp13-18

[28] Datasheet Philips Components, material grades Piezoelectric Ceramics, 1996, jun 27.

[29] Datasheet Philips Introduction Piezoelectric Ceramics, 1996.

[30] Datasheet Philips Components, PXE 5, Material grade specification, 1996, mar 27.

[31] PBNA Polytechnisch zakboekje, 48e druk, pp **A2**/31, ISBN 90 6228 266 0

[32] C.J.Morris, F.K.Forster, Optimization of a circular piezoelectric bimorph for a micropump driver, JMM 10, pp459-465, 2000

Chapter 6 : Detection Cell*

In this chapter the design and realization of a micromachined optical detection cell is presented. A theoretical background for light absorption by the reaction product and losses by reflection of light at interfaces is given. In order to obtain optimal detector sensitivity, a special etching technique is used for making 45-degree planes that reflect the light parallel into the detection channel. Measurements with the detection cell using a Lock-in Amplifier (LIA) setup indicate a more than 3 decades dynamic range which is in line with theoretical calculations. The non-ideal behavior of the detector is ascribed to the change in refractive index of the samples for higher concetrations.

6.1 Introduction

Concentrations of chemical compounds in solutions can be measured by a variety of detection methods, such as electrical, electrochemical, mechanical or optical methods (e.g. [1]-[5]). Of all these methods, the measurement of optical absorption is a commonly and routinely applied method. The solution to be measured is placed in a cuvette, through which light is guided. The intensity of the outcoming light is measured, from which the absorption of light by the sample is calculated. The intensity of the outcoming light is related exponentially to the concentration of the chemical compound in the sample. Increasing the path length through the cuvette makes the measurement more sensitive to lower concentrations.

This chapter shows the design of a micromachined detection cell. First the different causes for the losses of light in and around a detection cell will be treated. After that, an overview of known micromachined detection cells will be given, ending with the MAFIAS detection cell design. The last part of this chapter presents the results of measurements that were performed on realized detection cells.

---

* Part of this chapter has been published in: Proc. MME 2000, Uppsala, Sweden, (2000)

* Parts of this chapter have been submitted: R.M.Tiggelaar, T.T.Veenstra, R.G.P.Sanders, J.G.E.Gardeniers, M.C.Elwenspoek, A. van den Berg, A light detection cell for microfluidic analysis systems, Talanta, 6-4-2001

6.2 Theory

Two effects are of interest considering the intensity of a beam of light in a detection cell (cuvette). The first effect is the absorption of light by the sample that is present in the detection cell. The losses that correspond to this effect vary with the concentration of the sample. Second there are the losses related to the in- and out coupling of the light beam into and from the detection cell. This factor does not change for a fixed geometry, though can be influenced by the design of the detection cell itself. These two effects are treated into more detail in the next paragraphs.

6.2.1 Absorption of light in a medium

When a beam of light goes through a solution with a colored compound in it, the light is partly absorbed by this compound. The absorption or extinction can be related to the concentration of the compound using Lambert-Beer's law (eq. 1):

$$I = I_0 \cdot e^{-\varepsilon \cdot C \cdot d} \qquad \text{Eq. 1}$$

with:

I: measured light intensity at concentration *C* [W]

I_0: measured light intensity at concentration *0* [W]

ε: the extinction coefficient of the absorption material/compound [$l \cdot mol^{-1} \cdot m^{-1}$],

C: the concentration of the absorbing material/compound [$mol \cdot l^{-1}$],

d: the distance the light travels through the solution [m].

If the product $\varepsilon C d << 1$, equation 1 can be rewritten:

$$\frac{I}{I_0} = 1 - \varepsilon C d \qquad \text{Eq. 2}$$

So for small concentrations of a certain compound and a fixed path length, the light intensity is linear with concentration.

6.2.2 Reflection of light at a surface

Light hitting a surface is divided into two portions. Part of the light is reflected, whereas the remaining part penetrates the surface. The ability of a material to reflect light is quantified by the *reflectance R, R* being the ratio of the reflected power to the incident power. *R* strongly depends on the incident angle θ_i as well as on the refractive indices of the incident and reflecting media (Figure 1).

In order to calculate the reflectance *R*, Snell's law and the Fresnel equations are required [6]. Equation 3 gives the Snell's law of reflection:

$$n_i \cdot \sin(\theta_i) = n_t \cdot \sin(\theta_t) \qquad \text{Eq. 3}$$

with:

n_i: refractive index of the incident medium,

n_t: refractive index of the transmitting medium,
θ_i: the angle of incidence,
θ_t: the angle of transmission (or refraction).

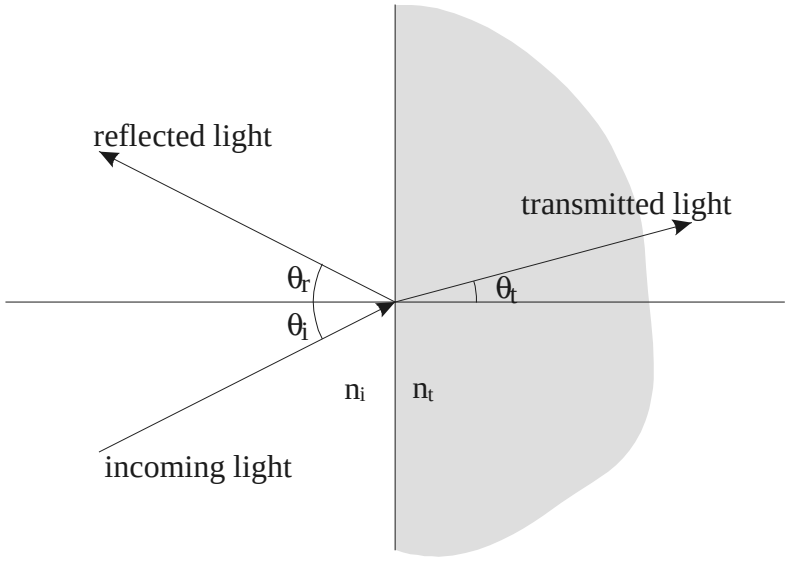

Figure 1: Variable denomination around the reflection and transmission of light on a surface.

The angle of incidence θ_i equals the angle of reflection θ_r.

The Fresnel equations couple the amplitude of the reflected light wave to the amplitude of the incoming light wave. These ratios depend on the polarization of the incoming light. For perpendicular and parallel-polarized light waves the Fresnel equations are given by eq. 4 (an exact derivation is given in [6]):

$$r_{\perp} \equiv \left(\frac{E_{0r}}{E_{0i}}\right)_{\perp} = \frac{n_i \cdot \cos(\theta_i) - n_t \cdot \cos(\theta_t)}{n_i \cdot \cos(\theta_i) + n_t \cdot \cos(\theta_t)} \qquad \text{Eq. 4a}$$

$$r_{\parallel} \equiv \left(\frac{E_{0r}}{E_{0i}}\right)_{\parallel} = \frac{\frac{n_t}{\mu_t} \cdot \cos(\theta_i) - \frac{n_i}{\mu_i} \cdot \cos(\theta_t)}{\frac{n_i}{\mu_i} \cdot \cos(\theta_t) + \frac{n_t}{\mu_t} \cdot \cos(\theta_i)} \qquad \text{Eq. 4b}$$

with:
E_{0r}: the amplitude of the electric field of the reflected light wave,
E_{0I}: the amplitude of the electric field of the incoming light wave,
$r_{\perp}$: the amplitude reflection coefficient (for the component of the *E*-vector parallel to the plane of incidence),
$r_{/\!/}$: the amplitude reflection coefficient (for the component of the E-vector perpendicular to the plane of incidence),
μ_i: the permeability of the incident medium,
μ_t: the permeability of the transmitting medium.

When both media forming the interface are simple dielectric media ($\mu_i = \mu_t$), the Fresnel equations (eq. 4) can be simplified using goniometric formulas. Eq. 5 are the Fresnel equations for dielectric media.

$$r_{\perp} = -\frac{\sin(\theta_i - \theta_t)}{\sin(\theta_i + \theta_t)} \qquad \text{Eq. 5a}$$

$$r_{\parallel} = +\frac{\tan(\theta_i - \theta_t)}{\tan(\theta_i + \theta_t)} \qquad \text{Eq. 5b}$$

If the amplitudes of reflection are known, the parallel and perpendicular reflectances $R_{//}$ and $R_{\perp}$ can be calculated by multiplying the found amplitude reflections with its own complex complement (eq. 6):

$$R_{\parallel} = r_{\parallel} \cdot r_{\parallel}^{*} \qquad \text{Eq. 6a}$$

$$R_{\perp} = r_{\perp} \cdot r_{\perp}^{*} \qquad \text{Eq. 6b}$$

Dependent on the polarization of light, with the use of eq. 6 the reflectance R can be calculated.
For unpolarised light the reflectance R can be calculated by means of eq. 7.

$$R = \frac{R_{\perp} + R_{\parallel}}{2} \qquad \text{Eq. 7}$$

In Figure 2 the theoretical curve of the reflectance R of a water-silicon interface is given as a function of the angle of incidence θ_i.

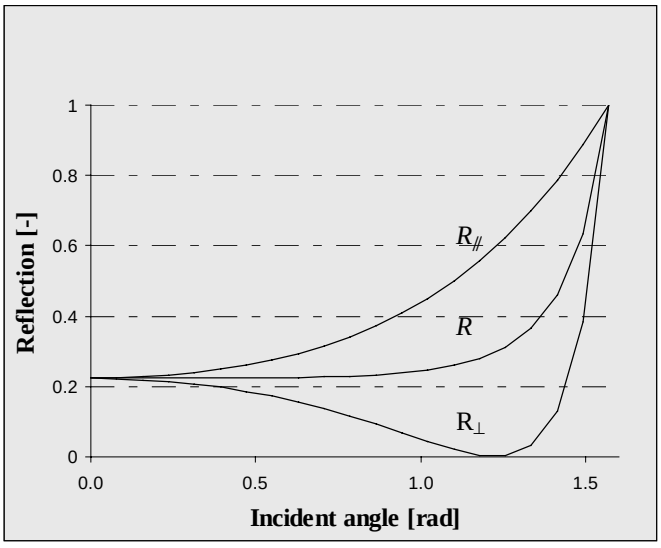

Figure 2: Curve of reflectance *R* as function of the angle of incidence for a water-silicon interface (wavelength 600 nm)

From Figure 2 it is seen that if the incident angle is less than 1 rad (~57°), the reflectance of a water-silicon interface for unpolarised light is nearly constant at 0.23.

For multiple reflections at a given angle of incidence θ_i, the decrease in light intensity may be expressed as a function of the reflectance R as given in eq. 8:

$$I = R^x \cdot I_0$$

Eq. 8

with:
I: the measured light intensity [W m^{-2}],
I_0: the original (or initial) light intensity [W m^{-2}],
x: the number of reflections [-].

The intensity of light entering a cuvette will be decreased by reflections as well as by absorption of light by the solution in the channel. Combining equations 1 and 8 results in an expression for the final light intensity:

$$I = I_0 \cdot R^x \cdot e^{-\varepsilon \cdot C \cdot d}$$

Eq. 9

From this equation it can be deduced that the light-power output is always lower than the input power. The intensity is decreased by a (for a fixed geometry) factor due to the losses from the reflections. The exponential factor is dependent on the concentration of the light absorbing solution. A longer path length makes the detection cell more sensitive to the light-absorbing compound.

Therefore it can be said in general, that an effective detection cell should have a long path length with as little as possible internal reflections. It should also be noted, that the reflectance R as well as the extinction coefficient ε are strongly dependent on the wavelength of the light. The absorbance of the chemical compound of interest (indophenol) has a Gaussian profile with its peak at 590 nm (Figure 4). The reflectance of silicon is finite for most of the visible light (Figure 3, [6], [7]).

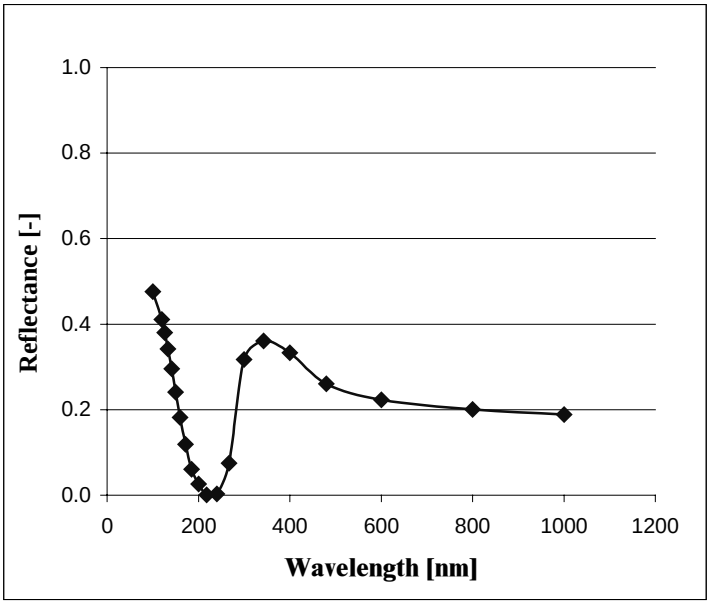

Figure 3: The wavelength dependence of the reflectance of a silicon-water interface. The reflectance is calculated for oblique incidence.

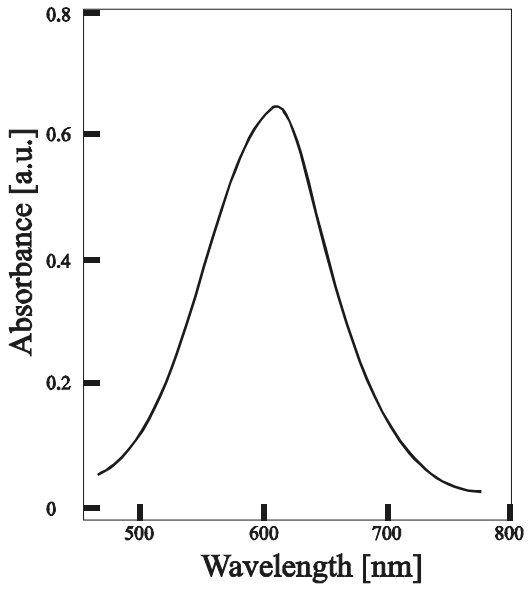

Figure 4: The wavelength dependence of the absorption of indophenol. Reproduced from [8].

The detection cell for the MAFIAS system has to measure the concentration of indophenol-blue, a compound with its absorption maximum at 600 nm. Therefore the light sent into the detection cell should be around this wavelength also for a maximum sensitivity.

6.3 Design – The device

For the actual design of a micro-cuvette, a number of possibilities exist. The cuvette in its simplest form will consist of a silicon wafer with a through hole [9], [10]. The silicon wafer is covered on both sides with a Pyrex wafer (Figure 5).

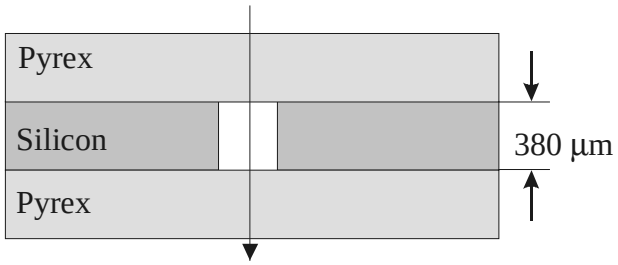

Figure 5: The simplest design of a microcuvette.

The main disadvantage of this type of cuvette is the very short light path that is created. The thickness of the silicon wafer determines the path length, which therefore will be 380 μm. Since this is not long enough for our application, the light path has to be designed such that it is in the plane of the wafer. In this way, any path length within the chip dimensions can be realized. The simplest approach to realize this is shown in Figure 6. The shown design [11-13] uses standard KOH etching techniques to create the channel and mirrors, which are the normal <111> sidewalls resulting from the KOH etching technique.

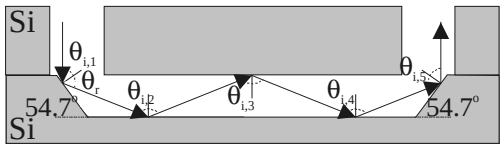

Figure 6: Simplest design for a light path lying in the plane of the wafer.

As is shown in Figure 6, the path the light beam travels within the detection cell has a number of reflections with the detection cell walls. Any of these reflections leaves only about 27% of the incoming light. This means that after 5 reflections only 0.15% of the original light power is left. This would require a very powerful light source. A better option to improve the efficiency of the cuvette is to reduce the number of reflections. This can be accomplished by coupling the light in under an angle ([14], [15], Figure 7). In this way the only reflections are those at the mirror walls at the beginning and end of the light path.

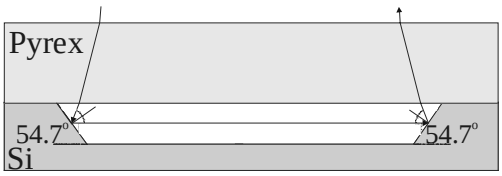

Figure 7: Incoupling of the light under an angle reduces the number of internal reflections.

The disadvantage of coupling the light in under an angle with the wafer surface is, that a change in refractive index of the sample will still result in a situation in which the light will reflect on the side walls of the detection cell. In order to get rid of all the disadvantages of the previous designs, the design as shown in Figure 8 is presented.

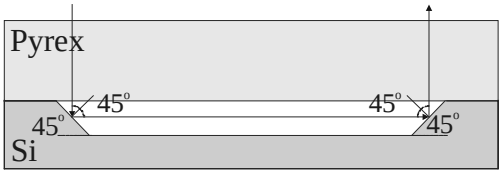

Figure 8: The final cuvette design.

This design cannot be realized with standard KOH-etching techniques. The normally used Si-etchant KOH will only reveal the <111> planes of the monocrystalline silicon. These <111> planes make a 54.7° angle with the surface. The planes that make a 45° angle with the surface are the <110> planes. These can be etched free with adapted etching techniques using KOH-IPA (KOH with IsoPropylAlcohol added to it) instead of standard KOH [17]-[19].

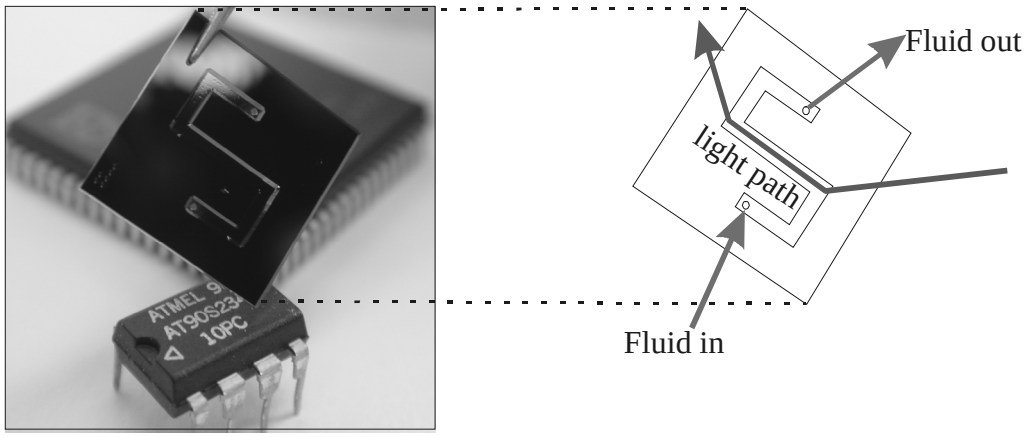

Figure 9: Photograph of a realized detection cell.

6.4 Design - path length

In this paragraph the needed length of the light path in the detection cell will be determined. The concentration range of indophenol that can be expected in the detection cell is estimated. The absorption from this concentration is calculated for a number of different path lengths. The path length at which the whole concentration range can be detected is chosen as the path length for the MAFIAS system.

The absorption for indophenol for a concentration range of 10^{-2}-10^{-5} mol l^{-1} and a path length of 10^{-1}-10^{-4} m was calculated using the software package Maple® (Figure 10). The absorption is calculated for indophenol with an extinction coefficient ε of 0.15×10^{6} l mol^{-1} m^{-1} [20]

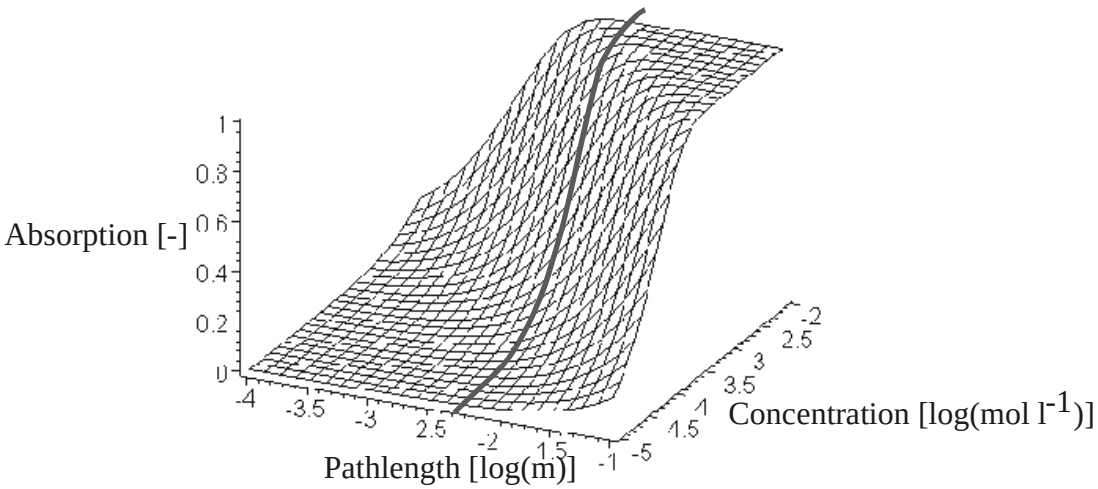

Figure 10: Absorption as function of the Indophenol concentration and the pathlength.

The concentration range that should be covered by the MAFIAS system is 6-600 µmol l^{-1}. In the MAFIAS system, the sample is diluted twice (chapter 2). Also the dispersion effect has to be taken into account (chapter 2). A dispersion of 10 is anticipated. This means that the concentration of indophenol in the detection cell will be in the range of 0.15-15 µmol l^{-1} (0.03-3 mg l^{-1}). From Figure 10 it now can be read that the path length for this concentration range should be about 4 mm. This pathlength guarantees the highest sensitivity in the whole needed range.

Anticipating a somewhat larger dispersion, the path length for the detection cell is chosen to be 6 mm. For this length, the desired concentration range can be detected as well as concentrations half a decade below the desired range.

6.5 Measurements

A number of sample cuvettes with several variations have been fabricated and tested. The variations include different path lengths for the light and covering of the channel with a reflective coating (platinum) to increase the reflection coefficient. All cuvette samples have been constructed such that the fluidic connections are fully interchangeable.

Measurements were performed to check if the detection cell actually could be used for the concentration range it is designed for. A series of indophenol solutions was prepared ranging from 4 µg l^{-1} to 10 mg l^{-1}. The used cuvette had a path length of 6 mm. A LED (light intensity peak at 590 nm, Agilent Technologies) was used as light source. A photodiode (Silonex) was used as the detector. To rule out influences from light from the lab environment measurements were done using an AC-modulated LED in combination with a lock-in amplifier (Stanford SR830) detection both at 1 kHz. Absorption measurements of the lowest and highest concentrations are shown in Figure 11.

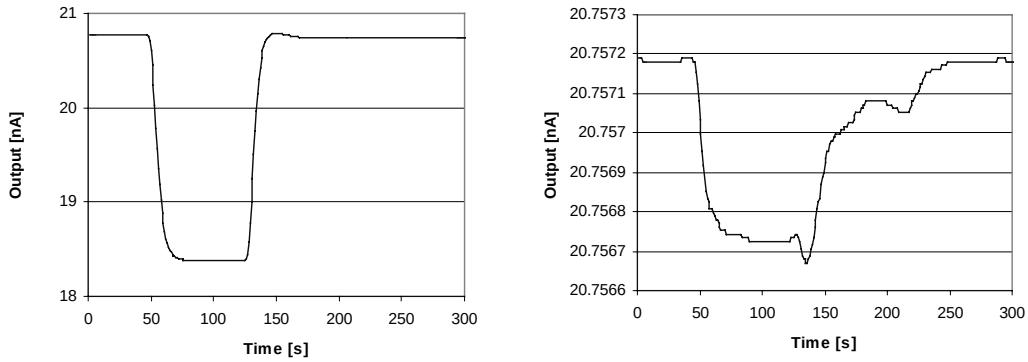

Figure 11: Typical responses from the measurements. The left graph shows the response from a sampleplug from the highest used concentration (10 mg l^{-1}). The right graph shows the response from the lowest used concentration (4 μg l^{-1}).

From Figure 11 it is seen, that the injected sample plug can be detected clearly. The response of the measurement system after the plug has passed the detection cell (clearest seen from the low concentration sample plug) is not understood. It might be an artifact resulting from the actuation of the valve that is used to change from reference fluid to sample fluid.
The results of the whole measurement series are shown in Figure 12.

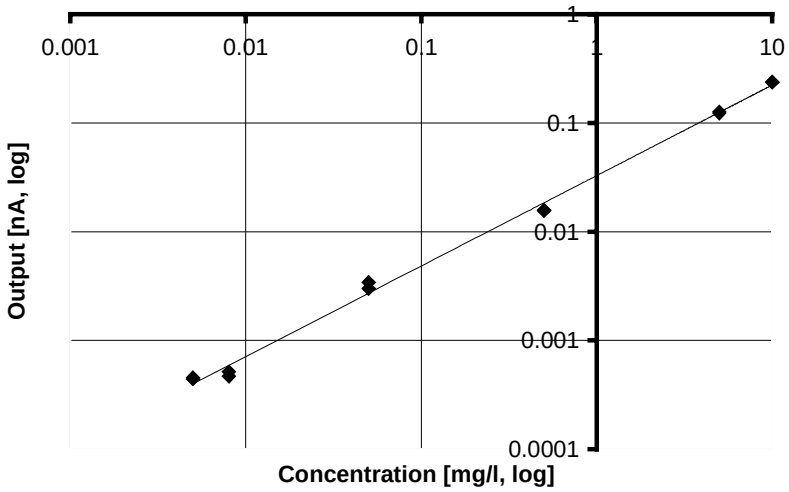

Figure 12: Measured output current as function of the concentration indophenol.

From these figures it is seen that the desired concentration range of 0.03-3 mg l^{-1} can easily be detected. The S/N ratio for the lower measurements lies in the order of 10. Therefore, the detection limit lies around 0.001 mg l^{-1}.

The fitted line in Figure 12 has a slope of 0.83 instead of a slope of 1 as expected from Lambert-Beer law (eq.2). The following reasoning explains this discrepancy.

The indophenol that is added to the water changes the refractive index of the sample with respect to pure water. Since indophenol is a larger molecule than water, the refractive index of the created samples will be larger as the refractive index from pure water [21]. Though the detection cell has been designed such that the lightpath does not alter for changing refractive indices, the reflectance (eq. 4-7) of the silicon sidewalls will be larger for a higher refractive index of the sample. Two effects now influence the intensity of the light that reaches the detector (see Figure 13). First, the light absorbance of the indophenol sample results in a dip in the detector signal. Second, the higher reflectance *R* of the mirrors cause more light to reach the detector, thus making the dip less deep then expected from only the absorbance. Therefore, the output for higher concentrations will be less as would be expected from the linearized Lambert-Beer law (eq.2).

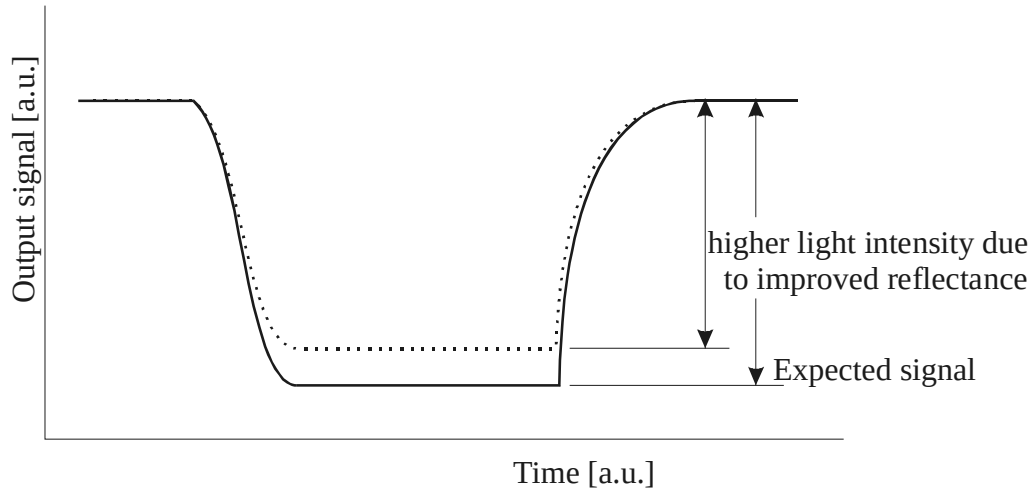

Figure 13 : The output signal is built from two effects. The absorbance causes the dip in the signal, whereas the improved reflectance results in more light reaching the detector.

6.6 Discussion and Conclusions

This chapter has presented the design of a micromachined detection cell for the optical absorption detection of indophenol blue. A number of considerations have to be made to come to an optimum design of the detection cell.

First, the wavelength of the light used as input to the detection cell has to match the wavelength at which the measured compound absorbs light. For a measurement on indophenol blue (absorption peak around 600 nm) red/orange light of that same wavelength has to be used to guarantee maximum sensitivity of the detection cell.

To come to a design with a light path length of more than 400µm, the light path has to be in the plane of the wafer. This introduces some problems for the in- and outcoupling of the light when using standard etching techniques. The 45° sidewalls resulting from KOH/IPA etching of silicon are used as mirrors to couple light into the detection cell. The reflections at the water-silicon interface will result in a light

intensity loss of about 23% at each reflection. The length of the light path in the detection cell is chosen to be 5 mm. For this length the MAFIAS concentration range is fully covered by the concentration range that can be detected with the detection cell.

Measurements have shown that the designed detection cell works adequately. Using a lock-in amplifier at 1 kHz as the control and readout electronics, a chemical concentration-span of more than three decades could be detected. The found concentration vs. output curve is not linear. This is probably caused by a change of the reflectance of the detection cell mirrors as a result of the change in refractive index of the sample due to the dissolved indophenol. This effect will be stronger for higher concentrations. To overcome this, a calibration measurement of the detection cell is needed.

6.7 Literature

[1] A.J. Nijdam, E. van Veenendaal, J. G. E. Gardeniers, A. P. M. Kentgens, G. H. Nachtegaal, M. Elwenspoek, ^{29}Si-Nuclear Magnetic Resonance on the Etching Products of Silicon in Potassium Hydroxide Solutions, Journal of The Electrochemical Society, 147 (6), pp2195-2198, 2000

[2] G. Pandraud, T.M. Koster, C. Gui, M. Dijkstra, A. van den Berg, P.V. Lambeck, Evanescent wave sensing: new features for detection in small volumes, Sensors and Actuators A 85, pp158–162, 2000

[3] A.J. Ricco, S.J. Martin, Multiple-frequency SAW devices for chemical sensing and materials characterization, Sensors and Actuators B 2, pp123-131, 1993

[4] Th. H. Gieling and H. H. van den Vlekkert, Application of ISFETs in closed-loop systems for greenhouses, Advances in Space Research 18, pp135-138, 1996

[5] S.Liu, P.K.Dasgupta, Sequential Injection Analysis in Capillary format with an electroosmotic pump, Talanta, 41 (II), pp1903-1910, 1994

[6] E. Hecht, Optics, 2nd edition, Addison-Wesley Publishing Company, 1987.

[7] D.R.Lide, Handbook of Chemistry and Physics, 80th ed, CRC Press, 1999-2000

[8] T.T.Ngo, A.P.H.Phan, C.F.Yam, H.M.Lenhoff, Interference in determination of ammonia with the Hypochlorite-Alkaline Phenol method of Berthelot, Analytical Chemistry 54, 1981, 46-49

[9] A.Daridon, M.Sequeira, G.Pennarun-Thomas, J.Lichtenberg, E.Verpoorte, D.Diamond, N.F.de Rooij, Comparative Kinetic Studies of the Berthelot Reaction in Microfluidic and Spectrophotometric systems, proceedings Eurosensors XIV, Copenhagen, Denmark, 2000

[10] M.A.Burns, B.N.Johnson, S.N.Brahmasandra, K.Handique, J.R.Webster, M.Krishnan, T.S.Sammarco, P.M.Man, D.Jones,

D.Heldsinger, C.H.Mastrangelo, D.T.Burke, An integrated Nanoliter DNA Analysis Device, Science, vol282 pp484-487, 1998

[11] E.M.J.Verpoorte, A.Manz, H.Lüdi, A.E.Bruno, F.Maystre, B.Krattiger, H.M.Widmer, B.H.van der Schoot, N.F.de Rooij, A silicon flow cell for optical detection in miniaturized total chemical analysis systems, Sensors & Actuators B 6, pp66-70, 1992

[12] D.J. Sadler, M.J. Garter, C.H. Ahn, S. Koh, A.L. Cook, Optical reflectivity of micromachined {111}-oriented silicon mirrors for optical input-output couplers, Journal of micromechanical microengineering, **7**, pp. 263, 1997.

[13] J.E. van der Linden, P.M. De Dobbelaere, P.P. van Daele, M.B. Diemeer, Micromachined photodiode submount with integrated mirror for efficient out-of-plane coupling to planar polymeric waveguide circuits, Japanese Journal of Applied Physics, **37**, pp. 3730, 1998

[14] P.Woias, K.Hauser, E.Yacoub-George, B.Hillerich, A Silicon-based Microreaction System for Analytical Applications, Proceedings IMRET3, FrankFurt, Germany, April18-21, 1999

[15] R.Miyake, K.Tsuzuki, T.Takagi, K.Imai, A highly sensitive and small flow-type chemical analysis system with integrated absorptiometric micro-flowcell, proceedings MEMS 97

[16] M.Elwenspoek, T.S.J.Lammerink, R.Miyake, J.H.J.Fluitman, Towards integrated microliquid handling systems, Journal Micromechanics and Microengineering 4, pp227-245, 1994

[17] L. Rosengren, Silicon microstructures for biomedical sensor systems, PhD. Thesis, Uppsala University, 1994.

[18] C. Strandman, L. Rosengren, H.G.A. Elderstig, Y. Bäcklund, Fabrication of 45° mirrors together with well-defined V-grooves using wet anisotropic etching of silicon, Journal of microelectro-mechanical systems, **4**, pp. 213, 1995.

[19] M. Vangbo and Y Bäcklund, Precise mask alignment to the crystallographic orientation of silicon wafers using wet anisotropic etching, Journal of Micromech. Microeng, **6**, pp. 279, 1996.

[20] P.L.Searle, The Berthelot or indophenol reaction and its use in the analytical chemistry of nitrogen - A review, Analyst 109, pp549-568, 1984

[21] P.W.Atkins, Physical Chemistry, 4th ed., Oxford University Press, p651

Chapter 7 : The monolithic MAFIAS

In this chapter the integration of the various components into one system is presented. First, all components and their respective fabrication technologies are summarized. Subsequently, the used technologies are simplified where possible, and streamlined so that ultimately one technological sequence enables the fabrication of the whole system. Particular attention is paid to the interconnections to the external "macro" world, both in the electrical and fluidic domain. It was found that only the detection cell, because of it's specific 45 degree reflecting planes, could not be realize with the technology of the other components, and therefore had to be integrated hybridly. Finally, the whole integrated MAFIAS was characterized and appeared to give reproducible measurement of ammonium for 10 and 20 mM respectively.

7.1 Introduction

In the preceding chapters of this thesis all theory needed for the MAFIAS system has been discussed. In chapter two the general system design (i.e. which components are needed to form the system), was presented. Chapter 3-6 resulted in specific designs and design rules for these components.

This chapter shows how all these components and design rules are combined into a complete system. First all components are shortly reviewed. After this, the processes needed for the realization of these components are presented and discussed. Then the connections needed to create all interfaces to the outside world are designed. After these preparing steps, the final system can be designed. First the process scheme is discussed, followed by an explanation of the layout of the final system. Finally the system is tested, and the obtained results are shown in the last paragraph of this chapter.

7.2 The components – A review

In chapter two the functional design of the system was given (shown again here in Figure 1).

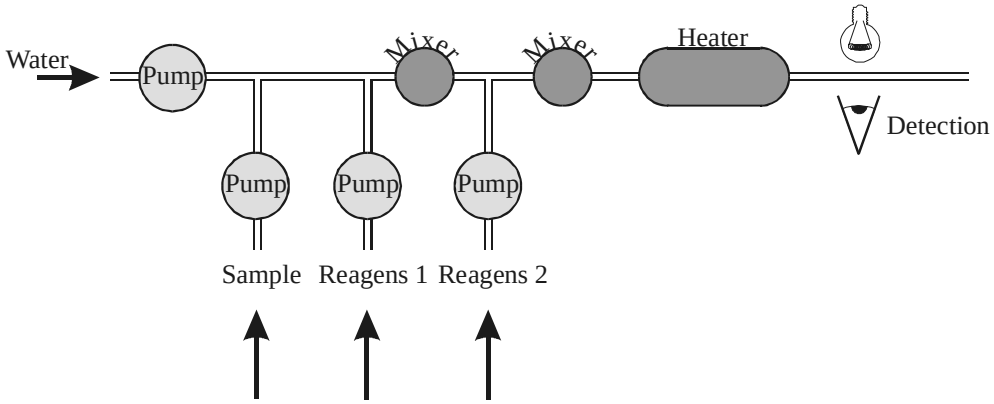

Figure 1: functional design of the system.

The components that are to be incorporated in the system are pumps, mixers, a reaction chamber and a cuvette (light cell). All these components have been treated in the chapters 3-6. A shortlist is presented in Table 1.

Component	Operating principle	Specs
Pumps	Peristaltic	10 µl/min, 70mBar
Mixers	Fast diffusion in narrow channel	Mixing of phenol in 3.3 seconds at a flow rate of 10 µl/min.
Reaction chamber	Long channel with electrical heater next to the channel. Temperature is measured using another resistor.	Temperature controlled at 37°C for 30 seconds.
Detection	Light cell.	5mm path length
Connecting channels	D-RIE etched channels.	200×200 μm^2 cross section
Electrical and fluidic connections	-	See this chapter.

Table 1 : shortlist of the fluidic components in the MAFIAS system.

The following paragraphs will treat the different fluidic components in more detail.

7.2.1 The pumps

The design of the pump is shown in Figure 2. The pumping principle is peristaltic; three pump chambers are located along a channel. Actuation of the three membranes in a specific sequence will result in fluid being propelled along the channel. The peristaltic pump has the property that reversing the actuation sequence will result in pumping action in the reverse direction.

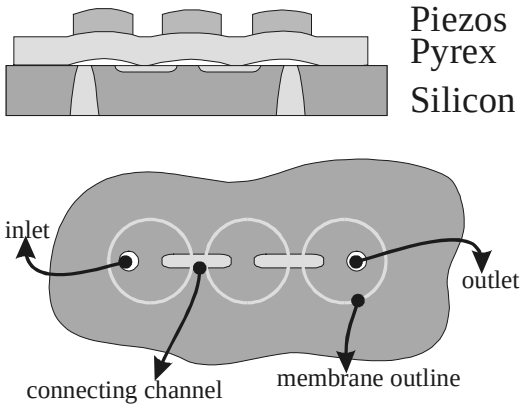

Figure 2: Layout of the micropump.

The pumps have to be capable of producing a net flow such that the whole system can be flushed once a minute. A rough estimate of the internal volume of the system is 10 µl (channels of 200×200 μm^2 with a total length of 25 cm). The pressure drop over a channel of those dimensions at the specified flow rate is about 70 mBar.

Therefore, the pump has to be capable of delivering 10 µl min^{-1} against a pump head of 70 mBar. The pump that has been presented in chapter 5 can meet these specifications, therefore that pump can be used for the MAFIAS system.

7.2.2 The mixers

The laminar flow regime in which microfluidics mostly stay, forces any mixing action to be based on diffusion. To ensure fast mixing, diffusion distances have to be chosen as small as possible. The way to minimize the diffusion distance that is chosen for the MAFIAS mixer is to create a narrow part in the systems main channel (Figure 3). In this narrow part chemicals can diffuse rapidly from one side of the channel to the other side.

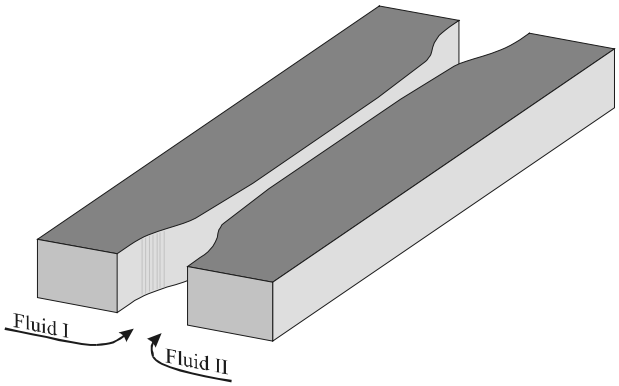

Figure 3: The mixer consists of a channel with a narrow part, in which diffusion is fast.

The width of the narrow part of the channel determines how much time it takes for a given particle to diffuse from one side to the other. The desired flow rate together with the cross-sectional area of the channel determines the needed length of the mixer. Care has to be taken that the geometry is chosen such that the pressure drop over the mixer won't be too high for the pumps to overcome.

The dimensions of the mixer that is to be implemented in the MAFIAS system are chosen as follows. The cross-section of the mixer-channel will be 100 μm wide and 200 μm deep. The mixing time at this width is 3.3 seconds. At a flow rate of 10 μl min^{-1}, the mixer channel has to be 27.5 mm long to keep the fluid the needed 3.3 seconds in the narrow part of the mixer. At these dimensions, the expected pressure drop over the mixer-channel is about 6 mBar.

7.2.3 The reaction chamber

The chemical reaction that has to be performed dictates that for a period of 30 seconds the temperature of the fluid in the system has to be kept at 37°C. This will be done by placing a heating element next to the systems main channel. The generated heat is conducted through the silicon to the walls of the systems channel. Since silicon is a very good heat conductor, the generated heat is distributed evenly over the silicon. Placing the heater on one side of the channel and a temperature sensor at the other side, a fair estimate of the fluid temperature can be made (see Figure 4). Heat diffusion through water (which will be the main fluid in the system) on the scale of 100 μm (the maximum distance that has to be covered in a channel of 200×200 μm^2) takes about 50 msec. Therefore it can be said, that if the temperature sensor measures a temperature of 37°C, the temperature of the fluid will indeed be at 37°C.

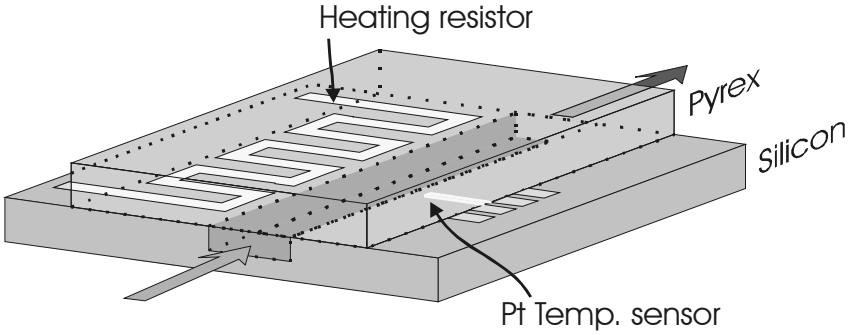

Figure 4: 3-D view of the reaction chamber of the system.

To increase the chemical resistance of the reaction chamber, the bottom wafer will be covered with a SiO_2 layer.

7.2.4 The optical detector

After completion of the chemical reaction converting ammonia into indophenol blue, the concentration of indophenol has to be measured. This will be done in a light cell (cuvette). Since a light cell with a path length of more than 1 mm is needed, a design had to be chosen with the light path in the plane of the wafer. Coupling light in and out of the light cell is done by using the sidewalls of the channel as mirrors.

The design used for the MAFIAS system is etched in KOH/IPA, which results in sidewalls making a 45° angle with the surface of the wafer (Figure 5). The reflection of light on a silicon surface under these conditions is such that only 25% of the incident power is reflected. Since the number of reflections is reduced to only two, the light efficiency is about 6%.

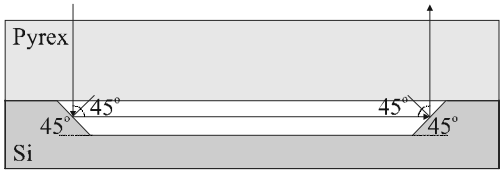

Figure 5: Cross-sectional view of the MAFIAS optical detector design.

The path length in the light cell together with the extinction coefficient of the chemical compound determines the concentration range that can be measured. The chosen length of 5 mm corresponds to a concentration range of 0.03-3.00 mg/l indophenol, corresponding to an initial ammonia concentration of 0.1-10 mg/l (dispersion is taken to be 10, dilution due to addition of reagent is 4).

Care has to be taken choosing the light source for the optical detection: the emission spectrum of the light source has to cover at least part of the absorption spectrum of the compound to be detected. The chemical compound indophenol blue has to be detected in the MAFIAS system. The absorption spectrum of indophenol has a peak at 610 nm. Therefore the light source to be used should be in this range also. A LED with output at 590 nm is used in the systems optical detector [Agilent Technologies]. This LED has sufficient overlap in the light spectrum with the absorbance peak to meet the specifications.

7.3 The components – Combining all processes.

In the previous paragraph all the components needed to build the microfluidic ammonium detection system were shown. These components have been realized separately and were proven to work [chapters 3-6]. Now these components have to be integrated into a monolithic realization.

Since all fabricated components were realized in a two-wafer stack, the monolithic design can probably be designed in a two-wafer stack also. Table 2 gives an overview of the different components as they were designed as standalone components.

In order to make the different process schemes compatible with each other, a closer look has to be taken to the reasons for the differences in the process schemes.

Table 2 shows that the fluidic channels for the four components are created using four different fabrication techniques. For the pump and the reaction chamber, the form of the cross-section of the channels is not important. Thus, for these components either the D-RIE used for the mixer or the KOH-IPA used for the detection cell can be used. The D-RIE etching technique is chosen because it allows a more flexible planar design of the channels.

The SiO_2 layer that is applied to the reaction chamber is a necessary feature. This layer has to prevent short-circuiting of the electrical wires on the Pyrex to the silicon. This SiO_2 layer can also be applied to all other devices without interfering with their functionality.

Pump	**Reaction chamber**	**Mixer**	**Detection cell**
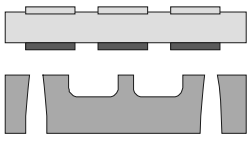	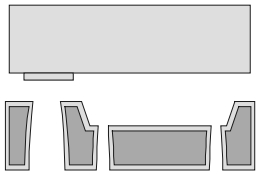	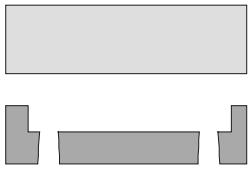	
Powder blasted channels	KOH-etched channels	D-RIE etched channels	KOH-IPA etched channel
Powder blasted through holes	Powder blasted through holes	Powder blasted through holes	Powder blasted through holes
Chromium anti-bond layer on bottom side of Pyrex	Platinum layer on bottom side of Pyrex for heating element and temperature sensor		
Platinum layer on top-side of Pyrex for electrical contacts for piezos	SiO_2 layer on Silicon wafer to prevent shorting of the Platinum layer		
Pyrex wafer is thinned to match the thickness of the piezodiscs			

Table 2: Comparison of the design of the different components.

The Pyrex wafer that is used for the pump membranes must be thinned down for proper pump operation. In order to maintain sufficient stability of the whole integrated system, it is decided to maintain the original Pyrex thickness for the other three components, and to thin down the Pyrex only locally, at the position of the micropumps.

The described changes can be implemented in the design of the different components, as illustrated in Table 3. At this point the process schemes of the different standalone devices are compatible enough for the devices to be integrated onto one wafer. Unfortunately the process scheme of the detection cell cannot be synchronized with the scheme of the other components since the sidewalls needed for the detection cell have to be at a 45° angle with the surface.

Pump	Reaction chamber	Mixer	Detection cell
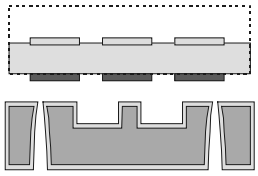	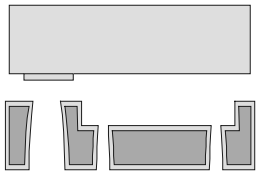	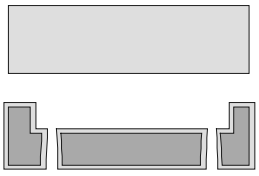	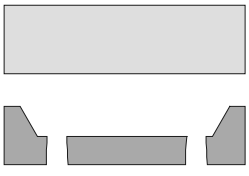

Table 3: The process schemes of the pump, reaction chamber and mixer as standalone devices have been synchronized.

Since the processes of the pump, reaction chamber and mixer now are compatible, these components can be combined into one layout. The result is shown in Table 4.

Pump	Reaction chamber	Mixer	Detection cell
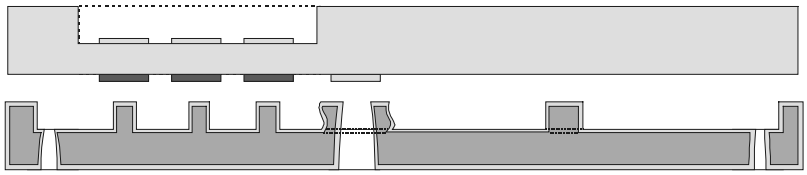			

Table 4 : The process schemes of the pump, reaction chamber and mixer are combined into one design.

Though the design as shown in Table 4 is feasible, one more change is made to the design. By moving the through holes for the electrical and fluidic connections to the top side of the wafer, all connections to the systems are available at the top side of the chip (see Table 5). This makes handling of the system much easier.

Pump	Reaction chamber	Mixer	Detection cell
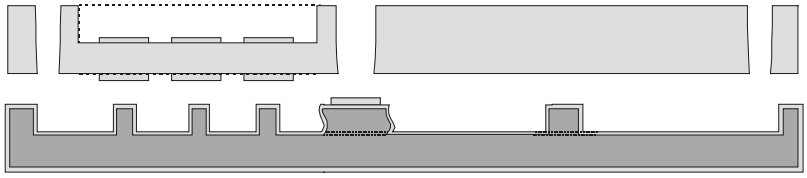			

Table 5: The through holes for the connections are moved from the bottom to the top wafer. Therefore the Platinum resistor layer for the reaction chamber has been moved to the bottom wafer.

The detection cell cannot be integrated in an efficient way into the systems design. It will therefore be fabricated separately and glued or bonded onto the system.

Rearranging the layout of the system as shown in Table 5 and placing the detection cell on top makes the system look as in Figure 6.

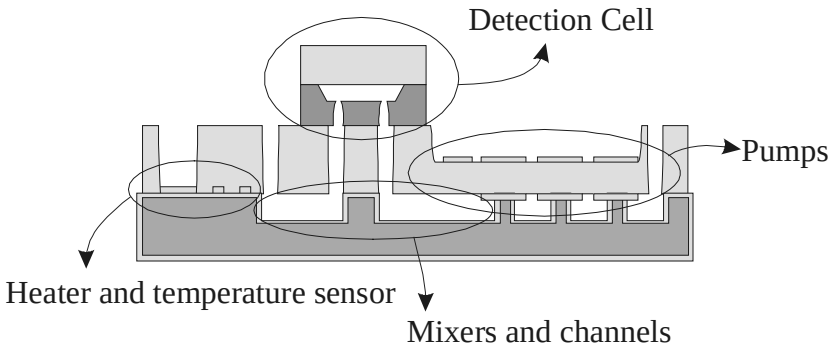

Figure 6: The cross-sectional view of the completed system.

So far the cross-sectional design of the system has been presented. The next paragraph will describe the connections that are used to link the chip to the outside world.
Though the detection cell has been drawn onto the main chip, the connection between the main chip and the detection cell might as well be implemented using separate pieces of tubing.

7.4 Connections to the macro world.

Interconnections to the outside world are essential for proper operation of the integrated system. Electronics are needed to control the reaction chamber and the pumps, and fluids have to be able to enter (and exit) the system. Though electrical and/or fluidic connections are needed for almost any device, no standard connection method exists. The considerations and solutions that are made for the connections for the MAFIAS system are discussed below. Since the realized chip is intended to be a prototype, it is considered of importance to end up with connections that can be disconnected rapidly and easily. This includes that all connections preferably should be on one side of the chip design: either all on the topside or on the bottom-side. This ensures that all connections on the chip are easily accessible and eventually will lead to easier packaging of the chip.

Electronic circuits have to be connected to the chip to change the chip from a piece of structured silicon into a working system. For small chips this is usually done using wire-bonds, a very fragile, one-time electrical connection which needs only little space on the chip. The chip is mounted on a macro carrier (often printed circuit board, PCB) and the wire bonds are created between the chip and this plate (Figure 7). Mostly these wire bonds are protected by covering the whole wire in glue. Further connections are made from the carrier plate.

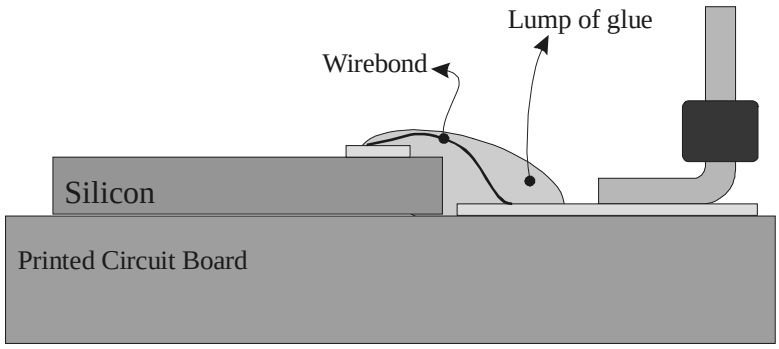

Figure 7: Principle of a wire bond electrical connection.

Since the MAFIAS chip is going to be a very large chip (one pump measures app. 4 cm^2, whereas four pumps are needed), the argument of saving chip space does not hold here. Therefore a more straightforward solution is chosen: the electrical connections will be made using standard PCB headers, soldered to the chip itself (Figure 8), instead of soldering these to the PCB. This method has proven to be very robust and reliable.

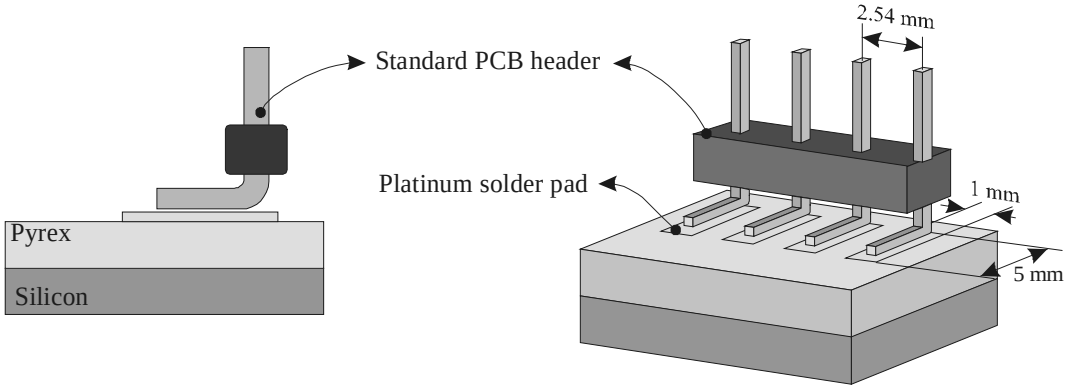

Figure 8: Standard PCB headers are soldered to the chip.

Creating high quality fluidic connections to any microfluidic system is demanding task. Most of the used methods come down to gluing a plastic or Perspex connection block to the fluidic chip [1,2]. This method is also used for the MAFIAS chip. A Perspex block with the .062 fluidic connecting system of The LEE® Company [3] will be used. This system consists of one part with threading being assembled on the tubing to the system whereas the threaded counterpart is glued to the chip (Figure 9). The The LEE Company connection system is used since it has a low dead volume and because it results in a mechanically strong link between the tubing and the system.

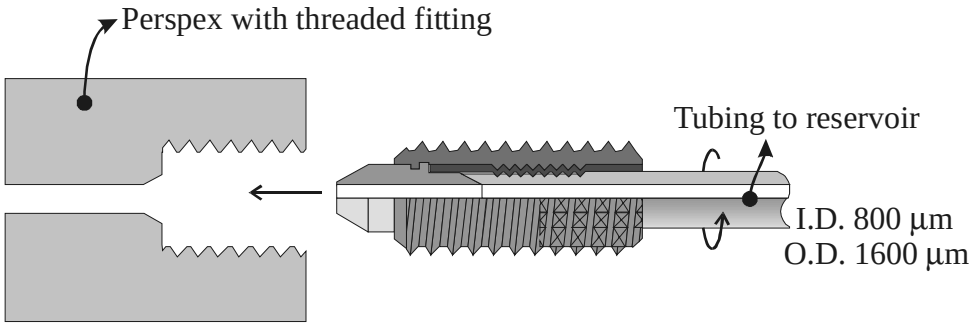

Figure 9: Schematic of the The LEE® company fluidic connection system.

It is found that a good connection is obtained when using a CNC controlled drilling machine to make the hole and thread in the Perspex® block to connect to the tubing. This Perspex® block is then glued to the wafer surface with an epoxy glue, resulting in a leak-free bond. To enforce the mechanical strength of the bond between the Perspex and the chip, the edge of the wafer/wafer interface is covered with an epoxy glue (Figure 10).

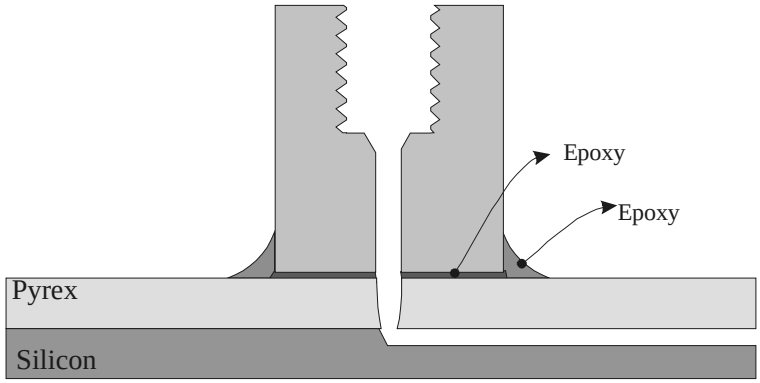

Figure 10: Connection of the wafer block to the wafer.

After describing the fabrication process of the system and the connection methods, the planar layout of the system will be shown.

7.5 The system – The design of the layout

In the previous section the process steps for the MAFIAS system were defined. This section shows the actual geometry of the different layers and how they all result in the final system. The chip design is made for a 4" (10 cm) wafer. The wafer-border is shown in all figures to give a reference for the size of all structures.

First the largest components will be placed on the wafer. The anti-bonding membranes (∅11mm) of the pumps are placed as shown in Figure 11.

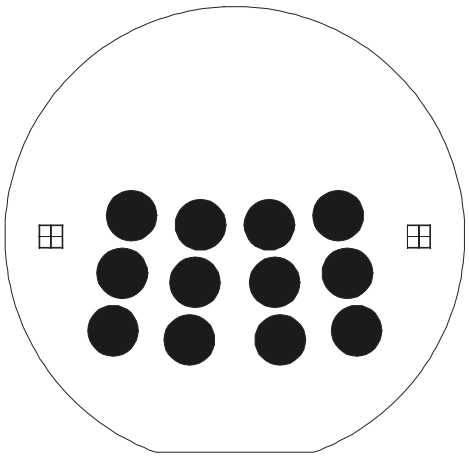

Figure 11: Placement of the anti-bond circles defining the pump membranes.

Four pumps are defined by each three membranes in a row. The pumps are placed under a slight angle with respect to each other in order to leave some space for electrical leads to the electrodes for the piezos.
The layout of these electrodes together with the solder pads for the connecting headers is shown in Figure 12. The 3D impression shows how the piezo will fit on the bottom electrode circle, as well as how the top-electrodes of the piezos are to be soldered to the electric leads. Soldering a wire from the top electrode to the leads on the wafer is an easy and reliable method of electrically connecting the piezo to the leads to the connector. The electric leads are made of platinum and are 400 μm wide and 100 nm thick.

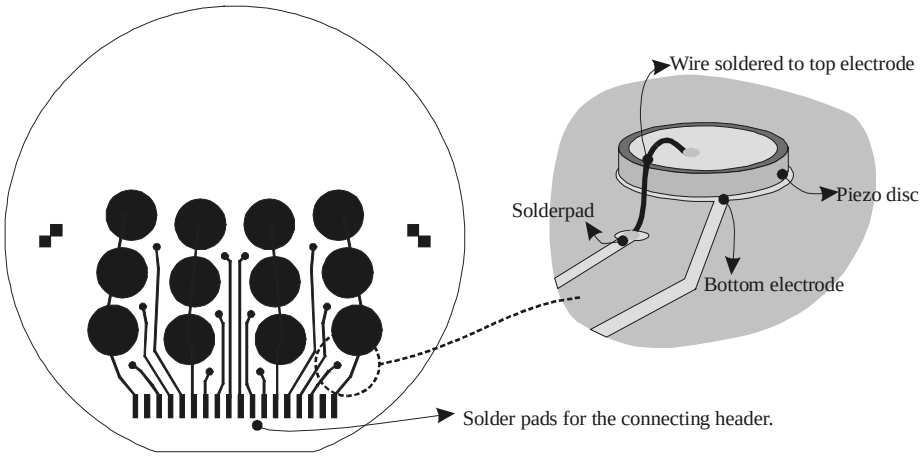

Figure 12: The layout of the electrodes for the piezodiscs.

The Pyrex top-wafer has to be thinned down to match the piezo-thickness in order to maximize the stroke volume of the pump membranes. The part of the Pyrex with the pump membranes is exposed to HF in order to be thinned down. A time-stop is used to define the thickness of the membranes. The part of the top wafer that is exposed to the HF etchant is indicated in the figure below.

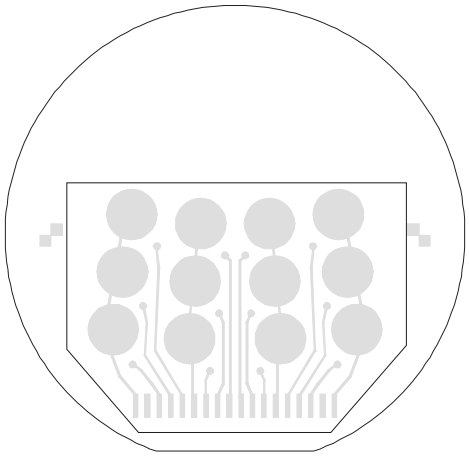

Figure 13: The part of the top wafer that will be etched is indicated with a black line. The electrodes are shown in gray for clarity.

Since the pumps are bi-directional, the in-/outlets can be chosen on either side of the pumps. A special Perspex® block is fabricated consisting of 5 fluidic The LEE® Company .062 connections (Figure 14). The inlets are drilled in one line and are spaced 6 mm. This block is to be glued on the wafer as shown in Figure 15. Four connections will be used as inlets, whereas the remaining connection will be the outlet of the system (waste).

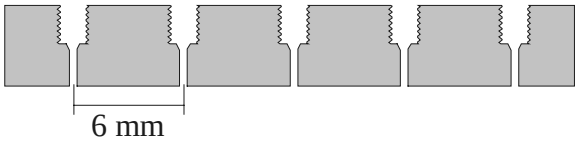

Figure 14: The connection block.

The most left pump uses the 2nd fluidic connection (carrier). The 2nd pump will be for the sample input. The 3rd pump then has to propel the first reagent into the system. Since the sample and the reagent have to be mixed at this point, a mixer structure as discussed in chapter 3 is inserted here. The last pump is for the second reagent. After insertion of the second reagent another mixer is needed. The mixer ends in the reaction chamber, which is a channel with a total length such that the fluid will stay in the channel for 30 seconds (12.5 cm channel length at 10 µl/min). Where the reaction chamber channel ends, an outlet has to be fabricated on top of which the detection cell can be mounted. The outlet of the detection cell then connects to the last piece of channel, which connects to the remaining fluidic connection.
All channels are 200 µm deep. The channels in the system are 200 µm wide; the channels from the inlets to the pumps and from the detection cell to the outlet all are 300 µm wide.

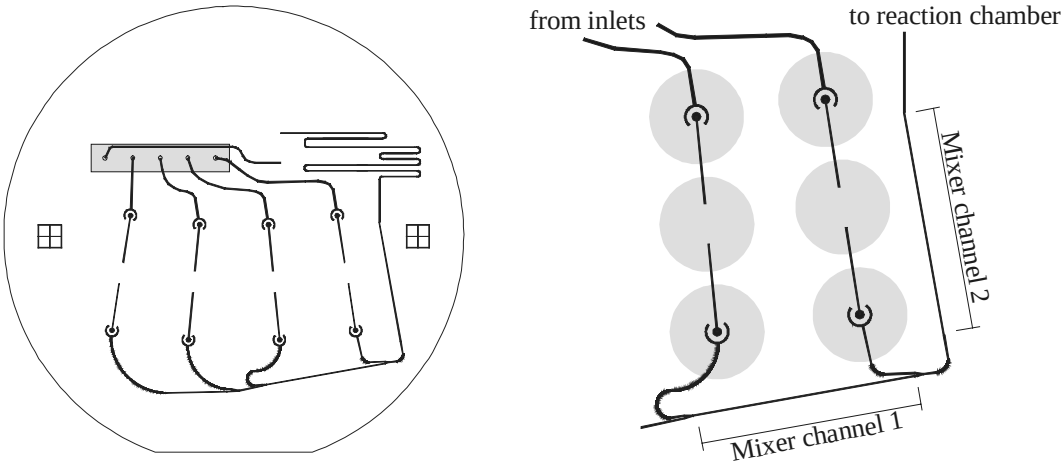

Figure 15: The channel layout of the system. The block left above is the fluidic connection block. The inset shows some details on the channels under the pump as well as the mixers.

The heater and sensor as described in chapter 4 will now be implemented. The temperature sensor will be a resistor of about 4 kOhms with double leads to be able to do a four-point resistance measurement. The heater resistor is designed to be 60 Ohms. The connections for these resistors are made in a similar way as for the connections for the pumps.

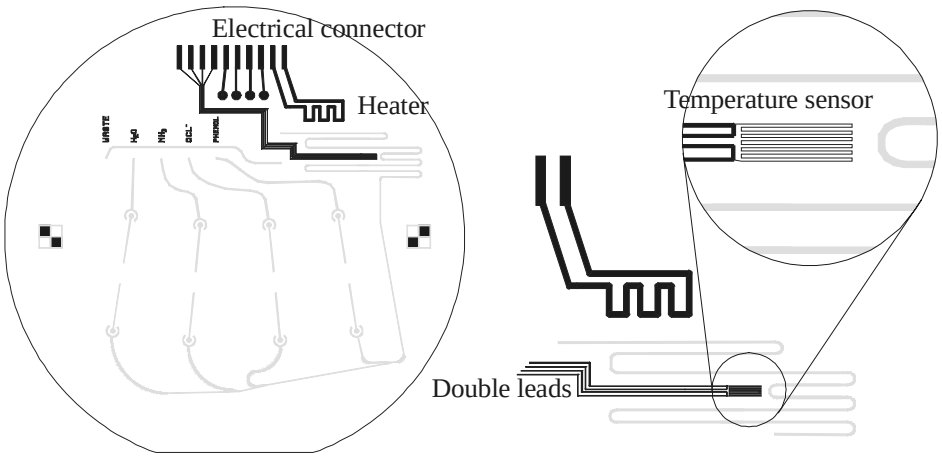

Figure 16: The heater and temperature sensor layout. The channel structure is shown in gray for clarity.

The four leads from the connector to the small circles are similar to the solder connections for the top electrodes of the piezo discs (see Figure 12). Here these solder connections will be used for the light source and detector for the detection cell.

The last process step involves the creation of through holes in the top wafer. These holes are made by so-called powder blasting. Since this technique can create holes only up to a certain aspect ratio [4], the mask can be designed such that –next to the through holes- smaller holes are created which do not reach the bottom side of the

wafer. These holes then can be used as alignment marks for the fluidic connection block as well as for the detection cell, which have to be glued to the topside of the wafer. The dimensions of the connection block are 30×6 mm^2, the detection cell will be 12×12 mm^2. A large hole will be created to be able to access the contacts for the heater and temperature sensor resistors.

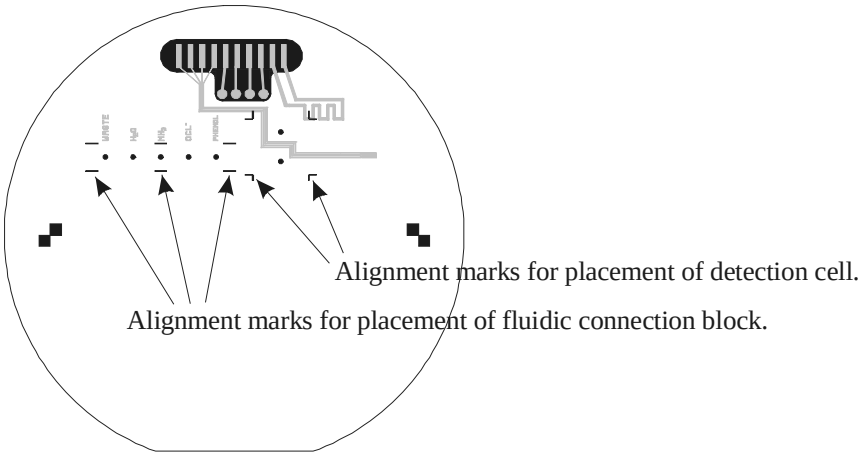

Figure 17: The powder blasted structures on the top wafer in black. The heater and sensor resistances are shown in gray for clarity.

Figure 18 shows the complete layout of the system on a one-to-one scale.

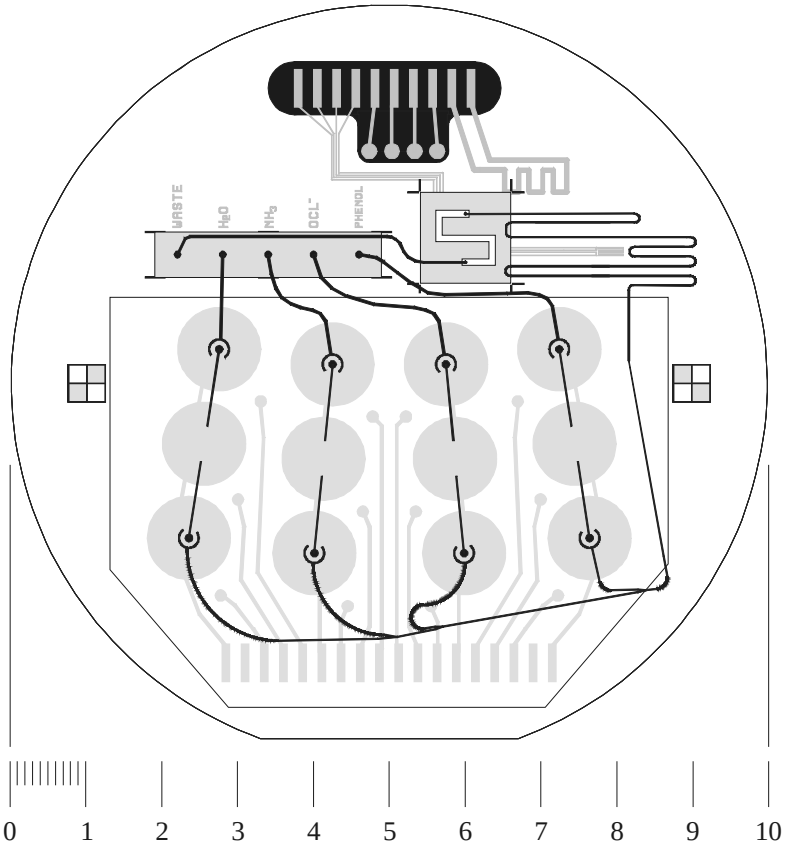

Figure 18: The whole system layout. The diameter of the chip is 10 cm.

Figure 19 shows a photograph of the fabricated system as it is after completion of the process steps. The piezo elements, the light cell and fluidic connections all are mounted to the chip.

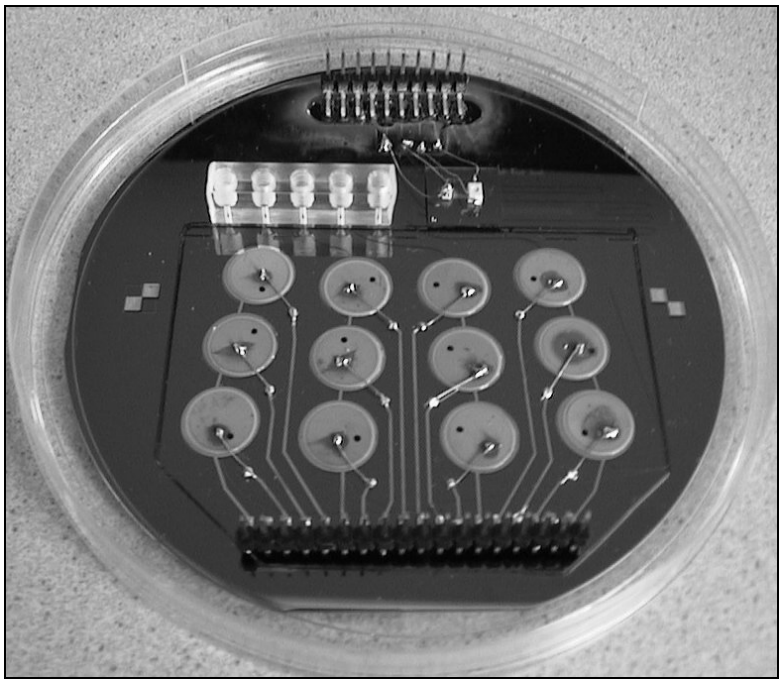

Figure 19: Photograph of the completed system.

7.6 The system – Characterization.

The system as shown in Figure 19 has been tested. The used setup is schematically shown in Figure 20. Every fluidic inlet is coupled through a 1 µm-filter to a small container. These containers initially are filled with the flush-fluid, but will later on be refilled with sample and reagent. All electric connections are led to the control electronics by using flat cable.

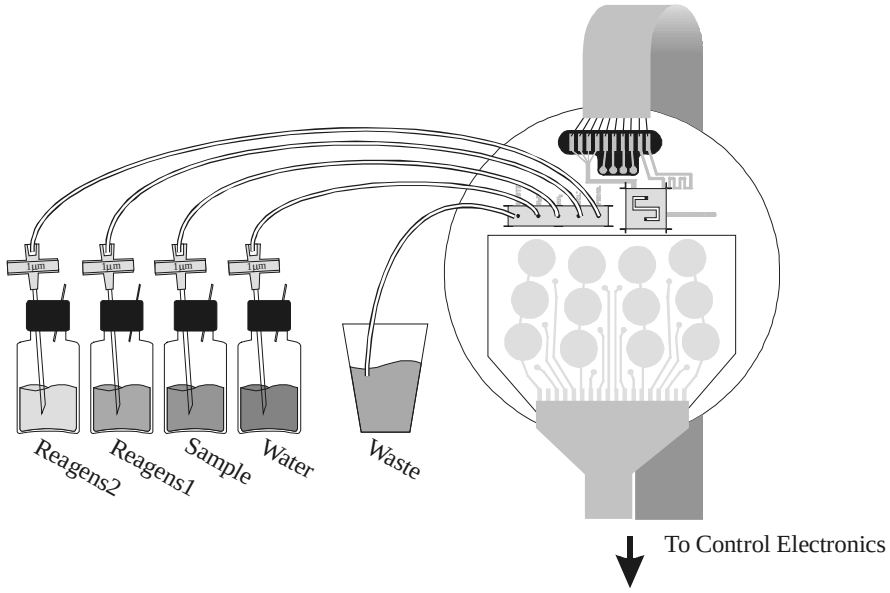

Figure 20: setup used to test the MAFIAS chip.

The first step in the testing procedure is to fill the whole system with the flush-fluid (ethanol or water). The fabricated chip easily primed itself with ethanol. All four pumps were able to suck-in the fluid and pump it through the whole systems main channel within one minute. Unfortunately, the anodic bond between the silicon and the Pyrex wafer failed after the ethanol had been in the system for a day. Figure 21 shows that the bond between and around two membranes has released, resulting in failure of the pumps.

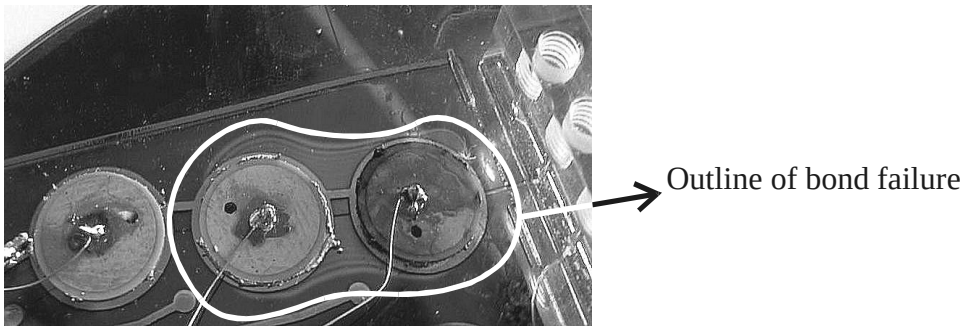

Figure 21: Photograph of the anodic bond after priming with ethanol. The newton rings indicate a gap between the silicon and Pyrex wafer.

The only principle difference with the stand-alone pumps was the silicon-oxide layer in between the silicon and the Pyrex. Therefore it is concluded that either the silicon-oxide layer cannot withstand ethanol or that the silicon-oxide to Pyrex bond is not as strong as a silicon to Pyrex bond.

Circumventing the bonding problem, a new chip was made. This time without the silicon-oxide layer on the silicon wafer. Since the silicon-oxide layer was needed to prevent short-circuiting of the electrical heater and temperature sensor through the silicon, the heater and temperature sensor were left out. The heating of the chip now is done by a thermal pad [5], whereas the sensing of the temperature is done using a standard Pt-100 element.

Using the chip in the described configuration a small series of experiments have been performed.

First, a number of plugs containing only hypochlorite or phenol have been injected, to ensure that the response of the light cell to these chemicals is known, and can be recognized later on. After this, a plug of ammonia was injected to which both reagents were added. This was repeated a number of times. After this, a series of ammonia plugs of only half the initial concentration were injected. Finally, the pump speed was varied to give the samples more time to complete the Berthelot reaction.

The resulting readings from the detection cell are shown in the following figure. First the two reagents were led through the system. The resulting peaks are labeled ‘phenol’ and ‘hypochlorite’. Next, two identical samples containing approximately 10 mM of ammonium were led into the system followed by addition of the two reagents. The resulting peaks are almost identical. The last two peaks are from ammonia samples of approximately 20 mM, and show a two times higher response.

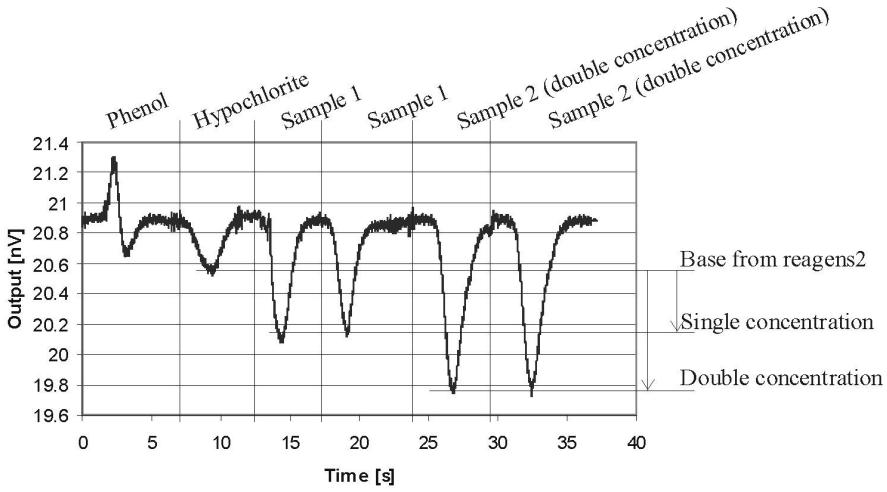

Figure 22: The readings from the detection cell while the different plugs are pumped through the system.

From the measurements shown in Figure 22 it is clear that the readings from the ammonia (which has been converted into indophenol) can easily be distinguished from the readings of phenol or hypochlorite.

The readings from the ammonia samples are combined from the reading from the first and second reagent as well as the reading from formed indophenol. From the first two injected plugs (reagents 1 and 2) a base-signal can be obtained. The additional signal that is seen during the measurement results from formed indophenol. From the injected ammonia sample plugs it is concluded that the reading due to indophenol corresponds to the injected amount of ammonium.

The ‘noise’ on the signal results from the pulsed pumping action. The light cell is attached to the main chip by using rubber rings. A pressure wave through the systems

channel results in a little tilt of the detection cell, which translates into the reading as a modulation on the output signal with the same frequency as the pumping frequency.

7.7 Discussion and Conclusions.

In this chapter the design of the layout of the MAFIAS system has been shown. From the process steps of the respective designs of the separate components the needed process steps for the final system were deduced. It was found, that the detection cell and the mixer cannot be made with the same etching techniques. The mixer channel is based on having straight sidewalls, whereas the detection cell needs 45° sidewalls for the in- and out coupling of light. Therefore the choice was made to fabricate the detection cell separate from the rest of the system. The detection cell can be added on to the system by gluing it to the system chip or using intermediate tubing.

Using standard PCB headers for the electrical connections and The LEE Company 0.062" fluidic connections will make the connections to the macro world. These last connections will be realized in a Perspex block, which is glued to the main chip. The headers for the electric connections will be soldered to the main chip. This will ensure fast and failsafe connections.

After the Process scheme was deduced, the actual physical layout of the system was determined. The first elements placed on the chip were the pump membranes and the electrodes for the pumps piezo-electric elements. Knowing the placement of the pumps, the channel structure of the system was planned. The fluid inlets are placed near each other so as the fluidic connections can be created in one piece of Perspex. The heating element and temperature sensor are connected to the outside world with the same type of header used for the pumps. The heater is placed on one side of the channel, the temperature sensor to the other side. The temperature sensor is connected with double leads to enable a four-point-measurement of the sensors resistance.

The placement of the external components (fluidic connections, light cell) is indicated by placement marks. These marks are created in the same powder blast process step as the creation of the through holes.

Testing of the chip as described so far, showed that the anodic bond between the silicon and Pyrex wafer was not strong enough to withstand the forces due to the bending of the membrane. This resulted in the failure of the anodic bond, causing the pumps not to work any more. The probable cause for a weak bond was the intermediate silicon-oxide layer. A second chip was fabricated without this oxide layer. Since the oxide layer was used to prevent the heater and temperature sensor from short-circuiting through the silicon, these two components were replaced by macro-versions.

A number of tests were performed on the system. It is seen that a sample plug with converted ammonia can clearly be distinguished from the readings from the separate reagents. It is also seen that a higher ammonia concentration results in a larger signal.

Though the results are preliminary, it can be concluded that the MAFIAS system works. Ammonia is actually converted into indophenol *on the chip*. The system therefore can be called a Full Lab on a Chip indeed!

7.8 Literature

[1] W.K.Schomburg, R.Ahrens, W.Bacher, J.Martin, V.Saile, AMANDA – surface micromaching and diaphragm transfer, Sensors and Actuators **76** (1999), pp 343-348

[2] G.Fuhr, T.Schnelle, B.Wagner, travelling wave-driven microfabricated electrohydrodynamic pumps for liquids, J.Micromech. Microeng. **4** (1994), pp217-226

[3] The LEE Company, Westbrook, Connecticut, USA

[4] H.Wensink, J.W.Berenschot, H.V.Jansen, M.C.Elwenspoek, High resolution powder blast micromachining, in Proc. 13th Int. Workshop Micro Electro Mechanical Systems (MEMS2000), Miyazaki, Japan, January 23-27 2000, pp769-774

[5] Jimi Heat, http://www.jimiheat.com

Chapter 8 : Selective Anodic Bonding

This chapter describes selective anodic bonding, a technology specially developed to realize peristaltic micropumps without dead volume. It was found that with the use of very thin (< 1nm) metallic anti-bonding layers a selective bonding was obtained. As mechanism for the selective bonding the absence of electrostatic attraction in case of the presence of such a thin metallic layer on Pyrex was proposed. It was found that the inability for oxygen ions to reach the silicon wafer results in either the development of oxygen gas at the interface or the oxidation of the intermediate layer.

8.1 Introduction

This chapter describes the investigations that were performed to come to a deeper understanding of the process of anodic bonding and in particular the process of selective anodic bonding. The first process is used to create a strong connection between a glass and silicon wafer, whereas the latter is used to prevent locally the formation of such a bond. Using this technique enables the user to create structures in silicon, which can be sealed from the environment using the simple and robust technique of anodic bonding, without causing those structures to be stuck to the glass wafer.

An article was written on the findings on the selective anodic bonding. This chapter contains a reprint from that article.

---

* T. T. Veenstra, J. W. Berenschot, J. G. E. Gardeniers*, R. G. P. Sanders, M. C. Elwenspoek, and A. van den Berg, Use of Selective Anodic Bonding to Create Micropump Chambers with Virtually No Dead Volume, *Journal of The Electrochemical Societ*y, **148** (2) (2001) G68-G72

Use of Selective Anodic Bonding to Create Micropump Chambers with Virtually No Dead Volume

T. T. Veenstra, J. W. Berenschot, J. G. E. Gardeniers,* ,z R. G. P. Sanders, M. C. Elwenspoek, and A. van den Berg

MESA+ *Research Institute, Transducers Technology Lab, University of Twente, 7500 AE Enschede, The Netherlands*

Membrane micropump chambers of 11 mm diam with virtually zero dead volume were realized using selective anodic bonding.The selective bonding was achieved with less than 1 nm thick metallic antibonding layers on the glass wafer. Experiments were carried out to come to a better understanding of the selective anodic bonding process. It was concluded that a conductive antibonding layer on the glass wafer prevents the formation of a bond, because in that case the electrostatic attraction between the Pyrex and silicon wafers will vanish upon contact. Chromium and Platinum were found to be suitable antibonding layers. Furthermore, it was found that during the anodic bonding process, the transport of oxygen ions from Pyrex toward the silicon-Pyrex interface results in the formation of SiO_2 , which forms the actual bond between both substrates. At positions of an intermediate antibonding layer the oxygen ions form oxygen gas. The Pyrex or silicon substrate may deform locally due to the buildup of oxygen gas pressure. This can be prevented by adding a gas outlet to the design.

Anodic bonding of Si to (Pyrex or similar types of) glass is a widely used process in the fabrication of micromechanical structures. Especially in the field of microfluidics, it is often used for tight sealing of cavities. The application discussed in this paper is the use of selective anodic bonding to define pump membranes on a Pyrex wafer.

An important factor for optimal functioning of membrane micro-pumps is the ratio of the membrane stroke volume over the dead volume of the micropump (DV/V_0 , see Fig. 1). This ratio determines whether the pump will be able to pump gas, will be self-priming, or will be bubble tolerant.[1] The most important contribution to the dead volume of the micropump generally is the volume directly under the pump membrane (the pump chamber). Although it is not the only contribution to the dead volume, an as small as possible pump chamber is highly desirable. In this paper, we discuss a selective bonding method to achieve micropumps with virtually no volume under the pump membrane.

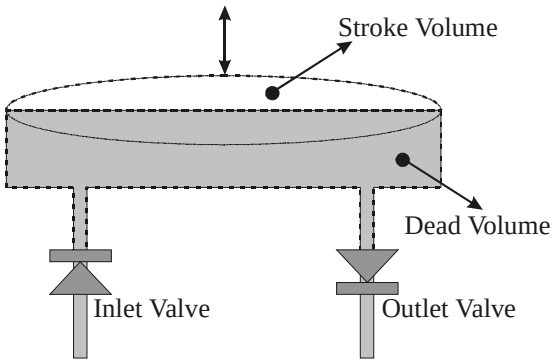

Figure 1. Schematic of membrane pump, describing the parameters mentioned in the text.

Experimental

It has been reported in literature that on locations where Cr patterns on Pyrex are present, bond formation between the Pyrex and Si is prevented, while bonding is perfect anywhere else on the wafer pair.[2-4] In order to test the suitability of this selective antibonding method for the creation of relatively large pump membranes, a num-ber of explorative experiments were

performed. These experiments proved the suitability of the method, but raised questions about the selective bonding mechanism, as it is known from literature. Therefore, the mechanism of selective anodic bonding technique was in-vestigated in somewhat more detail.

The experiments were performed on a typical anodic bonding setup. The Si (380 mm thick, 3 in. p-type <100>, resitivity 5-10 V cm) and Pyrex wafers (500 mm thick, 3 in., Corning) were placed on a hot plate which was kept at 425°C. A voltage of 500 V was applied across the Si/Pyrex package, using a point electrode as a cathode on the Pyrex and the hot plate as the anode that is in contact with the Si wafer. A temperature as high as 425°C is known to result in a relatively high mobility of the ions in the Pyrex, which causes the Pyrex to have a finite conductivity *(ca.* 10 Ω cm).[5] The high voltage across the Pyrex-silicon package is needed for two reasons: *(i*) to close the gap between the Si and the Pyrex, allowing intimate contact and stable bond formation,[6] and *(ii*) to create a high electric field in the Pyrex, which will drag sodium ions (intrinsic constituents of the Pyrex glass) toward the outer glass surface and oxygen ions [Whenever in this paper we speak about oxygen ions, the reader should be careful that it has not been clarified completely yet whether oxygen transport in Pyrex is by oxygen ions or by OH^- ions (see Ref. 7); these ions are either intrinsic constituents of the glass or present because of water absorption into the glass] toward the Si surface (Fig. 2), where they react with silicon, probably in an anodic oxidation process,[7] to silicon dioxide (SiO_2) that forms the actual bond.[8-12] Metal patterns were deposited by radio frequency magnetron sputtering through shadow masks. The metal layer thickness was measured with grazing-incidence X-ray diffraction, GIXRD (Cu Ka radiation, Philips PW3710). Surface profiles were measured with a Sloan Dektak 3030 mechanical surface profiler or with a Promap Optical Profiler.

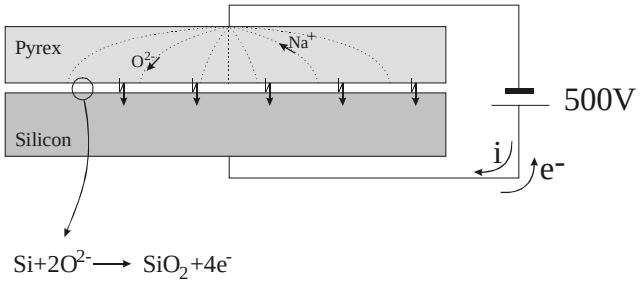

Figure 2. Ion movement during anodic bonding with point electrode.

Results and Discussion

For the first experiment, we patterned a Pyrex wafer with an 11 mm diam Cr circle with a thickness of *ca.* 5 nm. After anodic bonding of the Pyrex wafer to a Si substrate, it was seen that the silicon and Pyrex had bonded perfectly, except at the Cr patterns where no bonding occurred at all. By visual inspection, a large number of interference fringes were seen at these positions, indicating a large void between the Pyrex and the Si. Such interference fringes are generally considered to be indicative of local nonbonding. Measurement of the Pyrex surface profile revealed a 9.6 mm deflection of the Pyrex. This deflection decreased to 7.5 mm after a hole was scratched through the Si into the cavity (Fig. 3), indicating the presence of pressurized gas in the cavity. The experiment was repeated with a Cr layer with a thickness of only a few monolayers (measured with GIXRD) on the Pyrex. Again, the patterned region did not bond to the Si.

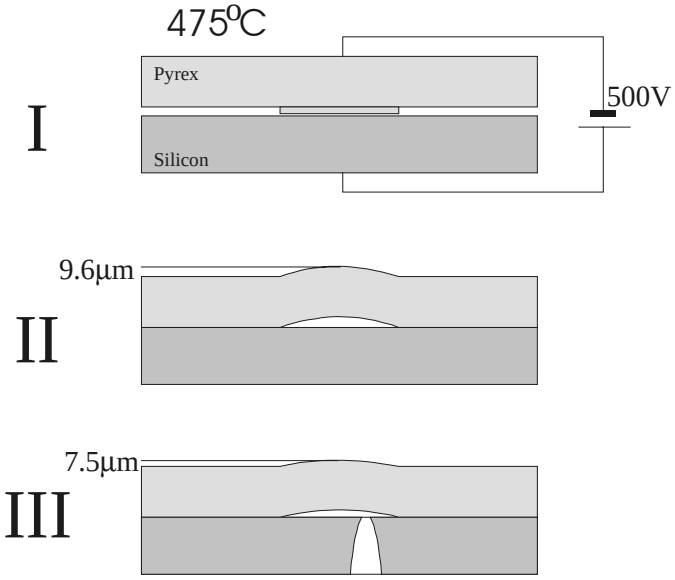

Figure 3. I. Starting situation; II. after selective bonding process; III. After scratching holes through the Si to open the cavities.

From these experiments it is easily concluded that anodic bonding is prevented at those locations where Cr is deposited at the Pyrex. It was speculated that formation of gas (presumably O_2 [13]) results in a pressure buildup underneath the membrane and caused the large deflection of the Pyrex. The experiment was repeated with an Al intermediate layer *(ca.* 25 nm) and with a Pt intermediate layer *(ca.* 25 nm). It was observed that Pt also prevents the formation of a bond, however, the Al circle bonded perfectly to Si. During the Al experiment, it was seen that when the bond front reached the Al, the bond front proceeded around the Al circle without a change in velocity. The bonding of the Al circle itself lagged behind (Fig. 4).

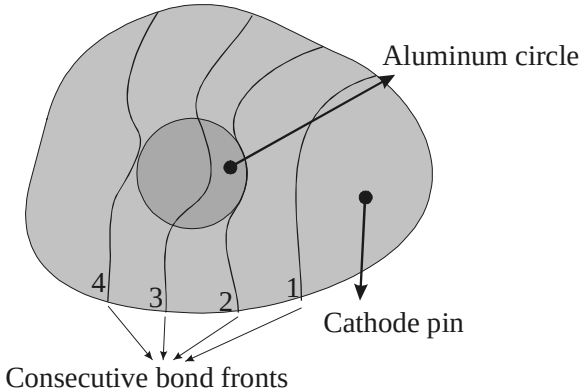

Figure 4. Figure showing bonding fronts during bonding of Pyrex with Al pads.

From the experiments so far one important thing that can be concluded regarding the antibonding mechanism is that the prevention of a bond is not caused by blocking the transport of oxygen ions toward the Si. This can be concluded from the fact that a very thin Cr layer (which can be considered permeable for oxygen at the conditions investigated) already prevents the formation of a bond, whereas a (relatively) thick layer of Al did not prevent a bond. The next set of experiments consisted of multiple membranes on one wafer, all located at a different distance from the needle cathode. In the first experiment, the Pyrex wafer was patterned with Cr circles and bonded to a bare Si wafer. It was observed that the membranes closest to the cathode showed the largest deflection after the bonding procedure (Fig. 5). The

second experiment was similar, except that the Si wafer had holes at those places where the mem-branes on the Pyrex were defined. The result of this experiment was that no deflection of the membranes could be detected (Fig. 6). From the first of this set of experiments, it was concluded that the strength of the electric field at the location of the membrane determines how much the deflection of the membrane will be relative to the other membranes. This makes sense, since the drift of oxygen ions is proportional to the electric field strength, so that underneath the membranes further away from the cathode pin, less oxygen gas is formed. Experiments in which the voltage on the electrodes was varied showed similar results, *i.e.*, a higher voltage gives rise to a larger deflection. The second experiment confirms oxygen formation. Any formed gas can escape from underneath the membrane into open air, so that no pressure is built up underneath the membrane and the membrane will not bulge out. Going back to the earlier experiments, it can now also be concluded that the de-flection is partly due to an elastic deformation (in the earlier experiment the deflection decreased after the overpressure was released through a hole through the Si into the cavity) as well as a plastic (permanent) deformation.

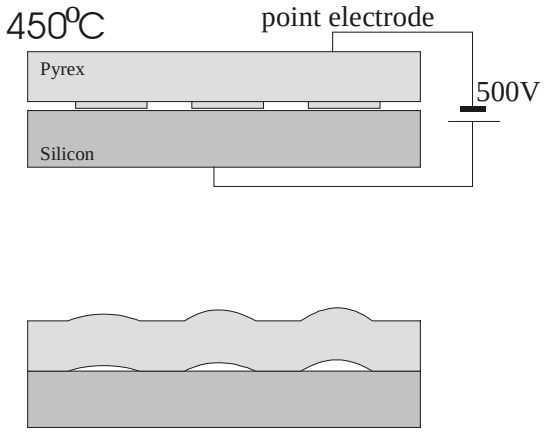

Figure 5. Bonding process with point electrode.

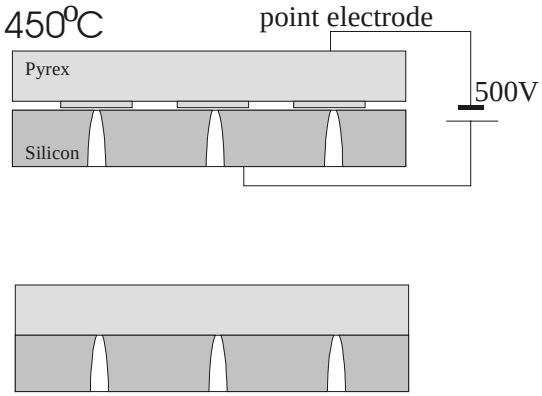

Figure 6. Bonding of Pyrex wafer with dicing cuts to Si partially covered with Cr.

The last set of experiments was performed to gather information on the amount of Si converted into SiO_2 during the bonding process. First, a 1 × 1 cm Pyrex was structured with parallel dicing cuts (the dicing cuts were 50 mm wide and spaced 150 mm). The bonding process was stopped after a total charge of *ca.* 0.1 C had been transferred. After the bonding process, the Pyrex and formed SiO_2 were etched away in 50% HF. The resulting surface profile now shows deep ditches (~ 30 nm) at the edges of the dicing cuts. At positions where the wafers had been bonded, the Si surface turned out to be 7 nm deeper than at regions where the Si had not been bonded, indicating that at these positions the Si indeed was oxidized during the experiment (Fig. 7 and 8). Mack and co-workers [9,13] also reported a step in the Si at

the edge of the glass sample after removal of the glass, but did not mention the relatively deep trench along the edge, probably because they only investigated the profile at the edge of a relatively large piece of glass bonded on Si (see Fig. 4 in Ref. 9), and not, as we did, a number of adjacent glass stripes bonded on Si. The experiment was repeated with an identically structured Pyrex wafer completely covered with a sputtered Cr layer. Again, after the transfer of a total charge of *ca.* 0.1 C, the bonding process was stopped. This time, the Pyrex did not bond to the Si at all. After oxide removal, again ditches were observed at the edges of the glass stripe structures, indicating the formation of SiO_2 : however, in this case, the ditches are only 4 nm deep instead of the 30 nm measured in the previous experiment, while at the positions where previously 7 nm of oxide was found, now no trace of oxidation was found. It might be that the 4 nm ditches in this case have arisen from oxida-tion by residual water of oxygen gas in the diced areas; this oxida-tion is locally enhanced by high electric fields *(i.e.*, at the sharp edges where the glass is in contact with the Si. This set of experiments has clearly shown that during the bonding process, oxygen (whatever its exact form may be, either O^{2-} or OH^{-} [7]) is transported towards the Si where it reacts to form SiO_2 .At the edges of the dicing cuts in the Pyrex, more Si is consumed than at the center of a bonded plane. We speculate that the mechanism causing this effect is the following: oxygen ions from the glass above the dicing cuts follow the electric field lines when they are pulled toward the Si and reach the Si it by drifting along the side of the dicing cut. Since at the edges of the dicing cuts the electric field lines can be expected to be more dense, a higher flux of oxygen ions per unit surface area of Si results at the positions where the cut edges contact Si, leading to a higher oxidation rate at these posi-tions. Definite and quantitative conclusions can however only be drawn when exact calculations of the electric field lines are per-formed. Note that the ditches mentioned above were only observed in cases where a sharp Pyrex edge touches the Si surface, in cases where the Pyrex is flat. In cases where the Pyrex is with or without chromium patches on it, such effects were never observed.

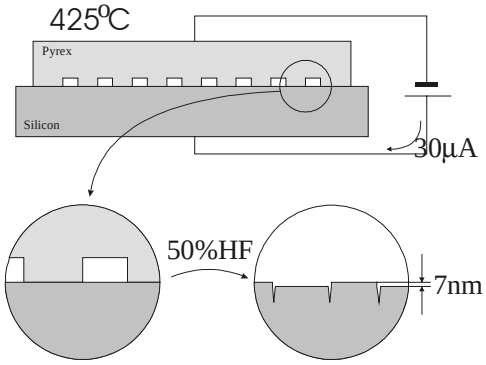

Figure 7. Procedure and final result of bonding experiment with dicing cuts (see text for details).

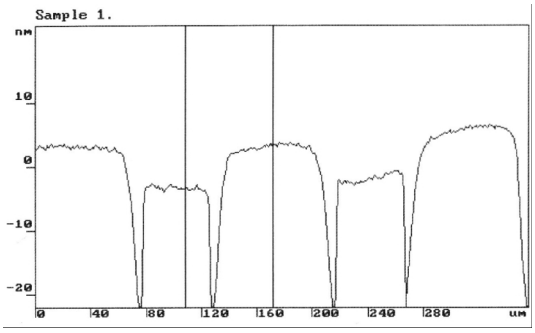

Figure 8. Surface scan of silicon surface after removal of the bonded Pyrex.

Proposed Bond-Preventing Mechanism

On the basis of the results from our experiments, we propose the following mechanism for the selective anodic bonding technique. The intermediate conducting layer causes the electric field be-tween both wafers to disappear as soon as the conducting layer makes contact with the Si. Without an electric field, at these locations, oxygen ions cannot be dragged from the glass to the Si surface to form silicondioxide while in contact with the other substrate. We think that the latter is an essential requirement for bonding to occur between the two wafers, *i.e.*, if there is no intimate contact between the two wafers when oxidation of the Si occurs, no bond will form. Without intimate contact, the oxygen ions will either react with the intermediate layer, oxidizing it, or form oxygen gas (Fig. 9). This theory seems to be in harmony with the experiment which showed that thin, *e.g.*, 10 to 20 nm, of Al does not act as an anti-bonding layer. We speculate that at the start of the experiment the Al layer removes the electric field, just like the Cr layer did, but as soon as the Al becomes oxidized completely, which oxidation gradually proceeds starting from the side where the Al layer is in contact with the glass, it does not conduct any more. This is in contrast to Cr, which according to several materials data handbooks will form only conductive oxides, and Pt, which does not form an oxide at all under these conditions. When oxidation of the Al layer is complete, the glass wafer will bond to the Si wafer. This is seen from the experiment in which the bonding front was observed to lag behind when it crossed over the Al circle: it takes a short period of time to completely oxidize the Al. When oxidation is finished, the local electric field between Si and the Pyrex is restored, and the now oxidized Al layer will bond.

The oxidation of an Al layer during bonding has also been reported by Schmidt *et al.*[7] In our experiments we also observed that if a relatively thick (100 nm or more) Al layer is used, no bonding is observed between the Al and the Si, because during the time span needed to complete the bonding process on uncovered regions of the wafer pair, the Al layer is not allowed to oxidize completely.

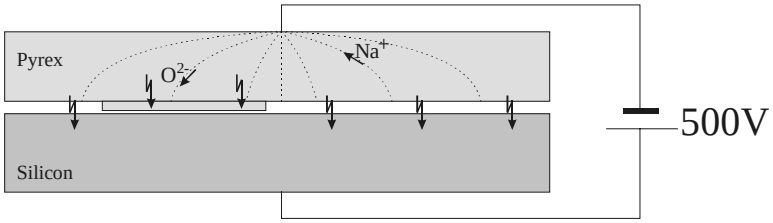

Figure 9. Schematic drawing of expected electric field lines and ion drift

Application

The Pyrex pump membranes were made directly on the Si with virtually no gap. The membranes were defined by patterning the Pyrex with a conductive layer (Cr or Pt). This technique allowed us to create a pump membrane which introduces a minimal dead volume, the only dead volume in the pump now originates from the used valves. The resulting stroke volume/dead volume ratio for our micropump is about 0.25, whereas a minimum of 0.08 is necessary for bubble-tolerant pumping.[1] Using the just described procedure, a peristaltic pump was realized (Fig. 10). The Pyrex wafer was patterned with three membranes, which were connected by two powder blasted channels.[14] An inlet and an outlet are created by powder blasting holes through the Si wafer. The membranes are activated by piezodisks glued on top of the membranes (Fig. 11 and 12). The only dead volume present in this pump is formed by the connecting channels. Experiments on the pump have shown that the pump in-deed can displace fluid with gas bubbles in it. A maximum pressure of 500 mBar could be built up. At that pressure, the Pyrex membranes broke. The maximum flow rate that the pump could reach was measured to be 9 mL/min.

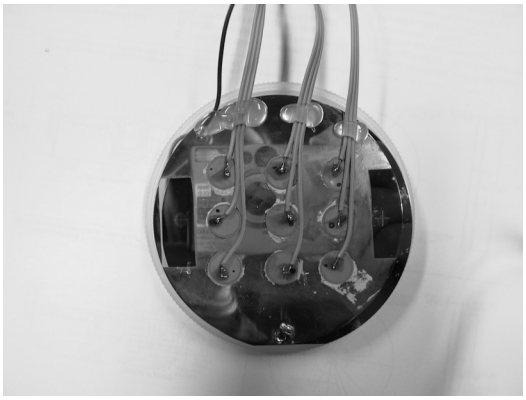

Figure 10. A picture of three completed micropumps, parallel to one another on a 3 in. substrate. The membranes are located underneath the piezo-discs.

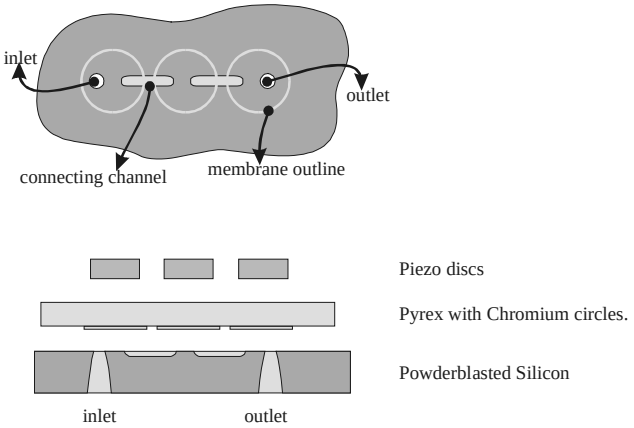

Figure 11. The fabrication process of the peristaltic micropump.

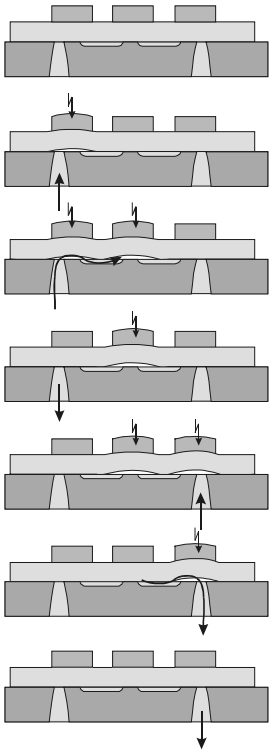

Figure 12. The working principle of the peristaltic micropump.

Conclusions

From the performed experiments, a number of conclusions can be drawn. The formation of SiO_2 and O_2 indicates that oxygen ions play an important role in the anodic bonding process. At positions where the oxygen ions cannot reach the Si, oxygen gas is formed or the intermediate layer is oxidized. It was seen that the local strength of the electric field determines how much oxygen is dragged out of the Pyrex. Further away from a point cathode the electric field is weaker, and consequently, less oxygen is formed. An intermediate conducting layer prevents oxygen transfer from the Pyrex to the Si and subsequent formation of SiO_2 , because it prevents the intimate contact between the two wafers during oxidation of the Si occurs, which is essential for bond formation. The intermediate layer has to be conductive throughout the whole bonding process. If the intermediate layer becomes oxidized, this oxide has to be conductive in order to prevent the formation of a bond. Both Pt and Cr work very well as antibonding layer, since Pt is not affected by oxygen, and chromium oxide is conductive. Al however, does not function as an antibonding layer, since the formed aluminum oxide is an insulator. As soon as Al oxidation is finished, bonding will proceed. The thickness of the antibonding layer is not critical. A thickness of only a few monolayers is already enough to locally remove the electric field between glass and Si.

With the aid of selective anodic bonding, a peristaltic micropump was realized. Since the dead volume in the micropump is very low, the micropump is capable of pumping against high pump heads. To further increase the pumping performance, the volume of the con-necting channels should be minimized, leading to an even higher pump head.

Acknowledgments

The authors greatly appreciate the financial support by the Dutch Technology Foundation (Stichting Technische Wetenschappen, STW), project no. TEL 3467. The tribology group at the Department of Mechanical Engineering of the University of Twente is thanked for performing the surface profiling measurements with the ProMap Optical Profiler (phase shift interferometry).

The Research Institute for Micro Electronics, Materials Engineering,Sensors & Actuators assisted in meeting the publication costs of this article.

References

1. M. Richter, R. Linneman, and P. Woias, *Sens. Actuators A,* **68**, 480 (1998).
2. D. Y. Sim, T. Kurabayashi, and M. Eshashi, *J. Micromech. Microeng.,* **6**, 266 (1996).
3. M. A. Huff and M. A. Schmidt, Paper presented at the Solid State Sensor and Actuators Workshop, Hilton Head Island, SC (1992).
4. T. R. Albrecht, Ph.D. Thesis, Stanford University, CA (1989).
5. E. Obermeier, in *Semiconductor Wafer-Bonding: Physics and Applications III*,C. E. Hunt, H. Baumgart, S. S. Iyer, T. Abe, and U. Gosele, Editors, PV 95-7, p. 212, The Electrochemical Society Proceedings Series, Pennington, NJ (1995).
6. G. Wallis and D. I. Pommerantz, *J. Appl. Phys.,* **40**, 3946 (1996).
7. B. Schmidt, P. Nitzsche, K. Lange, S. Grigull, U. Kressig, B. Thomas, and K. Herzog, *Sens. Actuators A,* **67**, 191 (1998).
8. A. Cozma and P. Huers, *J. Micromech. Microeng.,* **5**,98(1995).
9. H. Baumann, S. Mack, and H. Munzel, *Semiconductor Wafer Bonding: Physics and Applications III*, C. E. Hunt, H. Baumgart, S. S. Iyer, T. Abe, and U. Gosele, Editors, PV 95-7, p. 471, Electrochemical Society Proceedings Series, Pennington NJ (1995).
10. T. Rogers, *J. Micromech. Microeng.,* **2**, 164 (1992).

11.H. Henmi, S. Shoji, Y. Shoji, K. Yoshimi, and M. Eshashi, *Sens. Actuators A*, **43**,243 (1994).
12.T. Rogers and J. Kowal, *Sens. Actuators A*, **46-47**, 113 (1995).
13.S. Mack, Ph.D. Thesis, Jena, Germany, 1998 (in German).
14.H. Wensink, J. W. Berenschot, H. V. Jansen, and M. C. Elwenspoek, in *IEEE Proceedings of the 13th International Conference on Micro Electro Mechanical System*s, MEMS 2000, pp. 769, 774, Jan 23-27, 2000.

Chapter 9 : A microfluidic Compliance Structure

This chapter describes the design and realization of a micromachined compliance structure. The working of the compliance structure is based on the compression of a bubble of trapped air. First the response of the compliance is modeled. It is found that the dimensions of the channel in which the airbubble is trapped determine the frequency response of the compliance. Though dynamic measurements could not be done, it has been shown, that the compliance statically behaves as expected. The compliance has been integrated with a micropump. Measurements have shown that the performance of this pump is improved with a factor of four.

9.1 Introduction

This chapter describes the design and realization of a microfluidic compliance structure. A fluidic compliance is a system that takes up fluid as the pressure in the system rises. It is mostly used to dampen pressurewaves through a system in order to smoothen the flowrate in time. The research for this the compliance device was conducted at the University of Washington (Seattle, Washington) at the micropump lab of Prof. F.K.Forster.

An article is composed on the findings of the designed and fabricated compliance structure.

---

[*] T.T.Veenstra, N.R.Sharma[†], F.K.Forster[†], J.G.E.Gardeniers, M.C.Elwenspoek, A.van den Berg, The Design of an In-Plane Compliance Structure for Microfluidical Systems, submitted to Sensors and Actuators B (21-3-2001)

The Design of an In-Plane Compliance Structure for Microfluidical Systems

T.T.Veenstra, N.R.Sharma[†], F.K.Forster[†], J.G.E.Gardeniers, M.C.Elwenspoek, A.van den Berg
MESA[+]-research institute, Transducers Science and Technology Group, University of Twente, PO box 217, 7500 AE Enschede, The Netherlands
[†] University of Washington, Mechanical Engineering Department, Campus Box 352600, Seattle, WA 98195-2600, USA

Abstract

Two compliance structures for the use in liquid based microfluidic systems have been realized with the aid of silicon micro-machining (Figure 1). The basic principle is that these structures contain airbubbles, that dampen the flow and pressure variations that may arise from a micropump. The compliance structures were specifically designed to work with the NMPV (No Moving Parts Valve) pump [2]. The structures were modeled and simulated. From the results of these simulations and the model, design rules for the compliance are formulated.
Measurements on the compliance structures could only be performed for the steady state. These measurements were in very good agreement with the model. Working with two sets of pumps showed that pumps without the compliance structure needed an external compliance in order to get them to work, whereas the pumps with the on-chip compliance pumped right away.

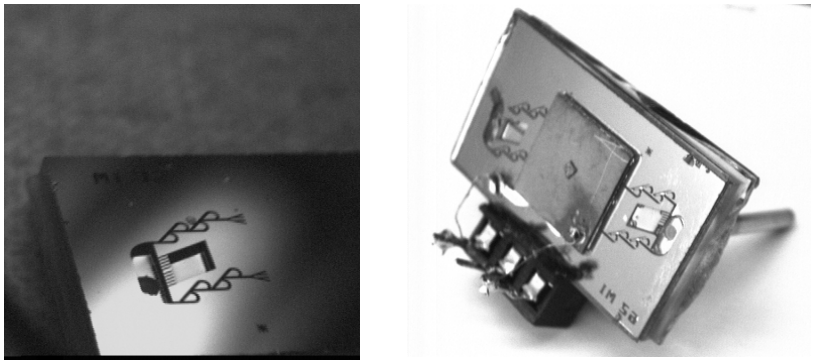

Figure 1 : Photographs of completed devices. A : standalone compliance. B : compliance combined with micropump.

Keywords

Microfluidics, compliance, pumps, micropumps, liquid

Introduction

Since in microfluidics most pumps are membrane pumps, the flow resulting from micro pumps will be pulsed in some sort of way [4-7]. Problems arising from this pulsed flow are summarized in [8]. For a micropump with checkvalves the flow will look more or less like a rectified sine. A pump with hydrodynamic valves (as the NMPV pump (No Moving Parts Valve pump)) produces a sinusoidal flow with an offset, resulting in a net flow. The

variations around this net flow are easily 5 times as large as the net flow itself. If there would be no compliance in the fluidic system, the flow variations would have to be present throughout the whole system, i.e. the whole column of fluid would have to be displaced. This would require a very strong membrane actuation and would very probably result in cavitation of the pumpchamber. The incorporation of an additional compliance directly before and after the micropump can solve this problem. The flow variations are taken up by the compliance whereas the net flow can go into the main fluidic system. Up to now, a macro-compliance was used to get the NMPV pump working.
In this paper we present a micromachined compliance, which consists of an airbubble trapped in a side branch of the main liquid transport channel.

Basic design

The actual compliance is formed with trapped air. The basic idea is that the compressible air bubble will dampen pressure pulses in the liquid stream. We designed two types of air traps. Both designs are shown in Figure 2. The first layout is designed to trap airbubbles in the far ends of the numerous narrow channels. The second layout consists of one large chamber next to the main channel.

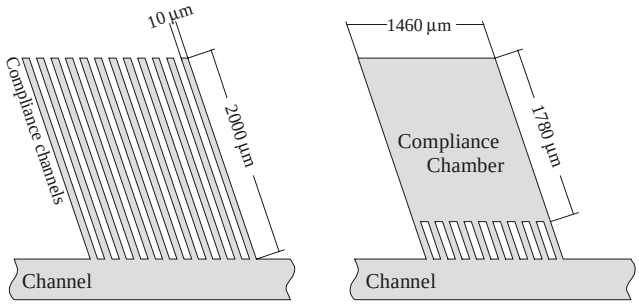

Figure 2 : The layout of the realized samples. The first layout consists of parallel channels, the other of a single chamber with multiple inlets.

Both structures were filled partly due to the surface tension which brings the fluid into the chamber or side-channel. This causes the pressure of the air in the structure to rise slightly. A pressure fluctuation in the main channel causes fluid to flow in (and out) the side structure. The fact, that due to the surface tension some fluid is stored in the side-channel makes both positive and negative flow variations possible.

For large flows into the compliance, the compliance does not act linearly. Since the air pressure will be raised due to the incoming fluid, the effort that is needed to get fluid into the compliance will increase.

Modeling

The static and dynamic behaviour of the compliance structures are modeled. From the full equation of motion, a steady state solution is derived. After this, the dynamic response of the system is calculated from the linearized system. For the compliance structure with the large chamber, a complete solution as for the little side-channel was not found. This is due to the fact, that the shape of the meniscus in the chamber cannot be predicted accurately.

For modeling the behavior of the side-channel, the fluid in the side-channel was considered as a mass (fluid in the side-channel) attached to a spring (trapped air) and a damper (fluid resistance of the filled part of the side-channel). The surface tension at the air-water interface introduces an offset for the mass-spring-damper system.
The model describes the position of the air-water surface as function of all other parameters of the system (Figure 3).

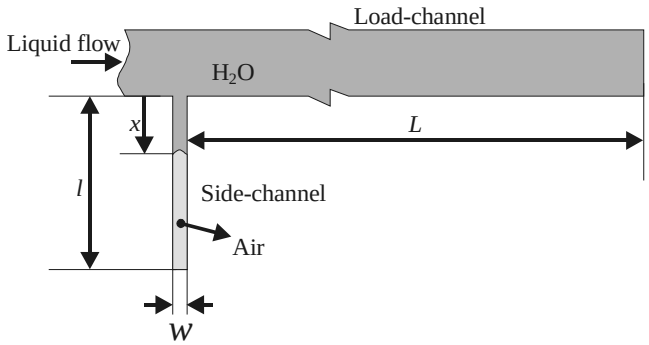

Figure 3 : The basic layout of the compliance structure.

The force balance is as follows:

$$M\ddot{x} = P_{fluid}\,wd + 2\gamma_s\,(w+d)\cos\alpha - P_{air}\,wd - w^2 d^2 R_{channel}\,\dot{x}\,, \qquad \textbf{Eq.1}$$

Where x is the position of the surface, M is the mass of the fluid in the side-channel, P_{fluid} and P_{air} respectively the pressure at the inlet of the side-channel and the pressure of the trapped air, w and d the width and depth of the side-channel, γ_s and α the surface tension and the contactangle of an air-water-glass interface and $R_{channel}$ the fluid resistance of the filled part of the side-channel.
Mass, resistance and trapped air pressure all depend on the position of the surface. The incorporated mass is:

$$M = \rho_{H_2O}\,dwx\,, \qquad \textbf{Eq.2}$$

where ρ_{H20} is the density of water.
The pressure of the trapped air depends on the frequency of the volume variations. For slow variations, there will be enough time to exchange heat between the gas and its surroundings. Therefore the isothermal approach is used for slow variations (Eq.3). However for variations with a frequency in the order of magnitude of the operating frequency of the NMPV pump (~3 kHz), the gas will not reach an equilibrium state. For these fast variations, the process is considered adiabatic (Eq.4). This was verified for a 10 µm wide channel. After a sudden temperature change of the gas, it takes appr. 200 µs to transport enough heat to (or from) the gas to keep the temperature of the gas at ambient temperature.

$$P_{air} = P_0\,\frac{l}{l-x} \qquad \text{(isothermal)} \qquad \textbf{Eq.3}$$

$$P_{air} = P_0\left(\frac{l}{l-x}\right)^{\gamma} \qquad \text{(adiabatic)} \qquad \textbf{Eq.4}$$

In these equations, P_0 is the initial pressure before compression, l is the length of the side-channel and γ is the specific heat ratio for the trapped gas (γ=1.4 for air). Both expressions were used, since the filling of the channel will be a slow process (there's enough time to exchange heat with the surroundings), so the isothermal law applies, whereas the actual flow variations will be fast variations (≈3 kHz for the NMPV pump) raising the need for the adiabatic equation. The final pressure from the isothermal equation will be the initial pressure for the adiabatic equation.

The fluid resistance of the filled part of the side-channel varies with the length of this filled part, x. However, care has to be taken which model is applied. If the channel width is much smaller than its depth, then the channel can be treated as a slit, but in case of depth and width being of the same order of magnitude, the fluid resistance should be considered as the resistance from a rectangular channel [10, 11]

$$R_{fluid} = \frac{3\mu_{H_2O} x}{w^3 d} \qquad \text{(slit, } d >> w \text{)} \qquad \textbf{Eq.5}$$

$$R_{fluid} = \frac{128\mu_{H_2O} x}{\pi D_{eff}^{\ 4}} \qquad \text{(rectangular, } d=O(w) \text{)} \qquad \textbf{Eq.6}$$

This effective diameter is given by

$$D_{eff} \equiv \frac{4A}{P} = \frac{2(wd)}{w+d}, \qquad \textbf{Eq.7}$$

in which A is the cross-sectional area of the channel, and P the wetted perimeter of the channel.

For the steady state, Eq.1 reduces to:

$$0 = P_{fluid} wd + 2\gamma_s (w+d)\cos\alpha - P_{air} wd \qquad \textbf{Eq.8}$$

in which P_{fluid} is the average pressure in the fluid at the inlet of the side-channel (pressure drop over the load-channel plus atmospheric pressure). From Eq.3 and Eq.8 the initial wick-in distance $\hat{x}$ (i.e. the distance the fluid enters the side-channel is easily derived :

$$\hat{x} = l - \frac{lP_0}{P_{fluid} + 2\gamma_s \frac{w+d}{wd}\cos\alpha} \qquad \textbf{Eq.9}$$

The dynamic behaviour of this system cannot be solved analytically, unless the nonlinearities are removed. The result of linearization about the equilibrium point will be a transfer function $H(j\omega)$, which will only be valid for small pressure variations

$$\overline{H}(j\omega) = \frac{\overline{x}(j\omega)}{\overline{P}(j\omega)} = k \frac{1}{1 + 2j\beta \frac{\omega}{\omega_0} - \frac{\omega^2}{\omega_0^{\ 2}}} \qquad \textbf{Eq.10}$$

In which k is the amplification factor, ß the damping constant, ω the applied frequency and ω_0 the natural frequency of the system. Rewriting Eq.1 into the above form and filling out

linearized equations for the mass, the air pressure and the fluid resistance in the side-channel, the natural frequency ω_0 is found to be:

$$\omega_0 = \frac{1}{l - \hat{x}} \sqrt{\frac{\gamma l P_{atm}}{\rho_{H_2O} \hat{x}}}, \qquad \textbf{Eq.11}$$

in which P_{atm} is atmospheric pressure.

Integration of Eq.10, and multiplying by the side-channels cross-sectional area {*wd*}, Eq.10 results in the side-channels admittance. The admittance of the load-channel is given by

$$\overline{A}_{load} = \frac{\overline{Q}}{\overline{P}} = \frac{1}{R + j\omega I}, \qquad \textbf{Eq.12}$$

in which *R* is the steady flow resistance of the channel and *I* the inertance of the fluid in the channel.

The admittance ratio of the side-channel and the load-channel now will determine the magnitude of flow variations in the load-channel due to pressure variations at the inlet of the load-channel. Figure 4 shows how the damping of flow variations can be derived from the admittances of the load-channel and the side-channel.

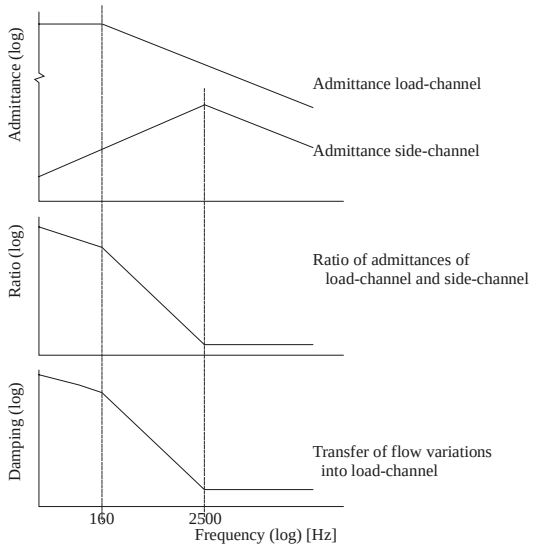

Figure 4 : Construction principle of the damping of flowvariations from the admittances of the load- and side-channel.

The higher corner frequency results from the corner frequency of the side-channel. The lower corner frequency is at the point where the admittance of both side- and load-channel are the same. For the calculation of the behavior, the following parameters were used for the dimensions of the side-channel and load-channel : ($d \times w \times l$=370×10×2000 μm^3) and ($d \times w \times l$=0.2×0.2×100 mm^3). The mean flow was 5 μl/sec. For this system, the cornerfrequency of the side-channel is 2500 Hz. The corner frequency of the load-channel is 160 Hz.

Eq.1 cannot be solved for the chamber compliance structure (Figure 2), since the shape of the meniscus that will be formed in the chamber cannot be predicted accurately. Therefore the force of the surface tension dragging fluid into the chamber cannot be predicted. Steady state measurements can be performed in which the pressure in the chamber as well as the length of the meniscus along the walls of the chamber can be measured. For these conditions, a modified Eq.8 still holds (see also Figure 5):

$$P_{atm}\frac{V_0}{V_1}ld = P_{fluid}ld + 2\gamma_s(l+d)\cos\alpha, \qquad \textbf{Eq.13}$$

in which l is the length of the meniscus (as seen from above), d the depth of the chamber and V_0 and V_1 the initial and real volume of the air in the chamber.

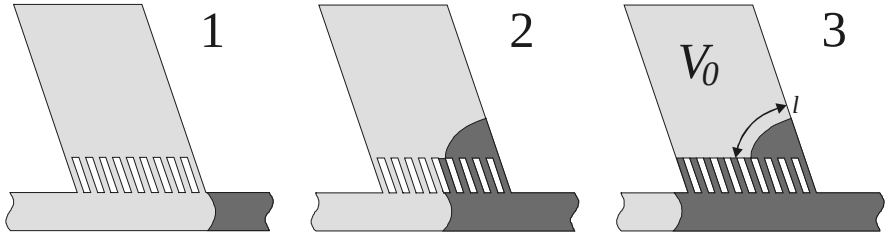

Figure 5 : meaning of V_0 and l for the chamber compliance structure.

Simulation

The compliance system was simulated using the simulation package Simulink [7]. The simulated system consisted of a load channel ($d\times w\times l$=0.2×0.2×100 mm^3) with 40 side channels ($d\times w\times l$=370×10×2000 µm^3). The flow that was specified at the inlet was a net flow of 5 µl/sec with a superimposed sinusoidal flow variation of 0.01 µl/sec. These flowvariations were kept this small to ensure the system would be in its linear region. The flowvariations at the output were calculated for different frequencies.
The results from these simulations are shown in Figure 6. These results closely match the frequency behaviour as predicted in Figure 4.

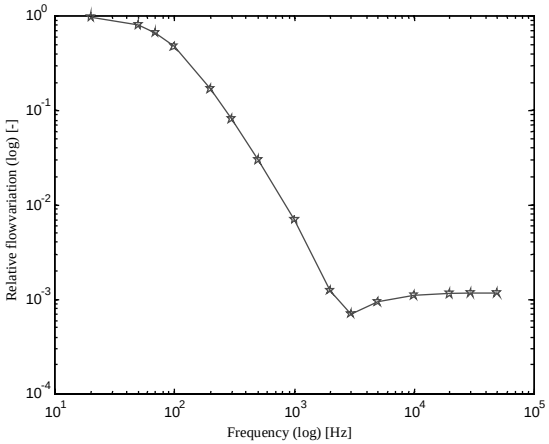

Figure 6 : simulated frequency dependence of the flowvariations in the load-channels respective to the imposed flowvariations on the whole system.

Realization

Samples were prepared using deep reactive ion etching (DRIE) to create the channels and chambers in silicon. The channels were covered by anodic bonding of Pyrex to the silicon. Holes were drilled through the silicon for the fluid connections. See Figure 7 for the principle of the fabrication process.

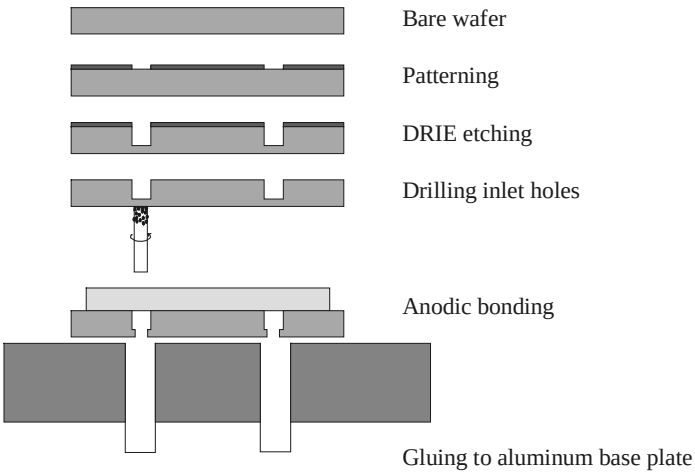

Figure 7 : The fabrication process of the samples.

Two types of samples were realized. The first type consists of a series of parallel side-channels, whereas the second type is a chamber next to the main channel with 10 parallel inlets into the chamber (see Figure 2). The chambers were 1460 μm wide and 1780 μm long. The side-channels were 10 μm wide and 2000 μm long. There were 384 side-channels on one sample. All etched structures were 373 μm deep.

Measurements

A measurement setup has been realized for the characterization of the compliance structure. The setup is schematically shown in Figure 8. A video camera is used to monitor the sample through a microscope. With this monitor, the position of the meniscus is measured. The system is pressurized with a syringe pump (1 ml B-D syringe on a KD-scientific syringe pump). The pressure in the system is read through a pressure sensor (Entran EPI-411, 3.5 Bar range).

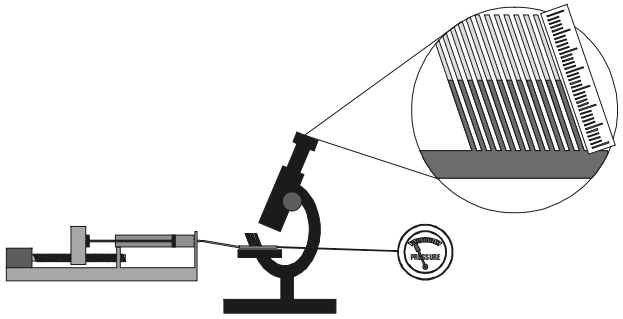

Figure 8 : schematic of the measurement setup. A microscope is used for the detection of the position of the membrane, a motor driven syringe pump for filling up the system and pressurizing it and a pressure sensor to monitor the actual pressure in the system.

The position of the meniscus was read through the microscope. From the so acquired data, the total volume of air and length of the meniscus can be calculated.

Due to the narrow but deep channel dimensions the channel did not allow visualization of the meniscus. Therefore it was not possible for us to obtain information on the position of the meniscus in the small channels. The dimensions of the compliance chamber elements however are such that the meniscus can easily be seen. Due to the multiple inlets into these chambers, the chambers first partly filled with water pushing air out of the chamber (Figure 9).

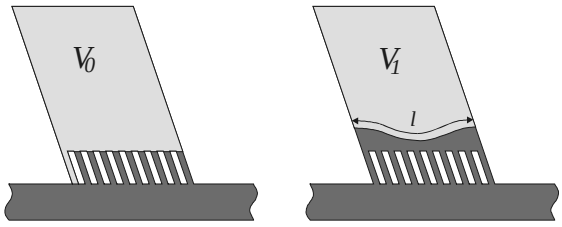

Figure 9 : The way the sample filled, the initial volume V_0 was smaller than meant to be. l denotes the length of the meniscus in the chamber.

Static measurements on this compliance could however still be performed. Starting with the reduced initial volume, the static pressure in the system was gradually increased, which caused the air to be compressed. The compression ratio of the air (initial gas volume over actual gas volume) and the corresponding fluid pressure (measured from the pressure transducer), air pressure (calculated from the measured air volume) and the theoretical

pressure due to the surface tension (from the measured length of the meniscus) are shown in Figure 10. The accuracy of the measurements on the airvolume and the length of the meniscus were about 5%.

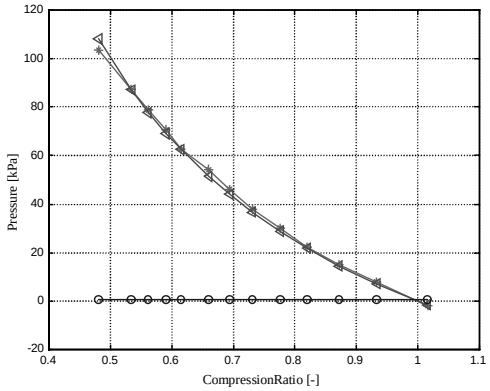

Figure 10 : The pressure in the fluid (*), results in compression of the air in the compliance chamber. The volumechange of the air corresponds to a pressure change of the air (◁). The pressure in the air due to the surface tension is also indicated (O).

Also measurements were performed on the comparison of a pump with the compliance structure and the same pumpdesign without compliance structure. The results are depicted in figure 11.

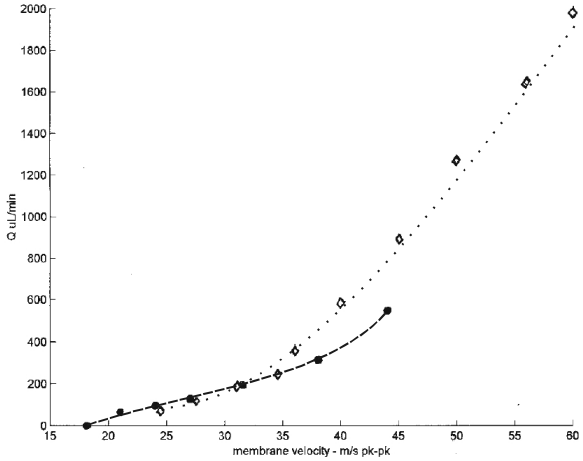

Figure 11 : Measurement results for a pump with (dotted line) and without compliance structure (dashed line)

The point where the lines stop indicate the point at which the pumps started cavitating. Cavitation is an indication for the fact that the fluid that is coupled to the membrane is too slow to follow the movements of the membrane. The compliance is used to decouple the fluid in the system from the pump membrane. From the figure it is clearly seen, that the pump with the compliance structure can reach higher membrane velocities and therefore higher flowrates as the pump without the compliance. The decoupling works well and therefore it can be concluded that the compliance structure works.

Conclusions and Future Work

A compliance for microfluidical systems has been designed to dampen flowvariations resulting from the NMPV pump. This micromachined compliance was used to replace a macro-world compliance which was required for good pump performance. Around the operating frequency of 3 kHz a theoretical damping of the flow variations of 30dB was established.

The proof of the working principle has been found in two ways. First, static measurements have been performed on the chamber compliance structure. It is seen, that a raise of the pressure in the system results in the compliance taking in fluid. The amount of fluid that is absorbed by the compliance matches theory perfectly. Second, two versions of the NMPV pump have been compared. The first version had no compliance structure, whereas the second had the designed compliance connected to its in- and outlet. From the comparison it was seen, that the compliance structure enables the pump to deliver almost four times as much fluid per unit time.

The current design of the chamber compliance with its multiple inlets (originally designed for lower resistance) can be improved by reducing the number of inlets to just one. This will prevent the filling of (part of) the chamber with fluid. Any amount of unwanted fluid in the chamber reduces the volume of trapped air and with that the effective compliance.

Acknowledgements

The research was funded by STW (Dutch Technology Foundation, project TEL 3467) and DARPA (contracts N660001-97-C-8632 and F30602-98-2-0151). Brian Williams is acknowledged for his help performing the comparison measurements.

References

[1] D.Maillefer, H.van Lintel, G.Rey-Mernet, R.Hirschi, A High-performance silicon micropump for an implantable drug delivery system, Proceedings MEMS 99, , 1999

[2] F.K.Forster, R.L.Bardell, M.A.Afromowitz, N.R.Sharma, A.Blanchard, Design, fabrication and testing of fixed-valve micro-pumps, Proceedings ASME Fluids Engineering division, 1995.

[3] R.Zengerle, M.Richter, Simulation of microfluid systems, Journal of Micromechanics and Microengineering 4, pp192, 1994.

[4] J.P.Krog, H.Dirac, B.Fabius, P.Gravesen, Requirements of pumps used in MicroTAS, microTAS'98, Banff, 1998

[5] Shih-I. Pai, Modern fluid mechanics (1st ed.), ch.II-2, Science press, Beijing, 1981

[6] F.M.White, Fluid mechanics, Mc.Graw Hill, NY, 1986

[7] Simulink, the Mathworks Inc. Natick, MA

[8] M.Richter, R.Linneman, P.Woias, Robust design of gas and liquid micropumps, Sensors & Actuators A 68, pp480-486, 1998

[9] M.Stehr, S.Messner, H.Sandmaier, R.Zengerle, A new micropump with bidirectional fluid transport and selfblocking effect, Proceedings MEMS '96, pp485-490, 1996

[10] J.Ulrich, R.Zengerle, Static and dynamic flow simulation of a KOH etched micro-valve using the finite-element method, Sensors & Actuators A 53, pp379-385, 1996

[11] M.C.Acero, J.A.Plaza, J.Esteve, M.Carmona, S.Marco, J.Samitier, Design of a modular micropump based on anodic bonding, Journal of Micromechanics and Microengineering 7 pp179-182, 1997

[12] T.Bourouina, A.Bosseboeuf, JP.Grandchamp, Design and simulation of an electrostatic micropump for drug delivery applications, Journal of Micromechanics and Microengineering 7, pp186-188, 1997

Chapter 10 : Conclusions and Discussion

In this final chapter, the balance of the presented work is drawn up. The choice for the system setup, definition and design of components and determination of technology are reiterated. The performance of the ultimate integrated system is critically evaluated and some drawbacks of the chosen approach are identified. Finally, an alternative approach for the realization of a MAFIAS, based upon modular integration of separate components onto a channel plate is discussed.

10.1 Defining the sub-systems

In the second chapter of this thesis, the Berthelot reaction scheme as used in MAFIAS was reviewed. This reaction, which involves the addition of several chemicals to the sample, is fairly representative for many schemes used in conventional FIA practice. The two-step Berthelot reaction converts ammonia into indophenol, a blue dye. The resulting amount of indophenol is measured using light absorption in a cuvette. Optimal reaction conditions are at pH 11 and T=37°C. The pH is controlled by premixing the first reagent with a pH 11 buffer. The temperature is controlled by microstructured thin film heaters integrated in the system. The above-mentioned conditions lead to a split of the whole system into four functional subsystems:

i) Propelling of the different fluids through the system is carried out by *micropumps*

ii) Different fluids present in the system (sample, reagent 1, reagent 2) have to be mixed at some point in the system. Thus *micromixers* are needed as subunits

iii) The second reaction step has to be controlled at a fixed temperature of 37°C. This temperature has to be maintained for 30 seconds. This function is realized with a *microreactor*

iv) After completion of the reaction, the indophenol concentration has to be determined. This is done in a *microfabricated cuvette*. Light is coupled into the cuvette from one side. The light intensity of the exiting light now will be a measure for the amount of indophenol present in the cuvette.

The profile of the sample plug that is injected in the system is distorted during its transport through the system. The combination of diffusion and the parabolic flow profile will lengthen and dilute the sample plug. *Dispersion* is introduced as the ratio of the theoretical peak (without dispersion) and the actually measured concentration peak. This ratio is a systems parameter, and should of course be kept as close as possible to unity. It is concluded that for minimal dispersion a small channel cross section in combination with a long (in relation to the channel diameter) sample plug length should be chosen.

10.2 Mixer

Typically in microfluidic systems, due to the small channel diameter (order of 100 μm) the flow regime in the channels will be laminar. This means that there will be no turbulence effects to enhance mixing. Mixing therefore has to be based on diffusion as principle of mass-transport.

On a large scale, diffusion is a relative slow process. The time it takes for a certain compound to diffuse from A to B is proportional to the square of the distance between A and B. The mixer design that is presented in this thesis is simply a narrowing of the main channel of the system, so that the diffusion distance is reduced. This results in a quadratic effect for the reduction in diffusion time. In the narrow part of the realized micromixer, diffusing from one side to the other takes only a few seconds.

The mixer has to be designed for a specific compound as well as for a certain flow rate. Choosing the width of the narrow part of the mixer defines the mixing time (this mixing time differs for different compounds, since the diffusion constant differs for different compounds). The channel has to be chosen as long as that the fluid stays in the narrow part of the channel for as long as is needed for diffusion to reach the other side of the channel.

After the geometry of the mixer has been decided, one should check the pressure drop that will be present over the mixer-channel. Not only will the narrow part of the channel have a higher fluidic resistance per unit length compared to the normal systems channel, but also the flow velocity in the narrow part of the channel is also higher, resulting in an even higher pressure drop over the channel. In general it can be stated that as long as the pressure drop is not a critical factor it is advantageous to create a mixing zone with the same channel cross section (same linear flow rate) but with the dimension perpendicular to the reagents interface reduced as much as possible.

10.3 Reaction Chamber

In chapter 4 the design and realization of a reaction chamber for the MAFIAS system was presented. The reaction chamber consists basically of a channel with a length corresponding to a residence time of 30 seconds at the chosen flow rate. The temperature of the fluid in the channel is controlled by using an electric heater and temperature sensor. Measurements on the reaction chamber were performed using

ethanol as fluid. These measurements showed that (after calibrating the temperature sensors) the temperature could be controlled very precisely. Since the channels are small (<200 μm), an even temperature distribution throughout the fluid is established very fast (~70 msec). Because it was found difficult to fully electrically isolate thin film heaters from the liquid when located on the glass cover directly in contact with the liquid, another configuration was chosen with the heater elements just beside the channel. The temperature control now controls the temperature of the whole silicon chip, but since the fluid is almost instantly at that same temperature, the chip temperature can be regarded the same as the fluid temperature. This choice has no disadvantages compared to the original approach.

10.4 Pump

In chapter five the design of the pump for the system is presented. This pump should be capable of driving the fluid through the system with the required flow rate. Further convenient features for a (micro-) pump are the capability of the pump priming itself and the capability of handling gas bubbles that might be present in the fluid. Those two features will make the handling of the pump much easier and less frustrating.

The pressure that is needed to push fluid at the desired flow rate through the system is approximated as follows. The fluidic resistance of the main channel of the system is calculated from an estimate of the geometry of that channel (25 cm length, cross-section of 200×200 μm^2). This channel has to be flushed about once a minute to come to the desired sample rate of 60 hr^{-1}. Therefore, the pump has to be capable of producing a flow rate of 10 μl/min at a back pressure of about 740 Pa (74 mBar).

In order to be self-priming or bubble-tolerant, the pump has to be able to overcome surface tension effects. A thin film of water between the pumps valve and the valve seat will actually put a force on the valve pulling it close. The pressure variations that are generated in the pump chamber have to be large enough to overcome this surface tension effect. According to the model of Woias and Richter [5.25] the extra pressure needed to overcome the surface tension forces is about 70 mBar. This brings the minimal head-pressure of the pump to approximately 150 mBar.

The peristaltic pumping principle is chosen for the pump. Using three membranes in a row interconnected with channels, pumping action can be achieved by sequential actuation of the membranes. An additional advantage of this principle is that it allows *bi-directional* pumping by changing the actuation sequence.

The pump is made of a silicon-Pyrex wafer stack. The membranes are defined by selective anodic bonding of the Pyrex to the silicon. The regions that are not bonded form the membranes. These membranes leave very little gap (~1μm) between the silicon and the Pyrex. This very small dead volume allows for a relative high compression ratio of the pump, enabling high pressures at the outlet of the pump. The membranes of the pump are actuated by a piezo disc, which is glued on top of the membrane. Putting an electric field over the piezo causes the piezo to expand in the

planar direction. Since the Pyrex does not expand, the Pyrex-Piezo is forced into a curve, creating some volume underneath the membrane. The used membranes have a diameter of 11 mm and are 200 μm thick. Using a 1 cm piezo disc of that same thickness results in a maximum center deflection of the membrane of about 5 μm, corresponding to a displaced volume of ~300 nl. The compression ratio of the pump is about 0.4 resulting in a theoretically maximum pressure of about 400 mBar.

Performance measurements of the pump have confirmed that the volume displacement indeed is about 300 nl. Since the realised channels have a volume of 480 nl, the maximum realizable pressure at the normal actuation voltage (120 V) is 625 mBar. Raising the actuation voltage to 130 V has shown that the pressure rises to 700 mBar, at which point the pump membrane breaks out of the top wafer. As this high pressure implies, the pump indeed is capable of priming itself as well as pumping an air/fluid mixture. The maximum measured flow rate was 25 μl/min (@1.4 Hz, 300 nl/stroke).

From all this it is concluded that the presented pump is more than suitable to drive the system. Disadvantage of the followed approach are the separate soldering of the piezo elements, and the relatively large surface area of the pumps.

10.5 Detection Cell

For the detection of ‘the amount of blue’ a detection cell has been designed and realized. From the desired detection range and the expected dispersion (Ch. 2), the needed length of the light path is determined to be 6 mm. In micromechanics, such a length can only be realized in the plane of a wafer. The design of the chip is based on wet-chemical etching using KOH-IPA as etchant. With this etching technique it is possible to create channels with 45° side walls. These side walls are used as in- and out-coupling mirrors. Using a light source that is placed perpendicular to the surface, this guarantees that the light travels from one side of the channel to the other without too many reflections.

Measurements were performed using a series of indophenol concentrations in the range of 4 μg/l to 10 mg/l. It was found that the detection cell could be used for the range from 10 μg/l up to 10 mg/l. The needed range for the MAFIAS system is 30 μg/l to 3 mg/l, which is neatly within the mentioned range.

The response of the detection cell is not linear (as would be expected from the Lambert-Beer law). This is caused by the fact that the reflectance of the mirrors in the detection cell improves with higher refractive index of the sample. The refractive indexe gets higher for higher indophenol concentrations, thus causing more light than expected to reach the detector. A calibration measurement series is needed before the detection cell can be used for the quantitative detection of indophenol.

10.6 Integration

Chapter seven describes how the different fluidic components were combined into one design. The designed system then was fabricated and tested. Because of the involved number of extra process steps, it was decided that the detection cell would not be included into the monolithic design. The detection cell can be glued (or anodically bonded) to the system or it can be attached to the system by intermediate tubing. The pump, mixer and reaction chamber all are integrated on one wafer. DRIE will be used to etch the channels in a silicon base plate and a Pyrex wafer will be used to close the formed channels and form the membranes for the pump. The Pyrex wafer has to be thinned locally to match the thickness of the used piezo discs.

Electric connections from the piezo discs and the heater and temperature sensor will be soldered to the chip. For this purpose, solder pads for a standard electronic header are sputtered on the chip. Testing of the chip has shown that the strength of the anodic bond between the silicon (with 200 nm silicon oxide) and Pyrex was not strong enough to withstand the forces and moments induced by the bending of the membranes. Therefore a second chip was fabricated without this oxide layer. Since this oxide layer was needed to protect the heater and temperature sensor from short-circuiting through the silicon, the heater and temperature sensor were not integrated into this second chip. The heater and temperature sensor could be implemented on the bottom side of the silicon wafer, but instead a standard heating mat and temperature sensor were used during the testing.

The testing of the chip has shown, that the system works. The formation of a blue dye was observed (as well by eye as by using the detection cell), and the performance of the systems was characterized. It was seen, that injection of only hypochlorite or phenol results in a change of the output signal of the detection cell. Running the system with injection of a plug of ammonia, hypochlorite and phenol results in the formation of indophenol. The resulting response from the detection cell is clearly different from the response from only one of the reagents. It was also observed that a twice diluted ammonia sample results in only half the output from the detection cell.

10.7 Selective anodic bonding

In order to gain insight in the selective anodic bonding technique of (Pyrex) glass to silicon this bonding process was investigated.

As was known from literature, a layer of chromium (~300 nm thick) locally prevents the formation of the anodic bond between silicon and glass. Normally, the anodic bond is formed by oxygen ions from the Pyrex reaching the silicon where they form silicon oxide, the actual bond. One hypothesis was that the intermediate layer blocks the path for oxygen towards the silicon, thus preventing the formation of a bond. A phenomenon, however, appeared to give a much better explanation of the non-bonding.

The actual mechanism was found to be the vanishing of the electric field between the Pyrex and silicon at those places where a conducting layer has been deposited on the Pyrex. As soon as this conducting layer touches the silicon, both sides will be at the same potential, resulting in zero electric field strength. From this theory two important conclusions are drawn. First, the intermediate layer may be much thinner than 300 nm. A 1 (one) nm thick chromium layer already prevents bond formation. This fact opens some new opportunities, since a one nm thick layer will hardly introduce stress in any of the bonded wafers due to the 'step-covering'.

The other conclusion is that the intermediate layer has to be conductive throughout the bonding process. The chromium layer will be oxidized during the process, but stays conductive. An aluminum intermediate layer will not prevent the forming of a bond since the oxidized aluminum is not conductive. Other materials that can be employed as anti bonding layer are e.g. platinum.

It is seen, that during the bonding process gas is formed at the antibond layer. This gas presumably is oxygen gas, formed from the oxygen ions that are pulled from the glass wafer towards the silicon. In closed regions, the formation of this gas will result in pressure build-up underneath the membrane defined by the antibond layer. This pressure will cause the membranes to bulge out. Introducing an outlet through which the formed gas can escape from underneath the membrane will prevent the deformation of the membranes.

10.8 A microfluidic compliance structure

The last chapter in this thesis describes a compliance structure for microfluidic systems. The compliance is based on a trapped air bubble. The air will be compressed slightly by a raise in the pressure, thus creating some volume to take up fluid.

The air is trapped in a narrow side channel of the main fluidic system. Due to the surface tension, the side channel will fill partly. The pressure in the air bubble will be above the ambient pressure. Since the side channel is partly filled, the compliance is capable of handling both over- and under- pressure.

The compliance channel has to be tuned to the system. The ratio of fluidic impedances of the compliance channel and the system determines the frequency dependence and the efficiency of the compliance structure.

The compliance has been applied to a micropump that is driven at 2 kHz, and has been designed to reduce flow variations at that frequency by a factor of 1000. Though the actual flow variations cannot be measured, it is observed that the pump performance has improved significantly from the addition of the compliance.

10.9 Discussion

The most important final conclusion of this thesis that can be drawn is that it appeared possible to realize a monolithically integrated FIA system for ammonium measurement with sufficient dynamic range and detection limit. Almost all of the initially stated specifications such as flow rate of 10 μl/min, sample rate of 1/min and dynamic range of 3 decades have been reached. The generic nature of the chosen analysis (based upon the Berthelot reaction) makes the followed approach and finally realized system easily applicable to a large variety of other determinations, which is a great accomplishment.

Nevertheless there are several drawbacks connected to the realized MAFIAS. It should be mentioned that the system is fairly vulnerable. Most important disadvantage of the chosen monolithic approach is that as soon as only one of the integrated components fails, the whole system becomes worthless. Since it is only the pumps that incorporate moving parts, these are the most likeliest to fail. Observed failure conditions involve too high backpressure (membranes break out of the Pyrex wafer) and dust/dirt. Such particles become trapped underneath the membrane (which lifts to a maximum of 5 μm) preventing the membrane to come down and close.

A way to get around this problem is to create a system in which the different components can be replaced. It is clear that this cannot be the case in a monolithic design. It has to be a design in which the components are either stacked [1] or placed on a fluidic channel plate.

The most promising modular approach of a (micro) fluidic system is the MATAS technology (Modular Assembly for Total Analysis Systems) [2]. This technology places the micromachined components in a small housing made from printed circuit board, which fits exactly in a corresponding hole in a PCB board. Electrical connections to the components are realized on top of the PCB, fluidic connections are provided by a channel plate glued underneath the PCB. See Figure 1 for more details.

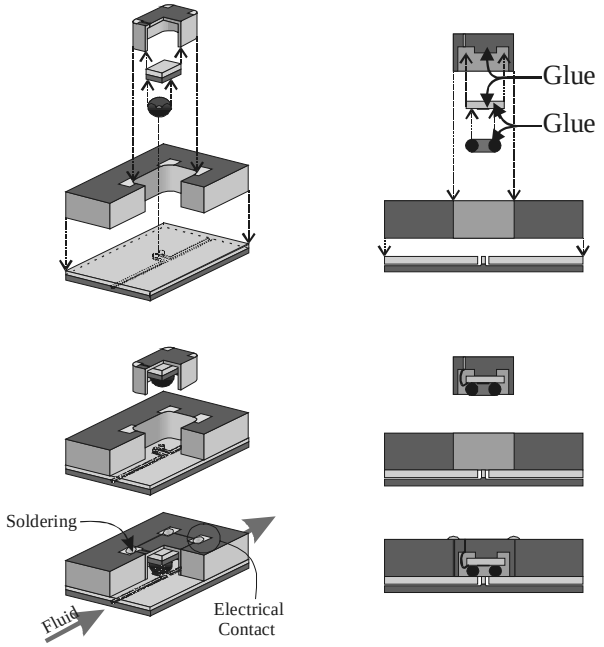

Figure 1 : The MATAS technology.

Using a technology as described, a component that fails can be replaced fast and easy, resulting in an again working system.

10.10 Literature

[1] B.H.vanderSchoot, S.Jeanneret, A.vandenBerg, N.F.deRooij, Modular setup for a miniaturized chemical analysis system, Sensors and Actuators B 15-16, pp211.

[2] T.T. Veenstra, R.M.Tiggelaar, R.G.P.Sanders, J.Wissink, A.Prak, J.G.E.Gardeniers, M.C.Elwenspoek, MAFIAS in modules, proceedings of the 3rd symposium on Microsystems in Practice, 20-21 janurai 2000, pp3

Summary

This thesis contains a full description of the complete design of the MAFIAS system. MAFIAS is short for **M**icro **A**mmonia **F**low **I**njection **A**nalysis **S**ystem, i.e. a micro mechanical system for the detection of ammonia.

The sequence of all the steps of the design is reflected in the sequence of the chapters.

Chapter 2 gives in inventarisation of the chemistry that is involved in the ammonia detection. From the chemistry, a number of constraints for the system are deduced. The concept of dispersion is introduced to the reader.

The following chapters 3-6 deal with the needed fluidic components. The mixer, reaction chamber, pump and detection cell that are made are described in those chapters. The designs, measurements and results are all described in the respective chapters.

In chapter 7, all components are integrated into one system. First, the process schemes for the different components are tuned to each other. After this, the layout of the components on the chip is decided. Fluidic and electrical connections to the macro world are described. Chapter 7 is concluded with a small measurement series. The measurements indicate that the desired reaction indeed takes place on the chip.

The last two chapters deal with two sidebranches of the performed research. Chapter 8 shows how the technology of anodic bonding can be used to create Pyrex membranes that have virtually no gap with the silicon. These membranes are employed in the design of the micropump of the MAFIAS system.

Chapter 9 describes a micro fluidic compliance structure. This structure is specifically designed to improve the performance of the micropump of the group of Prof. Forster (University of Washington – Seattle – USA).

Samenvatting

In dit proefschrift staat het volledige ontwerp van het MAFIAS beschreven. MAFIAS staat voor **M**icro **A**mmonia **F**low **I**njection **A**nalysis **S**ystem, ofwel: een micro mechanisch systeem voor de detectie van ammonia.

De hoofdstuk indeling van het proefschrift volgt de volgorde van de ontwerpstappen die zijn genomen.

Een inventarisatie van de benodigde chemie is weergegeven in hoofdstuk 2. Vanuit de chemie volgen een aantal randvoorwaarden voor het ontwerp van het gehele systeem. Een kleine beschouwing aangaande het fenomeen *dispersie* wordt ook in hoofdstuk 2 gegeven.

De volgende hoofdstukken geven de ontwerpen van alle benodigde componenten weer. De mixer, reactie kamer, pomp en detectiecel die zijn gemaakt worden beschreven in de hoofdstukken 3-6. Zowel de ontwerpen an sich alsmede de verrichte metingen en resultaten daarvan worden beschreven in elk van de respectieve hoofdstukken.

De componenten worden geïntegreerd tot één systeem in hoofdstuk 7. Eerst worden de verschillende proces schema's voor de losse componenten op elkaar afgestemd. Vervolgens wordt de layout van de componenten op de chip bepaald. Bijzondere aandacht wordt gegeven aan de verbindingen van de chip naar de buitenwereld. Hoofdstuk 7 wordt afgesloten met een kleine meetserie. De verrichte metingen geven aan, dat de chemische reactie daadwerkelijk plaatsvindt op de chip.

De laatste twee hoofdstukken geven twee zijpaadjes van het verrichte onderzoek weer. Hoofdstuk 8 laat zien hoe de technologie van het anodisch bonden kan worden gebruikt om Pyrex membranen te maken die zonder tussenruimte aanliggen op silicium. De membranen die met deze technologie zijn gemaakt zijn toegepast in het ontwerp van de micropomp voor het MAFIAS systeem.

Hoofdstuk 9 geeft de beschrijving van een kleine fluidische compliantie structuur. Deze compliantie structuur is specifiek ontworpen om de prestaties van de micro pomp van de groep van Prof. Forster (University of Washington – Seattle – USA) te verbeteren.

Dankwoord

De gedachtes en ideeen die in dit proefschrift staan zijn niet de mijne. Tenminste. Niet alléén van mij. Vele mensen hebben hun steentje bijgedragen. En velen van die vele mensen hebben dat onbewust gedaan. In dit laatste stukje van het proefschrift wil ik een ieder die mij tot steun is geweest in de afgelopen 4 jaren bedanken.

Eerst zijn daar de mensen die me de kans hebben geboden om het MAFIAS project te laten doen. Miko, Albert, ik dank jullie hartelijk voor alle geboden ruimte, adviezen en vrijheid. Ik vond het zo gaaf, dat ik met plezier nog een tijd blijf hangen.

De vakgroep MicMec vormt zo nu en dan een perfect team. Veel problemen worden met zijn allen opgelost. Een aantal MicMeccers zijn voor mij van bijzondere waarde geweest.
Remco aka Pino: samen met jou was er een heus MAFIAS-team. Een gavere meewerker had ik me nooit kunnen wensen!
Veel van de techonologie komt uit de handen van Erwin en Meint: dank voor alle hulp en ideeen.
In de vier jaren die ik met de opdracht bezig ben geweest heb ik een redelijke hoop begeleiders versleten. Theo, Remco, HenRIE, Theo (2e poging) en Gijs hebben het allen geprobeerd. Uiteindelijk is het Han dan gelukt om mij in een duidelijke richting te laten lopen. Allen, maar speciaal Han: heel erg dankjewel van Theo.
En dan was daar die student. Roald. Vriend en vijand verbazen zich over wat wij samenwerken noemen. Wij weten echter beiden wel precies hoe of dat dat zit…

Alle frustraties die je gedurende zo'n dagje onderzoek opbouwt moeten er ook zo nu en dan uit worden gelaten. Het zijn dan voornamelijk vrienden die de klos zijn. Namen die in dit rijtje zeer zeker genoemd dienen te worden zijn: Menne, Jeroen, Martin, Nicole, Roald, wErik, Ozzie en schEric. Maar dat zijn niet de enigen. Met veel plezier heb ik veel van mijn vrije tijd doorgebracht in en rond de CD-Uitleen. Het gaat te ver om hier alle vrijwilligers met name te noemen. Op gevaar af een enkeling (of twee) te missen noem ik hier diegenen die de meeste indruk hebben gemaakt: Herman, Peut,

BasB, Mark, Joost, Renie, Olaf, Paul, Pascal, Goris (leuk fontje joh), Dennis, BasL, Marcel, AndreG, JeroenB

Als laatste is er dan nog mijn familie. Pa, Ma, Rita. Precies begrijpen wat ik allemaal uitspook is er niet bij geweest. Maar voor alle aandacht en steun ben ik jullie zeer dankbaar.

T